A stomatin dimer modulates the activity of acid-sensing ion channels

Dissertation zum Erlangen des akademischen Grades des Doktors der Naturwissenschaften (Dr. rer. nat)

Eingereicht im Fachbereich Biologie, Chemie, Pharmazie der Freien Universität Berlin

Vorgelegt von

Janko Brand geboren in Aachen

Berlin im Jahr 2012

Diese Arbeit wurde in dem Zeitraum vom März 2008 bis Juli 2012 unter der Leitung von Prof. Dr. Oliver Daumke am Max Delbrück Centrum für Molekulare Medizin in Berlin Buch angefertigt.

Kommission der Disputation

Vorsitzender: Prof. Dr. Udo Heinemann
Vorsitzender (stellvertretender): Prof. Dr. Christian Freund
Gutachter: Prof. Dr. Oliver Daumke
Gutachter: Prof. Dr. Volker A. Erdmann
Gutachter (Vertretung): Prof. Dr. Markus Wahl

Akademischer Mitarbeiter: Dr. Christoph Weise
Akademischer Mitarbeiter (Vertretung): Dr. Peter Fürste

Disputation am 15.11.2012

"Men wanted for hazardous journey. Small wages. Bitter cold. Long months of complete darkness. Constant danger. Safe return doubtful. Honour and recognition in case of success."

Newspaper advertisement from Ernest Henry Shackleton for one of his antarctic expeditions.

Summary

Stomatin proteins oligomerize at membranes and have been implicated in ion channel regulation and membrane trafficking. To obtain mechanistic insights into their function, I determined three crystal structures of the conserved stomatin domain of mouse stomatin that assembles into a banana-shaped dimer. I could show that this dimerization is crucial for the modulation of acid-sensing ion channel 3 (ASIC3) and ASIC2a activities. A hydrophobic pocket at the inside of the concave surface is open in the presence of an internal peptide ligand and closes in the absence of this ligand, and we demonstrate a function of this pocket in the inhibition of ASIC3 and ASIC2a activity. In one crystal form, stomatin assembles via two conserved surfaces into a cylindrical oligomer, and these oligomerisation surfaces are also essential for the repression of ASIC3-mediated currents. The assembly mode of stomatin uncovered in this study might serve as a model to understand oligomerisation processes of related membrane-remodelling proteins, such as flotillin and prohibitin.

Zusammenfassung

Stomatin-verandte Proteine assemblieren an der Zellmembranen und spielen eine wichtige Rolle in der Regulation von Ionenkanälen. Um detailierte Aussagen über die Funktion dieser Protein zu erhalten wurden mittels Kristallröntgenbeugungsanalyse drei Strukturen vom Maus Stomatin gelöst. Die Analyse der Strukturen zeigte, das Stomatin als Dimer vorliegt, der eine bananenförmige Form hat. Im weiteren konnte gezeigt werden, dass diese Dimerisierung eine wichtige Rolle für die Regulierung der Ionen Kanäle ASIC3 und ASIC2a spielt. Eine hydrophobe Tasche in der Innenseite der konkaven Oberfläche des Stomatin Dimers ist geöffnet in der Anwesenheit eines kurzen internen Peptidliganden und schliesst sich, sobald dieser mutiert wird. Dass diese Tasche wichtig für die Funktion von Stomatin ist, konnte durch Mutagenese gezeigt werden. In einer der drei Kristallformen wurden Interaktionsflächen identifiziert, die zu einer zylindrischen Anordnung der Stomatin Dimere führt. Mutagenesen in diesen Interaktionaflächen verhindern die Modulation des ASIC3 Kanals. Dieser Aufbau der Stomatin Oligomers könnte einen wichtigen Beitrag zum Verständnis der Zusammensetzung von anderen SPFH Proteinen, wie z. B. Flotillin oder Prohibitin liefern.

Publications

Parts of this PhD thesis have been published in the following manuscripts.

Stomatin-domain as a target for therapy

The patent application is submitted.

A Stomatin dimer modulates the activity of acid-sensing ion channels.

Brand J, Smith E, Schwefel D, Poole K, Omerbašić D, Lapatsina L, Kozlenkov A, Behlke J, Lewin GR and Daumke O.

The EMBO Journal 2012 Jul 31. doi: 10.1038/emboj.2012.203.

Stomatin- domain proteins.

Lapatsina L, **Brand J**, Poole K, Daumke O, Lewin GR.

Eur J Cell Biol. 2011 Apr 16. PMID: 21501885

Table of Contents:

1. Introduction

1. 1. The Family of the SPFH domain containing proteins

The SPFH (Stomatin, Prohibitin, Flotillin, HflK/C) domain containing protein family is defined by the presence of a structurally conserved core domain of approximately 100 amino acids (Tavernarakis *et al.*, 1999). This domain also known as prohibitin domain (PHB-domain) or stomatin domain, was firstly considered to be evolutionary conserved until a recent report proposed that it emerged independently in different SPFH domain containing proteins by convergent evolution (Rivera-Milla *et al.*, 2006).

Members of the SPFH family are widely distributed among all kingdoms of life, including archaea (Green and Young, 2008), bacteria (Zorick and Echols, 1991), plants (Borner *et al.*, 2005) and mammals (Huber *et al.*, 2003; Schulte *et al.*, 1997a; Snyers *et al.*, 1998). In spite of the phylogenetic distance, the amino acid sequence of the SPFH-domain is remarkably conserved **(Figure 1. 1.)**.

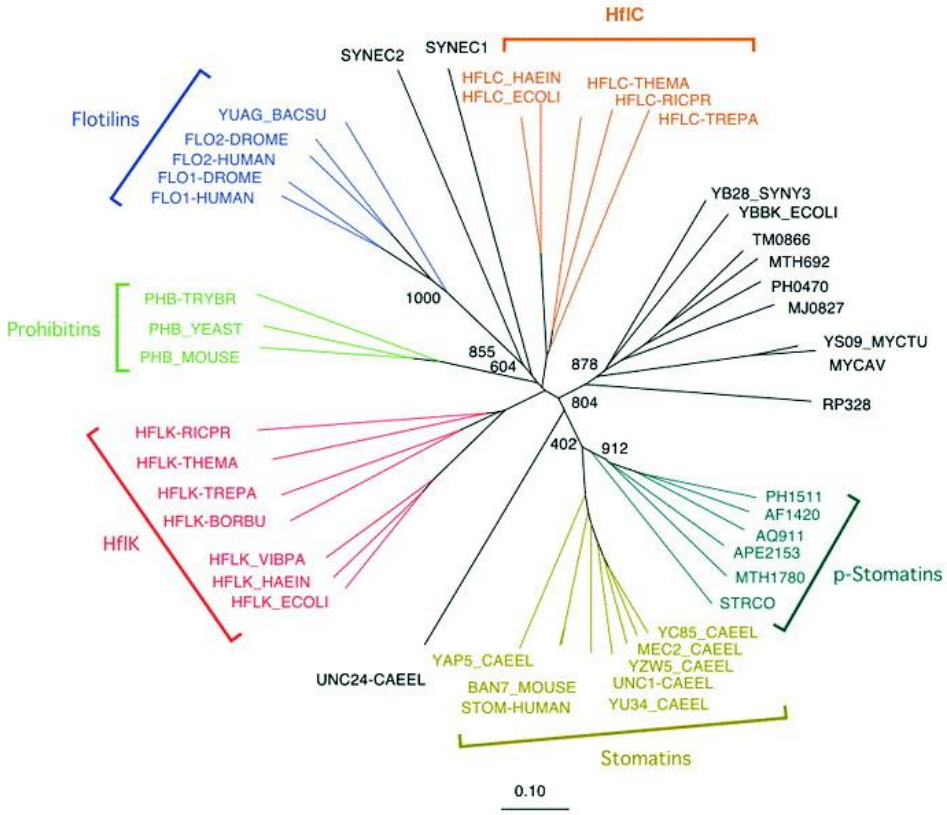

Figure 1. 1: Dendrogram of SPFH domain proteins
A dendrogram comprising 46 SPFH domain containing proteins, illustrates the evolutionary relationships between members of this class of proteins. Taken from (Tavernarakis *et al.*, 1999).

According to the Pfam database, 1583 SPFH domain containing proteins are descirbed across all organisms; of these 243 appear in animals and 96 in mammals (Browman *et al.*, 2007). The crystal structure of the *Pyrococcus horikoshii* (ph) stomatin, is the first structure of an SPFH domain and has elucidated the topological and structural characteristics of the stomatin family proteins(Yokoyama *et al.*, 2008) **(Figure 1. 2A)**. The phstomatin has a mixed α/β fold with the N-terminal β-strand 1 is subdivided into β1a and β1b by a short loop and together with β2 and β3 forms an anti-parallel, curved β-sheet. Helices α2 and α4 extend in parallel and occupy the groove of the sheet, whereas the short α1 and α3 helices are oriented perpendicularly at both ends of the sheet. N- and C-termini are located at opposing sides of the molecule. The phstomatin harbors an unique β-strand (β0) at the N-terminus **(Figure 1. 2)** and β0 mediates trimerization of phstomatin by forming an inter-strand contact to the neighboring molecule (Yokoyama *et al.*, 2008) **(Figure 1. 2B)**.

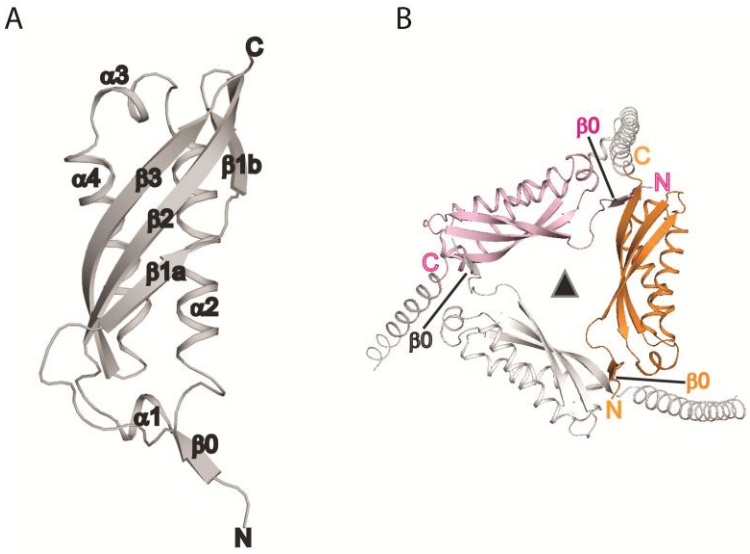

Figure 1. 2: The structure of the SPFH domain from *Pyrococcus horikoshii* (ph).
(A) the structure of the SPFH domain of *Pyrococcus horikoshii* (ph) has a mixed α/β fold. Residues at the N- termini form an additional β0 strand which contacts the C-terminus of the adjacent monomer which results in the trimeric assembly of the phstomatin shown in (B). The image was generated by PyMOL using pdb entry 3BK6 from the publication (Yokoyama *et al.*, 2008).

The structure of the mouse flotillin 2 was solved by NMR (pdb: 1WIN) followed by the crystal structure of the rat Major Vault Protein (MVP) (pdb: 2ZUO, (Tanaka *et al.*, 2009). Proteins containing the SPFH domain show the propensity to form higher order oligomers. For human stomatin, the C-terminus was identified to participate in this oligomerisation which is crucial for the function of these proteins (Umlauf *et al.*, 2006).

Indeed, hetero- and homo-oligomers have been demonstrated for many SPFH domain containing proteins (Boehm *et al.*, 2009; Tanaka *et al.*, 2009; Tavernarakis *et al.*, 1999). In the case of the cyanobacterial SPFH protein (Boehm *et al.*, 2009), prohibitin (Merkwirth and Langer, 2009) and erlins (Pearce *et al.*, 2007), ring like structures have been observed by electron microscopy **(Figure 1. 3)**.

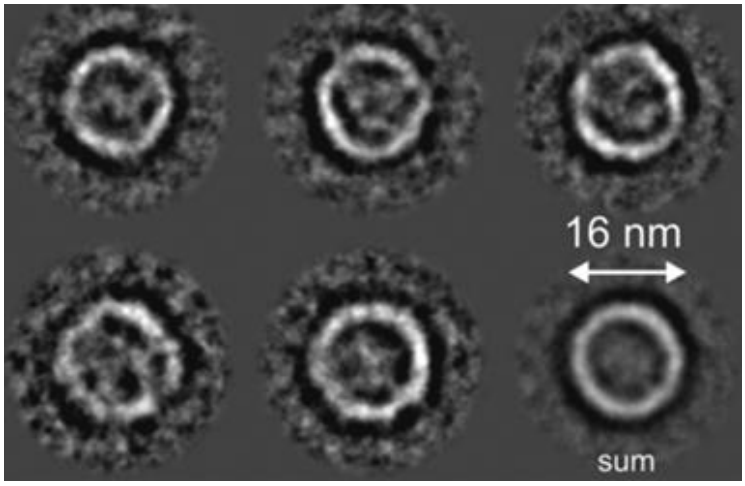

Figure 1. 3: Single-particle analysis of a cyanobacterial SPFH protein
Electron micrograph of negative stained cyanobacterial protein. The ring like protein complexes have an outer diameter of approximately 16 nm. For more detailed information, see publication from (Boehm *et al.*, 2009).

A typical SPFH-domain protein is an integral membrane protein with a single, relatively short, hydrophobic membrane insertion domain followed by the core SPFH domain. The N- and C-terminal regions of the proteins are cytoplasmic and are not conserved among the family members (Boute *et al.*, 2000; Owczarek *et al.*, 2001; Salzer *et al.*, 1993; Seidel and Prohaska, 1998). Stomatin and other members of the SPFH domain containing protein family have been found to be posttranslational modified by phosphorylation (Salzer *et al.*, 1993), palmitoylation (Snyers *et al.*, 1999) and myristolation (Neumann-Giesen *et al.*, 2004). Eukaryotic SPFH proteins localize to the plasma membrane (PM), the endosomes, Golgi network, endoplasmic reticulum (ER) and at perinuclear compartments **(Figure 1. 4)**.

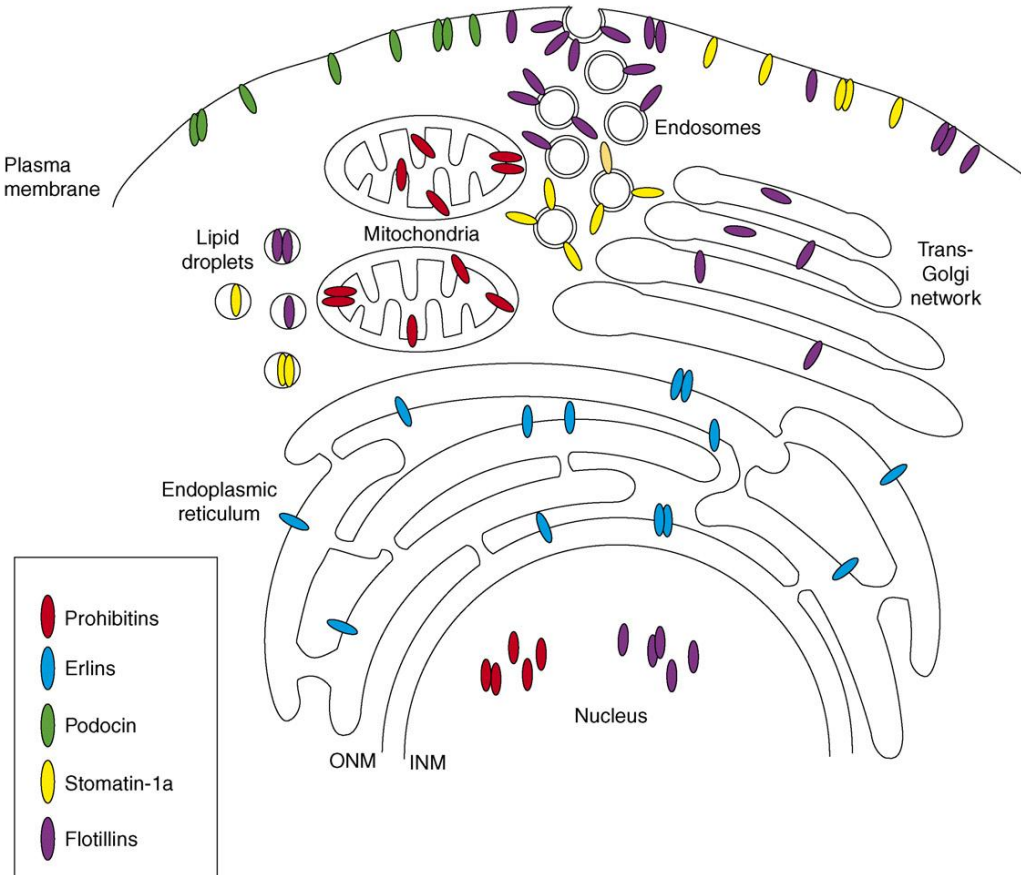

Figure 1. 4: Cellular localization of the SPFH domain proteins.
Subcellular distribution of mammalian SPFH domain containing proteins in epithelial or fibroblast cells. Prohibitins (red) are reported to localize to the inner mitochondrial membrane and in the nucleus. The erlin 1 and erlin 2 (blue) localize to the Endoplasmic Reticulum (ER), including the outer nuclear membrane (ONM). Podocin (green) is found at the plasma membrane (PM). Stomatin (yellow) localizes to the PM, endosomes and lipid droplets. Subcellular localizations of flotillin-1 and -2 (purple) include the PM, endosomes, lipid droplets, trans Golgi network (TGN) and the nucleus. Picture taken from the review (Browman *et al.*, 2007).

Reports of lipid droplet (Umlauf *et al.*, 2004) and lipid raft (Snyers *et al.*, 1999a) association have also been described. Consistent with their diverse cellular localization, SPFH domain containing proteins influence different functions in the cell ranging from mechanotransduction to modulation of channel signalling events to endocytic processes. A more detailed description of the selected members will be given in the following paragraphs.

1. 1. 1. MEC-2

The MEC-2 protein was identified in a genetic screen for touch-insensitive mutants in *C. elegans* (Huang *et al.*, 1995). Worms lacking the alleles of the *mec-2* gene are touch insensitive; beside this no morphological changes were observed (Huang *et al.*, 1995; O'Hagan *et al.*, 2005). The 481 amino acids of MEC-2 show 35% sequence identity and 48% similarity to stomatin. Like other SPFH domain containing proteins, MEC-2 is anchored to the plasma membrane via an N- terminal patch of 25 hydrophobic amino acids. Mutagenesis studies showed that alanine mutations of cysteines 140 and 174, results in misslocalization of the MEC-2 protein and impaired function (Huber *et al.*, 2006). Later it was shown that these residues at the N- terminus are palmitoylation sites (Browman *et al.*, 2007). MEC-2 features a proline rich domain which implicates involvement of MEC-2 in protein/protein interactions (Huang *et al.*, 1995). MEC-2 is able to bind to cholesterol and to localize to lipid rafts (Huber *et al.*, 2006).

Biochemical and electrophysiological studies have revealed that MEC-2 functionally interacts with a multiprotein-channel complex, containing the acid sensing ion channels (ASIC) -related degenerin Na^+ selective ion channels composed of MEC-4, MEC-10 and MEC-6, which was shown to convert mechanical stimuli into a nerve signal (Goodman *et al.*, 2002; Huang *et al.*, 1995; O'Hagan *et al.*, 2005).

Expressed alone in Xenopus oocytes, MEC-2 has no effect on membrane currents, but increases the amplitude of amiloride-sensitive channel currents approximately 40-fold when co- expressed with MEC-4 and MEC-10 (Brown *et al.*, 2008; Goodman *et al.*, 2002). Several other studies showed that different proteins such as MEC-12 and MEC-7 (α and β tubulins) and MEC-1, MEC-5 and MEC-9 (components of the extracellular matrix) are involved in the formation of mechanosensitive complexes in *C. elegans* (Chalfie, 2009) and **(Figure 1. 5)**. These complexes localized as punctuated structures along the axons of mechanosensory neurones in the worm (Zhang *et al.*, 2004). The formation and localization was shown to be cholesterol dependent and requires the core SPFH-domain of the MEC-2 protein (Cueva *et al.*, 2007; Zhang *et al.*, 2004). This suggests that MEC-2 might serve as a structural scaffold for other proteins at the membrane.

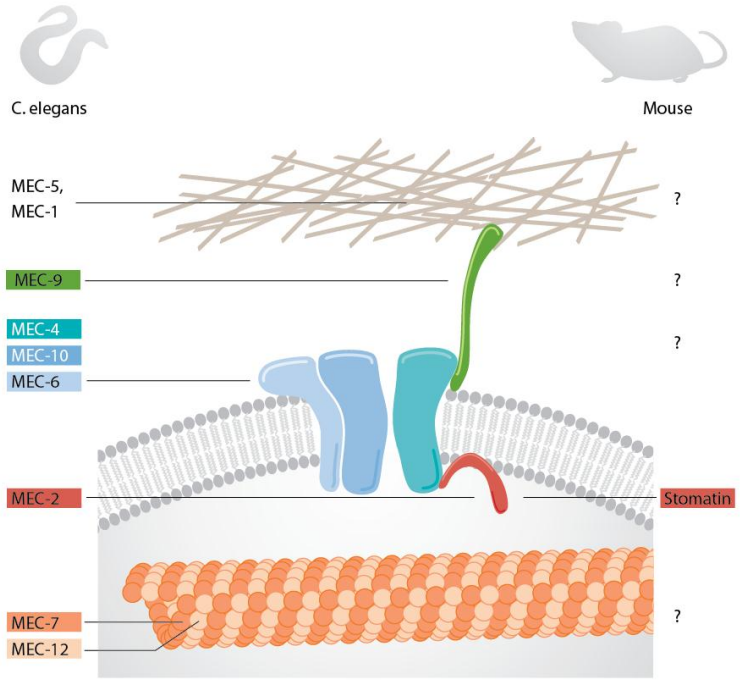

Figure 1. 5: Comparison of the touch sensation apparatus in *C. elegans* and mouse
For *C .elegans* several indispensable proteins for the mechanotransduction were identified. MEC-5 and MEC-1 are proteins of the extracellular matrix which are connected via a tether consisting of MEC-9 to the transduction channel composed of MEC-4, MEC-10 and MEC-6. MEC-2 plays a central role in the mechanotransduction process, because it directly interacts with the transduction channel and may link the tubulins MEC-7 and MEC-12 to it. In mouse SLP3 and possibly stomatin were shown to be indispensable for the mechanotransduction. Picture adopted from (Lechner and Siemens, 2011).

The essential role of MEC-2 in mechanosensory transduction raised the speculation that the mammalian SPFH-domain proteins may also have a conserved role in regulating mechanosensory processes in vertebrates. Interestingly, coexpression of mammalian stomatin with MEC-2 showed a dominant negative effect on MEC-2 function, indicating the possible formation of hetero- oligomers between MEC-2 and stomatin (Goodman *et al.*, 2002). Furthermore, a series of studies showed that mammalian SPFH- domain containing proteins such as stomatin (Lapatsina *et al.*, 2012b; Price *et al.*, 2004) and SLP-3 (Wetzel *et al.*, 2007) are also modulators of ion channels involved in mammalian mechanotransduction and pain sensation.

1. 1. 2. Stomatin

Stomatin was cloned and identified as a major protein of erythrocyte membranes (Hiebl-Dirschmied *et al.*, 1991a; Hiebl-Dirschmied *et al.*, 1991b). Subsequent studies showed that its mRNA is ubiquitously expressed (Stewart *et al.*, 1992). A quantitative reverse transcription polymerase chain reaction (qRT- PCR) study identified stomatin in different mouse tissues (Wetzel *et al.*, 2007) **(Figure 1. 6)**.

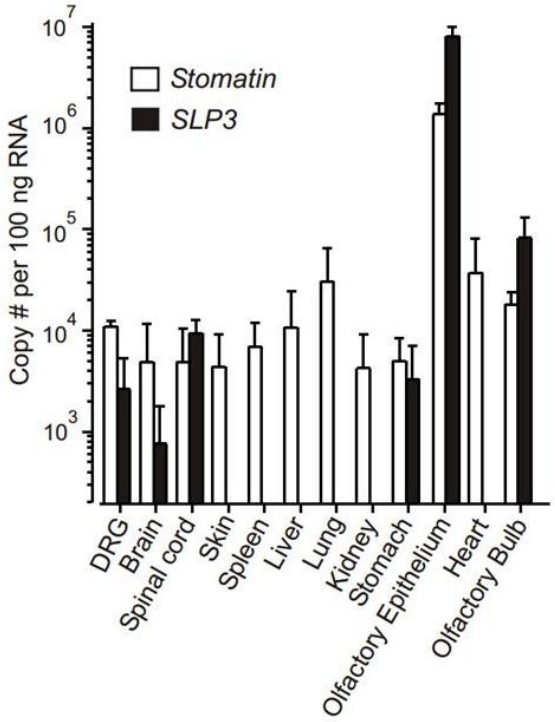

Figure 1. 6: Expression profile of stomatin and SLP-3 in different mouse tissues.
The mRNA expression profile of SLP-3 and stomatin in different mouse tissues identified by qRT-PCR. Picture taken from (Wetzel *et al.*, 2007).

The 31 kDa protein is expressed in many tissues and cell lines (Unfried *et al.*, 1995; Wetzel *et al.*, 2007). Stomatin is associated with detergent-resistant, cholesterol- and sphingolipid-rich membranes, also known as lipid rafts (Mairhofer *et al.*, 2002; Salzer and Prohaska, 2001; Snyers *et al.*, 1998; Snyers *et al.*, 1999a). Furthermore stomatin localises to the plasma membrane, the endoplasmic reticulum (ER) and to late endosomes, depending on the cell type **(Figure 1. 4)**.

Stomatin shares the topology of other members of the SPFH domain family **(Figure 1. 7)**. The N-terminal stretch of 20 amino acids allows the proteins to associate with membranes. Cysteine 29 and 86, which flank the hydrophobic region can be palmitoylated (Snyers *et al.*, 1999) which likely modifies the interaction of stomatin with membranes.

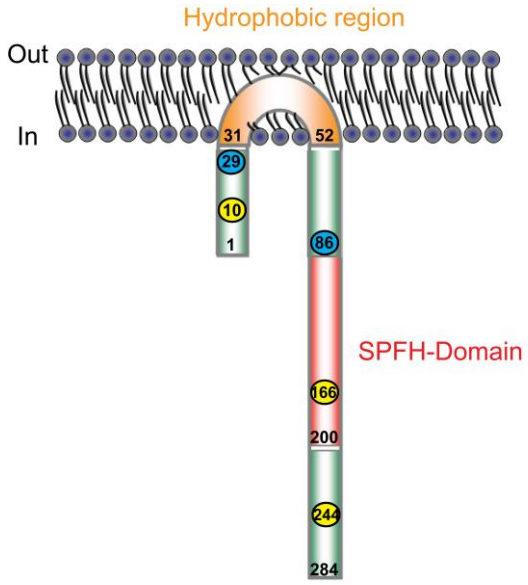

Figure 1. 7: Topology of stomatin
Protease protection experiments revealed that the N- and C-terminal portions of stomatin are oriented towards the cytosol. Serines 10, 166 and 244 can be phosphorylated (yellow circles). The cysteines 29 and 86 (blue circles) flanking the hydrophobic region (orange) are palmitoylation sites.

The very N-terminal 30 residues, the SPFH domain and the C-terminus of the protein were shown to be insensitive to protease K treatment on intact erythrocytes, suggesting that both the N- and C- termini are located in the cytoplasm (Hiebl-Dirschmied *et al.*, 1991a). The fact that the serines at positions 10, 166 and 244 can be phosphorylated supports the idea that stomatin has a lollipop or hairpin topology, similar to the topology proposed for caveolin related proteins (Salzer *et al.*, 1993).

A alternative topology, different from the hairpin structure, was recently proposed by Kadurin and colleagues; these authors reported that a proportion of stomatin proteins exists in a single pass transmembrane form with a highly glycosylated extracellular C-terminal region (Kadurin *et al.*, 2009). They also showed that a single point mutation in the hydrophobic region, P47S, converts stomatin into a transmembrane protein (Kadurin *et al.*, 2009).

Stomatin was shown to form 9- to 12mer oligomers of approximately 300 kDa in human amniotic cells (UAC) (Snyers *et al.*, 1998); in erythrocytes (Salzer and Prohaska, 2001) and platelets, the oligomers can capture 600 kDa (Mairhofer *et al.*, 2002) **(Figure 1. 8)**.

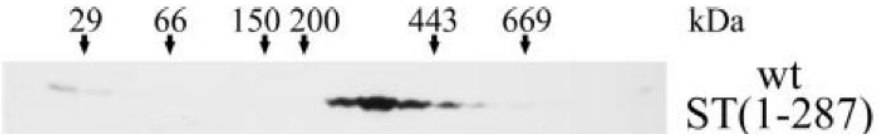

Figure 1. 8: Oligomerisation of human stomatin
Sucrose gradient centrifugation experiments revealed that human stomatin can form higher-order oligomers of 9-12 subunits in erythrocytes and UCA cells (Umlauf *et al.*, 2006).

A more detailed analysis by sucrose gradient centrifugation showed that single point mutations in the SPFH domain and the C-terminal residues can disrupt human stomatin oligomers but did not affect lipid raft localization (Umlauf *et al.*, 2006).

Stomatin is important for the Na^+ homeostasis in mature red blood cells and appears absent from erythrocytes in patients suffering from overhydrated hereditary stomatocytosis (OHSt) (Gallagher and Forget, 1995; Stewart *et al.*, 1993) where an increased permeability for Na^+ and K^+ ions leads to osmotic stress and a reduced lifespan of the erythrocytes. A detailed analysis of the stomatin gene in OHSt patients revealed no mutation in the gene or the promoter region (Fricke *et al.*, 2003). It was shown that erythrocyte precursors from OHSt patients contain the same amount of stomatin and that only the mature red blood cells lack the stomatin protein (Fricke *et al.*, 2004).

Analysis of a stomatin knockout mouse showed no apparent phenotype and the erythrocytes remained intact (Zhu *et al.*, 1999). Nevertheless, in human erythrocytes stomatin was shown to interact with and is able to modulate the activity of the glucose transporter type 1 (GLUT1) (Montel-Hagen *et al.*, 2008; Zhang *et al.*, 2001). A reciprocal relationship was observed between the levels of stomatin and GLUT1 mediated transport activity in human cells (Montel-Hagen *et al.*, 2008), however the mechanisms by which stomatin regulates the activity of GLUT1 remain undetermined, and the conclusions of this study have been questioned (Carruthers and Naftalin, 2009).

A recent study showed that stomatin co- localize and can be co- immunoprecipitated with a gap junction protein called pannexin-1 (Panx1) channel (often referred as Panx1 hemichannel) (Zhan *et al.*, 2012). Furthermore it was shown that stomatin can modulate

the activity of this hemichannel, which is involved in ATP release in erythrocytes (Locovei *et al.,* 2006) and has been implicated in the cellular response to mechanical stress (Bao *et al.,* 2004).

A long line of experimental evidence revealed that stomatin and acid sensing ion channels (ASICs) co- localize and directly interact with each other. This was shown by co-immunoprecipitation assays and co- localization studies (Lapatsina *et al.*, 2012b; Price *et al.*, 2004). Furthermore, it was shown that stomatin can modulate the activity of members of the ASICs family (Lapatsina *et al.*, 2012b; Price *et al.*, 2004), similar to the function of MEC-2 in *C.elegans* as a modulator of mechanosensory transduction (Huang *et al.*, 1995). Indeed, analyses of stomatin knock-out mice revealed a reduced mechanosensitivity of a sub-population of skin mechanoreceptors (Martinez-Salgado *et al.*, 2007). The effects of stomatin gene deletion on mechanotransduction were, however, much less pronounced than the effects found for the closely related SLP-3 protein (Wetzel *et al.*, 2007) **(Figure 1. 6)**.

In spite of these progresses, the molecular mechanisms by which stomatin exerts its functional effects have remained enigmatic. Stomatin is the founding member of the stomatin family, which in mammals includes stomatin-like proteins (SLP) 1-3 (Lapatsina *et al.,* 2012a). These related proteins, which share 40 to 84% sequence similarity in the SPFH-domain and have a similar membrane topology and domain organisation, and will be discussed in the following.

1. 1. 3. SLP-1

Stomatin-like protein-1 (SLP1), also known as STOML-1 (Lapatsina *et al.*, 2012a), STORP (Gilles *et al.*, 2000), slipin-1 (Green *et al.*, 2008) or hsUNC-24 (Smith *et al.*, 2000) is comprised of 397 amino acids. A patch of 30 hydrophobic N- terminal residues allows the protein to associate with membranes. SLP-1 is expressed in brain, heart and skeletal muscle (Seidel *et al.*, 1998) and at lower levels in other tissues (Wang and Morrow, 2000); a recent study revealed the expression of SLP-1 in sensory neurons of the dorsal root ganglion (DRG) (Gary Lewin, personal communication). The SPFH domain and a C-terminal sterol carrier (SCP-2) domain face the cytoplasm. This bipartite domain architecture is also found in the *C. elegans* protein UNC-24, which also contains

an SCP-2 domain (Barnes *et al.*, 1996), suggesting that SLP-1 might also play a role in sterol/lipid transport and transfer in the cell. In a recent analysis from Mairhofer *et al*, a targeting signal was identified which allows SLP-1 to localize to late endosomal compartments (Mairhofer *et al.*, 2009). Furthermore, a direct interaction of SLP-1 with stomatin was shown *in vitro* and *in vivo* (Mairhofer *et al.*, 2009). By blocking cholesterol trafficking from the late endosome, it was demonstrated that SLP-1 is important for cholesterol transport to the lysosyme and late endosome.

Despite its role in lipid and cholesterol transport, SLP-1 has not yet been studied in detail. A *slp-1*$^{-/-}$ mouse was recently generated and preliminary results indicate that the *slp-1*$^{-/-}$ mice shows impaired mechanosensory functions (Gary Lewin, personal communication). Further detailed experiments with these *slp-1*$^{-/-}$ mice may elucidate the precise role of this protein in general and with special regard to its role in the nervous system and in the physiological modulation of ion channels.

1. 1. 4. SLP-2

The cloning of SLP-2 revealed that it does not contain the hydrophobic N- terminal domain typical of all other members of the stomatin family (Wang *et al.*, 2000). SLP-2 and stomatin show with 17% the lowest homology in amino acid conservation in the stomatin family, which implies the greatest evolutionary difference between these two proteins (Green *et al.*, 2008).

Like stomatin, the expression profile of SLP-2 shows a broad distribution in a wide range tissues and cell lines, and it has also been detected in red blood cells and recently in T cells (Christie *et al.*, 2012). SLP-2 was described as a peripheral cytoplasmic membrane protein which can form higher-order oligomers (Kirchhof *et al.*, 2008; Wang *et al.*, 2000). In a proteomic analysis of human endothelial cells using two-dimensional gel electrophoresis and mass spectrometry, the protein was identified to be lipid raft associated (Sprenger *et al.*, 2004). More recently, several studies have shown that SLP-2 localizes to mitochondrial inner membrane (MIM) and is able to interact with mitofusin-2, a dynamin-like protein involved in the fusion of mitochondria (Da *et al.*, 2010; Hajek *et al.*, 2007; Reifschneider *et al.*, 2006; Schmitt *et al.*, 2006). In line with these localization studies, it was demonstrated that SLP-2 may be required to protect

mitochondria from stress-induced hyperfusion (Tondera *et al.*, 2009). The exact function of SLP-2 has not yet been resolved, but it was shown that SLP-2 is unregulated in different cancer types. Furthermore cancer cell lines transfected with antisense SLP-2 showed decreased growth and tumorigenecity, suggesting a correlation between SLP-2 up- regulation and the transformation of normal cells into cancer cells (Zhang *et al.*, 2006).

Several important questions remain to be clarified. Attempts to generate SLP-2 mutant mice revealed that the loss of SLP-2 function is lethal (Heppenstall, Seifert and Lewin unpublished). For a more detailed analysis of the physiological function of SLP-2, more comprehensive mouse genetics experiments will be necessary.

1. 1. 5. SLP-3

SLP-3 or STOML-3 (Wang *et al.*, 2000) was discovered in sensory neurons and probably evolved by a gene duplication of the stomatin gene in mammals (Kobayakawa *et al.*, 2002). SLP-3 and stomatin share similar domain architecture with a short cytoplasmic N-terminus, followed by a hydrophobic region and a long cytoplasmic C- terminal domain comprising the SPFH-domain. SLP-3 shares about 33% identity in its amino acid sequence with MEC-2 and 60% with stomatin.

A quantitative reverse transcription polymerase chain reaction (qRT- PCR) study in different mouse tissues revealed that, in contrast to the ubiquitously expressed stomatin, SLP-3 expression is restricted to only a few tissues and that it is found predominantly in neuronal tissues including mechanosensory neurons of the dorsal root ganglia (DRG) **(Figure 1. 6)**.

A comprehensive cell biological analysis in HEK-293, CHO and DRG cells revealed a punctuated staining pattern and association of SLP-3 with the plasma membrane as well as co- localization with stomatin (Lapatsina *et al.*, 2012b). SLP-3 was found in mobile, rab11 positive compartments, suggesting its involvement in the formation of rab11 containing vesicles (Lapatsina *et al.*, 2012b). Furthermore, it was shown in HEK-293 and CHO cells that SLP-3 can be co- immunoprecipitated with all members of the ASIC family (Lapatsina *et al.*, 2012b; Wetzel *et al.*, 2007) and that this interaction depends on its N-terminal hydrophobic patch (Lapatsina *et al.*, 2012b). Interestingly, a previously

published mutation (Kadurin *et al.*, 2009) in the mouse stomatin, P47S, affected the localization of the protein and a similar effect was observed for the corresponding mutation P40S in SLP-3 (Lapatsina *et al.*, 2012b).

By generating *stoml-3*$^{-/-}$ mice, it was demonstrated that SLP-3 is functionally orthologous to the MEC-2 protein (Wetzel *et al.*, 2007). Around 40% of the neuron in *stoml-3*$^{-/-}$ mice were insensitive to mechanical stimuli applied by a nanomotor **(Figure 1. 9)** and this phenotype could be rescued by the reintroduction of a cDNA encoding wild type SLP-3 (Wetzel *et al.*, 2007). Accordingly, *slp-3*$^{-/-}$ mice have a much reduced tactile acuity compared to wild type mice (Wetzel *et al.*, 2007).

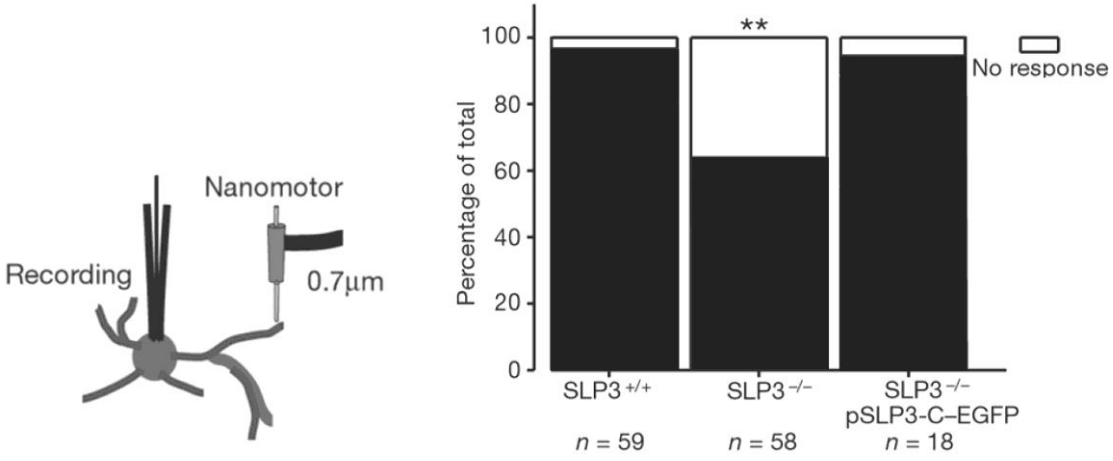

Figure 1. 9: SLP-3 is essential for mechanotransduction in the mouse
The *slp3-/-* knockout mice show a defect in mechanotransduction. A mechanical stimulus applied by a nanomotor revealed by electrophysiological recordings that 40% of the *slp3-/-* neuron did not respond to the mechanical stimulus. This phenotype was rescued by introducing an over- expressing plasmid SLP3-eGFP in the same neuron. Picture taken from (Wetzel *et al.*, 2007).

Thus, SLP-3 is not only necessary for the function of mammalian mechanotransduction complexes but it also plays a physiological role in regulating ASIC channels in sensory neurons without affecting the surface expression of ASICs (Lapatsina *et al.*, 2012b).

1. 1. 6. Podocin

Podocin (NPHS2) is a kidney-specific member of the SPFH domain containing protein family. Podocin localizes to the slit diaphragm of podocytes in the kidney (Roselli *et al.*, 2002) where it is involved in plasma filtration during primary urine formation (Boute *et al.*, 2000). Interestingly, podocin interacts with proteins involved in tight junction formation (Shono *et al.*, 2007) and colocalizes with nephrin and the actin cytoskeleton and thus act as a scaffolding protein that organizes lipid-protein domains (Saleem *et al.*, 2002).

The *NPHS2* gene was first identified as being mutated in patients suffering from hereditary nephrotic syndrome, a dysfunction of the kidney that causes the release of proteins in the blood vessel which increases the risk of clot formation and may affect the blood supply of organs (Boute *et al.*, 2000). Subsequent genetic studies showed that mutations in the podocin gene are the most common cause of hereditary nephrotic syndrome in humans (Boute *et al.*, 2000; Tsukaguchi *et al.*, 2002).

Similar to other SPFH domain containing proteins, podocin can form higher- order oligomers (Huber *et al.*, 2003). Like MEC-2, podocin can also directly bind to cholesterol in the membrane and thereby contributes to the formation of a megadalton protein-lipid complex (Huber *et al.*, 2003).

Podocin is 40% identical to MEC-2 and SLP3. Which both are involved in mechanotransduction. This led to the hypothesis that podocin may also participate in mechanotransduction events within the slit diaphragm in the kidney. Indeed, recent studies demonstrated that podocin binds directly to the transient receptor potential ion channel (TRP), TRPC-6, and also associates with cholesterol in the membrane (Huber *et al.*, 2006). Nevertheless, podocin has so far not been shown to directly modulate the gating properties of ion channels, although it is indispensable for the proper formation of the slit diaphragm (Roselli *et al.*, 2004).

1. 1. 7. Prohibitin

In mammals, there are two ubiquitously expressed genes known to encode for prohibitin1 (PHB1) and prohibitin2 (PHB2), both of which feature a conserved SPFH domain (Coates *et al.*, 1997). Prohibitin homologues have been identified in *C. elegans*, plants, yeast and in the mouse (Artal-Sanz and Tavernarakis, 2009; Browman *et al.*, 2007; Merkwirth *et al.*, 2008). PHB1 comprises 272 amino acids and PHB2 is 299 amino acids in length with a sequence identity between them of 50%. Prohibitin can associate via an N- terminal hydrophobic patch of amino acids to the inner mitochondrial membrane (IM), whereas the 30 kDa remainder of the protein localizes to the inner mitochondria space (IMS) (**Figure 1. 10**).

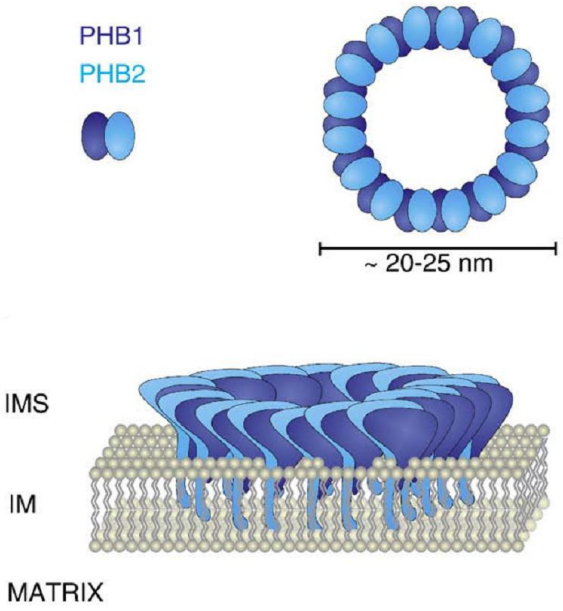

Figure 1. 10: Model of prohibitin assembly in the inner mitochondria membrane
Possible mode of the prohibitin heterodimer complexes in the mitochondria inner membrane. Picture taken form review of (Merkwirth *et al.*, 2009). (IM) = inner mitochondria membrane; (IMS) = inner mitochondria space.

PHB1 and PHB2 can form heterodimers in the IMS and, like other SPFH domain containing proteins, are able to form higher order heterooligomers of 1 MDa in mass (Nijtmans *et al.*, 2000).

From single particle electron microscopy studies of purified prohibitin, Tatsuta *et al.* **(Figure 1. 10)** confirmed complex formation by prohibitin and could show that these complexes have a ring like shape with a diameter of 20-25 nm (Tatsuta *et al.*, 2005a), suggesting a scaffold function for these proteins. Prohibitin knockout studies revealed

severe phenotypes: It was shown that prohibitin is crucial for embryonic development in *C. elegans* (Artal-Sanz *et al.*, 2003) and in mouse (Merkwirth *et al.*, 2008; Park *et al.*, 2005). Additionally, a direct interaction of prohibitin with a mitochondrial AAA-protease was demonstrated (Steglich *et al.*, 1999), indicating a role in protolytic activity. In a sequential knockdown study in yeast where either PHB1 or PHB2 were deleted, a reduced survival rate of the cells was observed (Coates *et al.*, 1997). A subsequent study confirmed this finding in *C. elegans*, as the prohibitin knockdown worms showed impaired fat metabolism and a reduced lifespan (Artal-Sanz and Tavernarakis, 2009).
These findings make prohibitins an interesting target for studying events like senescence and cell survival.

1. 1. 8. Major Vault Protein

Vaults were first discovered in 1986 at UCLA School of Medicine in search for biogenesis of lysosomal enzymes (Kedersha and Rome, 1986). The late discovery was a surprise, because the vault ribonucleoproteins are among the largest known intracellular macromolecular assemblies with a molecular mass of 13 MDa - about three times the size of a eukaryotic ribosome.
In mammals, the vault ribonucleoprotein complexes are composed of three proteins, the vault polymerase (vPAPR) (193kDa), the telomerase-associated protein-1 (TEP1) (240 kDa) and the Major Vault Protein (MVP) (104kDa), in addition to a small untranslated RNA (vRNA) of 141 bases. The MVP, which builds the outer shell of the vault, contributes more than 70 % of the mass of the complex (Scheffer *et al.*, 1995a).
The first structural information emerged from negative stain EM analysis (Kedersha *et al.*, 1986), followed by an EM reconstruction with a resolution of 31Å (Kong *et al.*, 1999), that revealed the barrel like structure of the complex. In the ensuing, years the resolution o fthe EM reconstruction was improved (Kong *et al.*, 2000) until in 2009, the precise molecular assembly became clear with the crystal structure of the native rat vault protein, solved to a resolution of 3.5 Å (PDB: 2ZUO, 2ZV4, 2ZV5) (Tanaka *et al.*, 2009) **(Figure 1. 11)**.

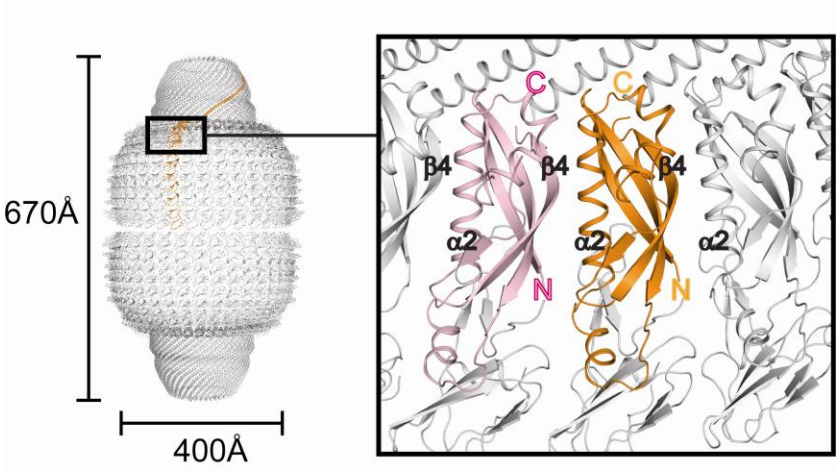

Figure 1. 11: Oligomerisation of the SPFH domain of the MVP protein.
On the left, the vault composed of 78 MVP monomers shown in grey with one subunit highlighted in orange, the dimensions of the complex at 67x40 nm are indicated. On the right, the so called shoulder domain of the MVP is shown at higher magnification, where two SPFH domains are depicted in orange and pink. The lateral contacts are established by α2 and β4. The N- and C- termini of the SPFH domain are not involved in the assembly of the higher-order oligomers. Picture modified from (Tanaka *et al.,* 2009) and newly generated with PyMOL.

The structure revealed that the vault consists of 2 half vaults, which can fuse at the 'waist' to form a barrel-like complex with overall dimensions of 67 x 40 nm Each half of the vault is built from 39 identical MVP subunits, so that a whole vault complex consists of 78 monomers. The SPFH domain at the shoulder of the vault **(Figure 1. 11)** builds lateral, hydrophobic contacts with adjacent SPFH domains.

Vaults have been detected at plasma membranes and lipid rafts (Kowalski *et al.,* 2007). A more detailed localization analyses revealed that vaults are found near the nuclear pore complex, leading to the suggestion that vaults could play a role in nuclear-cytoplasmic transport (Chugani *et al.,* 1993).

Vaults are evolutionary highly conserved and are present in a broad spectrum of tissues, suggesting an important function in cellular processes (Kedersha *et al.*, 1990). Evidence for a function of vaults in multi drug resistance (MDR) have come from *in vitro* and clinical studies (Scheffer *et al.*, 1995b). Since then, numerous studies have been carried out to study the relationship between vaults and MDR: while some studies indicated MVP as a prognostic marker of response to chemotherapy, others failed to show any of these correlations (Scheffer *et al.,* 2000). Although vaults have been reported to play a role in transport mechanisms, regulation of signaling pathways and drug resistance (Scheper *et al.,* 1992), a definitive answer regarding their function has not been assigned.

MVP knockout mice have not confirmed any of the *in vitro* observations (Mossink *et al.*, 2002).

Interestingly, a pH dependent opening and closing mechanism was described that would allow the vault to encapsulate substances or proteins. This bservation raised the interest of nanoparticle researchers hoping to exploit vaults as drug delivery systems for example, to treat lung tumors (Kar *et al.*, 2011).

1. 1. 9. Flotillins

Flotillins are the functionally best characterized members of the SPFH domain containing family. The two flotillins genes were first identified in a screen aimed to identify proteins which are important for epidermal structure (Schroeder *et al.*, 1994). Later, they have been found in the axon of goldfish retinal ganglion cells (Schulte *et al.*, 1997). It was discovered that these proteins were insoluble in TritonX-100 and float after sucrose density centrifugation, hence their protein named flotillins (Bickel *et al.*, 1997), or alternatively reggie respectively. Flotillins have been found in all mammalian cell types thus far tested (Bickel *et al.*, 1997; Volonte *et al.*, 1999) and flotillins homologous have been reported in bacteria (Lopez and Kolter, 2010), plants (Haney and Long, 2010) but surprisingly up to now not in *C. elegans* or yeast. The mouse flotillins have a mass of 47 kDa, and share 50% amino acid sequence identity. Both proteins contain two conserved hydrophobic domains, one at the N-terminus and one in the middle of the protein, which allow the proteins to associate with membranes **(Figure 1. 12)**. Anchoring of the proteins into the inner leaflet of the plasma membrane is mediated by a palmitoylation site (Morrow *et al.*, 2002) and for flotillin 2 an additional myristoylation site (Neumann-Giesen *et al.*, 2004) at the N- terminus (**Figure 1. 12)**. In a large scale proteomic analysis of putative lipid raft proteins, flotillin 1 and flottillin 2 were part of a set of 241 proteins identified (Foster *et al.*, 2003) and are now routinely used as marker proteins for lipid rafts because they are strongly enriched in these low density, cholesterol rich structures (Bickel *et al.*, 1997; Volonte *et al.*, 1999).

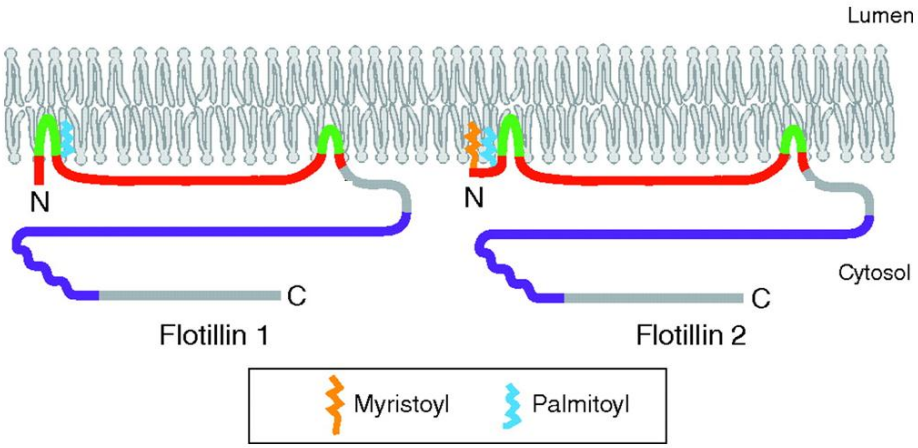

Figure 1. 12: Schematic topology of the flotillins.
Comparison of flotillin 1 and flotillin 2 showing the identified palmitoylation (cyan), myristoylation (orange) sites as well as the two hydrophobic amino acid patches (in green) which allow the protein to associate with the inner leaflet of the membrane. In red the SPFH domain and in blue the flotillin domain is shown. Picture taken and modified form the commentary of (Otto and Nichols, 2011).

It has been shown that flotillin 1 and flotillin 2 heterodimerise and that the absence of one flotillin leads to reduced stability of the other (Frick *et al.*, 2007). Furthermore, it was suggested that the heterodimer may form higher order oligomers through which they exert their physiological functions in the cell, possibly by generating scaffolds at the membrane (Frick *et al.*, 2007). In a study where flotillin 1 was knocked down, a reduced internalization of the cholera toxin B subunit was observed suggesting that flotillin 1 plays a role in endocytotic processes (Glebov *et al.*, 2006). In addition Frick et al. could show by light and electron microscopy, that flotillin containing microdomains colocalize with membrane invaginations, supporting the idea of membrane remodeling propensities for these proteins (Frick *et al.*, 2007).

The structure of the SPFH domain for the mouse flotillin-2 was solved by NMR (PDB entry 1WIN) and the overall fold is very similar to those of the SPFH domain from phstomatin, rnMVP and the mouse stomatin.

1. 2. BAR domain proteins

Bin/amphiphysin/Rvs (BAR) domain proteins do not belong to the SPFH domain protein family; nevertheless both protein families share some important features. BAR proteins can oligomerise at membranes and are able to introduce and maintain curvature on membranes (Takei *et al.*, 1999). This has been shown by lipid binding and lipid

tubulation assays and the demonstration that Drosophila amphiphysin exhibits a binding preference to negatively charged liposomes and can recognize highly curved membranes (Peter *et al.*, 2004). Besides this, Protein interacting with C kinase 1 (PICK1), carrying also a BAR domain, has been shown to interact and modulate ASICs (Baron *et al.*, 2002). The first structural information on these proteins came from the BAR domain of amphiphysin (PDB 1URU) (Peter *et al.*, 2004) and revealed that the minimal building block of Drosophila amphiphysin is a banana-shaped dimer **(Figure 1. 13)**. In the following years, numerous structures of the BAR domain family were solved (Henne *et al.*, 2007; Millard *et al.*, 2005; Shimada *et al.*, 2007) all of which showed similar dimeric species differing only in the degree of their curvature **(Figure 1. 13).** The conclusion from these studies is that the degree of curvature of the dimeric proteins determines the degree to which they can induce/recognize curvature in their target membranes; the most concave dimers, like amphiphysin, can induce the greatest degree of negative membrane curvature, the I BAR (inverse) family members can induce positive curvature and more linear shaped dimers, like in FCHo2, can maintain nearly planar stretches of membrane **(Figure 1. 13).**

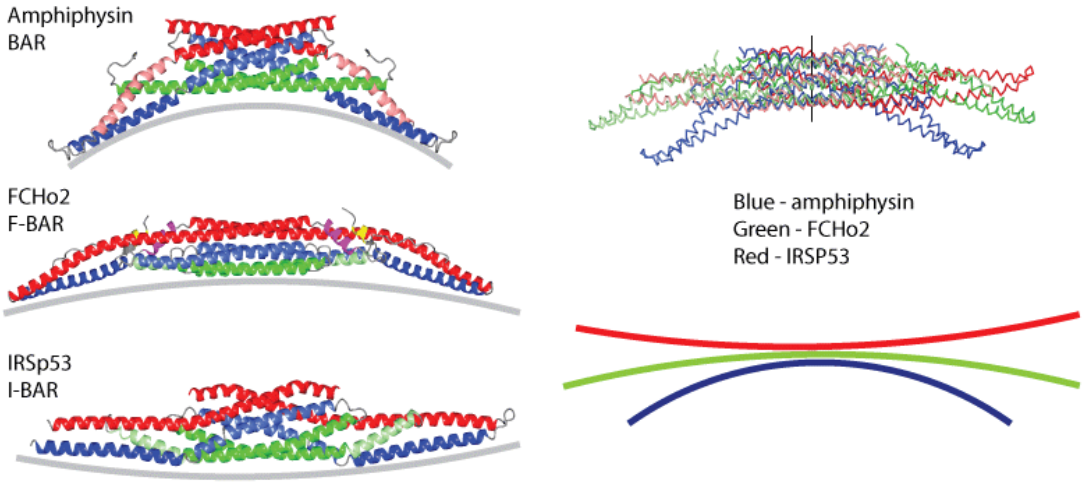

Figure 1. 13: Structural comparison of different BAR domain containing proteins.
The structure of the BAR domain containing proteins were helical protomers formed from dimers having a banana like shape with different degrees of curvature. Picture taken form the webpage www.endocytosis.org.

Due to their diverse shapes and functions, BAR domain containing proteins play a critical role in neurophysiological processes like signal transduction at the synaptic cleft (Llobet

et al., 2011). Furthermore, BAR domain proteins are important for endocytic processes: interactions of N- BAR domain proteins with dynamin and synaptojanine have been reported (Mim *et al.*, 2012).

1. 3. Acid Sensing Ion Channels (ASIC)

The Acid sensing ion channels (ASICs) belong to the epithelial sodium channel/degenerin (ENaC/DEG) family of cation selective ion channels. In 1981, the first proton gated ion channel that mediates Na^+ inward currents in mammalian sensory neurons was described (Krishtal and Pidoplichko, 1981a; Krishtal and Pidoplichko, 1981b). Since that time, ASICs consisting of 500-560 amino acids have been cloned from tunicates (Coric *et al.*, 2008), lamprey (Coric *et al.*, 2005), sharks (Coric *et al.*, 2005), bony fish (Paukert *et al.*, 2004), chicken (Coric *et al.*, 2005) and many different mammals (Price *et al.*, 1996; Waldmann *et al.*, 1995).

In mammals, the ASIC- family comprises 4 members (ASIC 1-4) for two of which isoforms exist. In rat, all ASICs share 41-50 % amino acid identity, with major deviations in their cytosolic N- and C-termini. ASICs mRNA and the corresponding proteins have been detected in an array of tissues of the central nervous system (CNS) as well as in the peripheral nervous system (PNS) (Paukert *et al.*, 2004). ASICs can sense the pH of their environment. In response to a drop of pH, the channel pore opens and allows cations, like Na^+ or Ca^+, to enter the cell. Upon pH stimulus, the ASIC family typically shows transient currents that can be blocked by a substance called amiloride (Waldmann *et al.*, 1997). A detailed analysis of the ASIC family revealed that each ASIC exerts unique current and that these electrophysiological traces can be clearly distinguished from each other (Lingueglia, 2007) and **(Figure 1. 14)**.

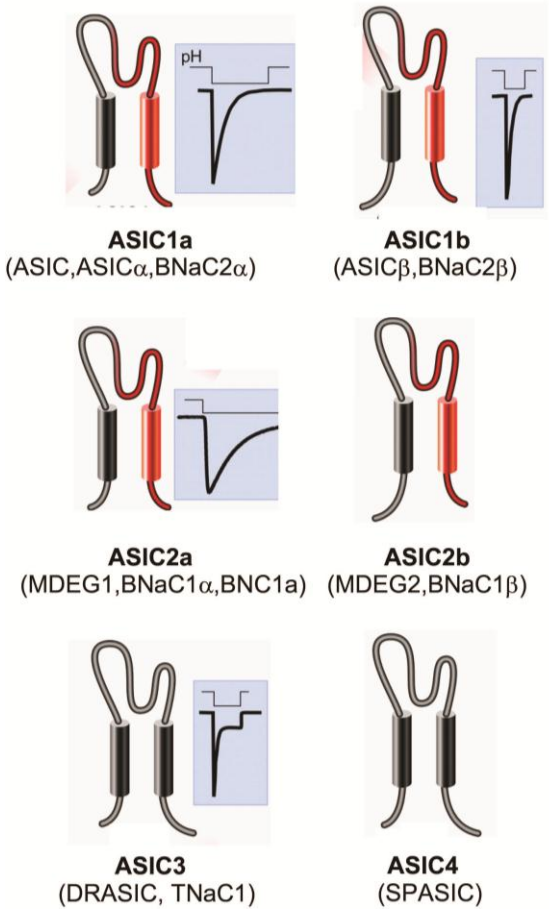

Figure 1. 14: Members of the ASIC family
Members of the ASIC family, with alternative names found in literature in parentheses. For ASIC1, two isoforms with distinguishable ion currents were identified. For ASIC2, also two isoforms were identified, but only ASIC2a showed sustained currents. Regions shared by the splice variants are shown in *red*. Picture adapted from review (Lingueglia, 2007).

ASICs have been implicated in mechanotransduction, nociception, fear-related behavior, inflammatory pain and seizure (Deval *et al.*, 2010; Wemmie *et al.*, 2002; Wemmie *et al.*, 2006). In apparent contrast, ASIC2a/ASIC3 double knockout mice show no obvious phenotype and no significant differences in mechanically gated currents in DRG neurons were detected (Drew *et al.*, 2004). This could be explained by the fact that in DRGs all four ASICs subunits are expressed and that the loss of one can be compensated by another subunit (Benson *et al.*, 2002). From this, one could also conclude that the ASICs subunits can form heterooligomers, which was later shown by (Benson *et al.*, 2002).

Before the first structure of an ASIC channel was solved, there were conflicting results regarding the minimal subunit composition necessary to form a functional channel. Most of the biophysical and cellular studies proposed a tetrameric assembly (Anantharam and

Palmer, 2007; Berdiev *et al.*, 1998; Firsov *et al.*, 1998) while other studies supported a nonameric assembly (Snyder *et al.*, 1998; Staruschenko *et al.*, 2004). Some groups predicted a homo- and heterotrimerization (Bassilana *et al.*, 1997) of ASICs which was supported by colocalization of different ASIC subunits (Alvarez *et al.*, 2002) and by co-immunoprecipitation experiments (Askwith *et al.*, 2004).

Confirmation had to wait until 2007 when the group of Eric Gouaux crystallized the chicken ASIC1a channel and solved its structure to the remarkably high resolution of 1.9Å (Jasti *et al.*, 2007). The structure of the chicken ASIC1a verified the previously proposed trimeric assembly of the channel (Jasti *et al.*, 2007). The crystallized construct contained truncations at the N- and C- termini resulting in a non-functional ASIC. Meanwhile, a trimeric assembly of ASIC1a was also shown by atomic force microscopy (Carnally *et al.*, 2008). A follow up study form the Gouaux group using a N- and C-terminally extended and thereby functional construct resulted in a crystal that diffracted to 3 Å resolution (Gonzales *et al.*, 2009). The trimeric assembly and the overall fold of the subunits with the two transmembrane (TM) helices, a large extracellular region (ECR) and the N- and C- termini facing the cytoplasm was the same in both structures **(Figure 1. 15.)**. The main difference between the two structures is the symmetric orientation of the TMs in the low resolution structure of the functional channel, allowing the formation of an ion channel pore (Gonzales *et al.*, 2009) whereas the TMs in the high resolution structure show an asymmetric arrangement (Jasti *et al.*, 2007).

The ASICs ECR consists of approximately 370 amino acids and for ASIC1a four glycosylation sites were identified (Kadurin *et al.*, 2008). The ECR includes 14 conserved cysteines which stabilize different domains by forming disulfide bonds (Firsov *et al.*, 1999), the clearly defined domains were named finger, thumb, palm, knuckle and β-ball **(Figure 1. 15).**

A gating mechanism of ASIC1a upon pH drop in the environment has been proposed based on the structural data (Gonzales *et al.*, 2009; Jasti *et al.*, 2007) a pH induced conformational changes in the rigid thumb and finger domain which are transmitted over the wrist domain, leading to rearrangement of the TM helices that open and close the ion pore. Since both ASIC1a structures were solved at pH 5,6 and 6,5, it is likely that both structures represent a desensitized conformation of the channel.

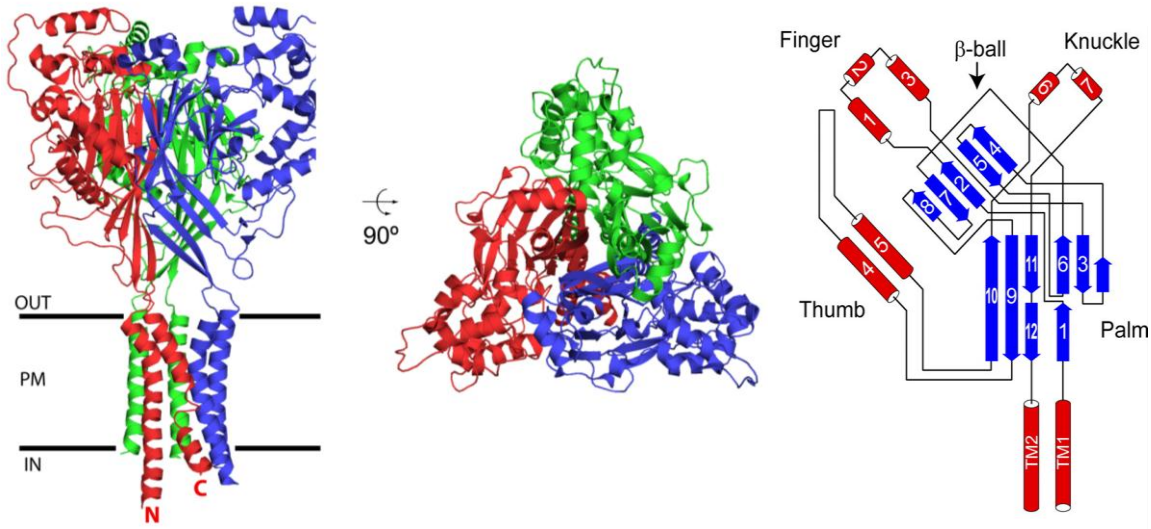

Figure 1. 15: The structure of the chicken ASIC1a.
The structure of the chicken ASIC1a shows a trimeric assembly with a central cavity having a diameter ranging between 4 and 18 nm. Both the N-and C-termini of the subunits face the cytosol. Figure prepared using PyMOL form the PDB entry 2QTS and the publication (Jasti *et al.*, 2007). Far right, the topology diagram of one ASIC1a subunit with helices in red and beta strands in blue, including the domain names, adopted form (Kashlan and Kleyman, 2011).

The molecular basis of ASIC activation and modulation is so far poorly understood. It was reports that protein that interacts with C kinase 1 (PICK1) interacts with the C-terminus of ASICs and protein kinase-C (PKC) simultaneously (Hu *et al.*, 2010). This raised the interesting possibility that (PKC) could regulate ASICs by phosphorylation events (Duggan *et al.*, 2002; Hruska-Hageman *et al.*, 2002). Indeed, a phosphorylation site at position 39 of ASIC2a was identified (Baron *et al.*, 2002).

ASIC modulation by protease cleavage was proposed (Hughey *et al.*, 2004) and functionally relevant protease cleavage sites were identified in the ECR of the channel (Passero *et al.*, 2008). Especially the finger domain, appeared to be accessible to furin and elastase proteases (Kleyman *et al.*, 2009).

Subsequently, the so called "ball and chain" mechanism by which the stomatin C-termini modulates ion channels was proposed (Stewart, 1997) but was never convincingly proven by additional experiments.

Yeast two hybrid analysis identified an interaction of ASIC3 with the multivalent PDZ (PSD-95 *Drosophila* discs-large protein 1) domain containing protein CIPP. Further experiments showed that this interaction increases the maximal ASIC3 peak current density by a factor of five and that the C-terminus of ASIC3 is required for this acceleration (Anzai *et al.*, 2002). From this data it was speculated that CIPP could be a

scaffolding protein that enhances ASIC3 surface expression and could bring together ASIC3 subunits in the membrane of sensory neurons (Deval *et al.*, 2004).

Several studies demonstrated that ASICs and stomatin are functionally linked (Lapatsina *et al.*, 2012b; Price *et al.*, 2004; Wetzel *et al.*, 2007). Colocalization and co-immunorecipitation analyses suggested that ASICs can interact with stomatin. Electrophysiological recordings further revealed that stomatin could be a functional modulator of the ASICs channels (Price *et al.*, 2004). This ASICs/stomatin interplay is of particular interest and will be described in detail in the next section.

1. 4. ASIC and stomatin

Several proteins involved in the formation of a mechanotransduction channel have been identified in *C. elegans*. It was shown by a genetic screen in *C. elegans* that, MEC-4, MEC-6 and MEC-10, are required for mechanotransduction in touch receptor neurons, suggesting the formation of a transduction channel composed of these proteins (Huang *et al.*, 1995). In mammals, the involved proteins remain mostly unknown.

Experimental results from different groups have provided evidence that stomatin and SLPs play a significant role in membrane organisation and the regulation of membrane and membrane-associated proteins, including ion channels such as ASICs (Lapatsina *et al.*, 2012b; Price *et al.*, 2004; Wetzel *et al.*, 2007). Indeed, it has been reported that stomatin can associate with ASICs and is able to modulate the acid evoked ion current. Using whole cell patch clamp electrophysiological recordings, the cation current induced by a change in pH in the extracellular fluid can be monitored. For this experimental setup, Chinese Hamster Ovarian (CHO) cells have been shown to be best suited because they completely lack ASICs (Cadiou *et al.*, 2007). In a study from Price and coworkers, ASIC3 tranfected CHO cells showed an increased current upon application of a stimulus of pH 5 (Price *et al.*, 2004)

The so called transient current results from a rapid opening of the ASIC3 pore followed immediately by a rapid closing of the same even during the remaining low pH stimulus **(Figure 1. 16 A left)**.

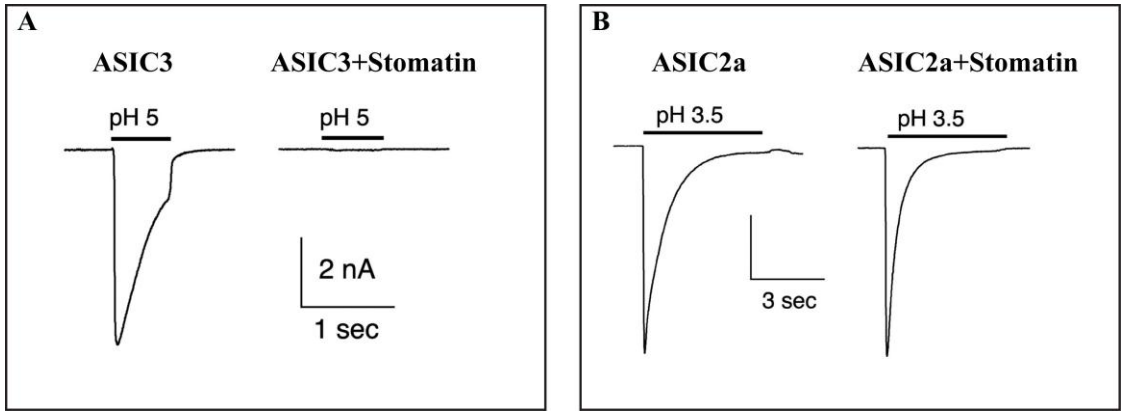

Figure 1. 16: Effect on ASIC3 and ASIC2a by stomatin.
(A) CHO cells expressing ASIC3 show transient currents after a stimulus of pH 5 in the extracellular medium. Upon co-expression of ASIC3 and stomatin this transient current is significant reduced. (B) When ASIC2a is expressed alone in CHO cells the so called sustained currents appear after a stimulus of pH 3.5; if ASIC2a and stomatin are co- expressed, the time of inactivation is significantly reduced. Picture taken from (Price *et al.*, 2004).

If the same experiment is conducted in cells co-expressing ASIC3 and stomatin, the former detected transient current is drastically reduced, suggesting negative regulation by stomatin of ASIC3 **(Figure 1. 16 A right)**. ASIC2a and ASCI3 share 46 % amino acid identity with the main differences being found in the N- and C-termini. ASIC2a is also activated by a drop in pH but the channel pores remain open for a longer time (called sustained current) period compared with ASIC3 when the pH stimulus is applied **(Figure 1. 16 A** and **B both left)**. Price *et al*. showed by co- expression of ASIC2a and stomatin that the inactivation time was reduced, suggesting that stomatin can negatively modulate the sustained currents of ASIC2a **(Figure 1. 16 B)**. Furthermore, Price *et al.* could demonstrate in COS cells that stomatin can be co-immunoprecipitated with all members of the ASIC family, suggesting a physical interaction which was underlined by fluorescence microscopy studies showing co-localization of the two proteins (Price *et al.*, 2004). The loss of pH induced ASIC currents by stomatin co- expression was observed independently of changes in membrane expression of the channels (Lapatsina *et al.*, 2012b).

1. 5. Objectives of this PhD thesis

SPFH domain containing proteins are important for many functions in the cell, like mechanotransduction, endocytosis and ion channel regulation. For stomatin, a major membrane protein of the erythrocytes, the role in the modulation of acid sensing ion channels (ASICs) was described. Despite intensive effort, the exact mechanism of how the SPFH domain containing proteins fulfill their functions remains unclear.

At the beginning of my work, no high resolution structure of a mammalian stomatin was available. The objectives of this thesis were therefore to determine the atomic structure of the SPFH domain of the mouse stomatin. Furthermore, this work aimed to biochemically characterise the mouse stomatin and to elucidate the oligomerisation state of the protein. These data should serve as basis for a detailed structure-based biochemical and functional studies to investigate its mechanism of action.

As shown previously by electrophysiological recordings, stomatin has a strong regulatory effect on the ASICs function. The electrophysiological recordings technique could be used as a read out system to determine the effects of the stomatin mutations identified in the structural and biochemical investigations.

Cellular localization studies in combination with co- immunoprecipitation analysis could help to further identify specific interactions and the localization of different stomatin mutants.

A detailed characterization of the stomatin protein could help to understand the mechanisms of other members of the SPFH domain containing protein family, e.g. flotillin or prohibitin. To understand the oligomerisation of one SPFH domain containing

protein would most probably provide a key to understanding the mode of action of the whole class of proteins. Finally, this work might help to understand the molecular mechanism of how stomatin modulates ASICs ion channels. This could help in the future to find new medical targets for the treatment of inflammatory pain.

2. Materials and Methods

2.1. Materials

2.1.1. Instruments

The instruments used in this study are listed in **(Appendix 9. 3).**

2.1.2. Chemicals

Chemicals from the following companies have been used: Roth (Karlsruhe, D), Calbiochem (Darmstadt, D), Jena Bioscience (Jena, D), GE Healthcare (Piscataway, USA), Sigma-Aldrich (Steinheim, D), Avanti (Alabaster, USA) and ROBOKLON (Berlin, D). They are listed in **(Appendix 9. 4).**

2.1.3. Enzymes

Enzymes used in this study are listed in **(Appendix 9. 3).**

2.1.4. Kits

Kits used in this study are listed in **(Appendix 9. 3).**

2.1.5 Bacteria strains

- E.coli TG1 K12, genotype supE, hsd_ *5*, thi, _(lac-proAB), F'[traD*36*, proAB+,lacq, lacZ_ M*15*] (Promega, Mannheim, D)
- E.coli BL21 (DE3) Rosetta, genotype F- ompT hsdsSB (rB- mB-) gal dcm (DE*3*)pRARE (CmR) (Novagen, Darmstadt, D) with pRARE containing the tRNA genes argU, argW, ileX, glyT, leuW, proL, metT, thrT, tyrU and thru

2.1.6 Plasmids

- pGex6P1 (AmpR, GE healthcare, Piscataway, USA)
- pSKB-LNB (KanR, O. Daumke, MDC Berlin)
- pEGFP-C3-MCS (KanR, based on pEGFP-C3, Clontech, Mountain View, USA;MCS exchanged against MCS from pGex-6P-1, O. Daumke, MDC Berlin)
- pmCherry-C (KanR, based on pEGFP-C1, Clontech, Mountain View, USA;EGFP gene exchanged against mCherry gene, AG Lewin, MDC Berlin)
- pIRES2-eGFP (KanR, Clontech, Mountain View, USA; was a gift from AG Lipp, MDC Berlin)
- pcDNA-6B His-cMyc (AmpR was a gift from AG Lewin, MDC Berlin)
- pBiFC-VN173 (AmpR was a gift from AG Lewin, MDC Berlin)
- pBiFC-CN155 (AmpR was a gift from AG Lewin, MDC Berlin)

2.1.7 Cell lines

- CHO cells (Chinese Hamster Ovarian cell line) (SCHERER et al., 1953) were a generous gift from Marion Papst, MDC Berlin

2.1.8 Media and buffers

Media used in the present work are listed in **(Appendix 9. 3)**, and their compositions are also shown in **(Appendix 9. 3)**.

2.2. Molecular biology methods

2.2.1 Polymerase chain reaction

Amplification of DNA fragments were conducted using Pfu or Pfu plus polymerase from ROBOKLON, Berlin, Germany; according to the manufacturer's protocol.

2.2.2 Restriction digest

The DNA was digested using enzymes from New England Biolabs, Frankfurt am Main, Germany, according to the protocol of the manufacturer.

2.2.3 Agarose gel electrophoresis

Agarose gels were prepared and run according to standard procedures.

2.2.4 DNA purification

DNA bands were extracted from agarose gels using the QIAquick Gel Extraction Kit, Qiagen, Hilden, Germany; according to the manufacturer's protocol. Quantification of the DNA was performed with a NanoDrop Thermo Scientific Wilmington, USA.

2.2.5 Ligation

For the ligation, 12 ng plasmid and a six fold molar excess of insert were combined with T4 DNA ligase from New England Biolabs, Frankfurt am Main, Deutschland, according to the manufacturer's protocol.

2.2.6 Preparation of chemically competent *E. coli*

Chemically competent *E. coli* cells were prepared according to (Chung et al., 1989).

2.2.7 Transformation of chemically competent *E. coli*

Plasmids were transformed using the heat shock method according to standard protocols (Schneider et al., 1977). For plasmid maintenance and amplification, the *E.coli* TG1 strain was used. For protein expression, the *E.coli* BL21 (DE3) Rosetta phage resistance strain was employed.

2.2.8 Preparation of *E. coli* cryo stocks

For long-term storage of bacteria, cryo stocks were prepared by mixing 1 mL of a overnight bacteria culture with 0.5 mL sterile 100% glycerol. Cryo stocks were stored at -80°C.

2.2.9 Site-directed mutagenesis

Site-directed mutagenesis was performed using the QuickChange kit according to the manufacturer's protocol.

2.2.10 Survey of prepared constructs

A survey of the constructs used in the present study can be found in the **(Appendix 9. 1** and **Appendix 9. 2).**

2.3 Protein expression and purification:

2.3.1 Antibiotics

Ampicillin was used at a final concentration of 100 µg/mL. Chloramphenicol was used at a final concentration of 34 µg/mL. Kanamycin was used at a final concentration of 10 µg/mL in liquid cultures and at 50 µg/mL in agar plates.

2.3.2 Protein expression and purification.

All mouse stomatin constructs were expressed as N-terminal GST or His-fusion proteins in *E. coli* BL21 DE3 phage resistant Rosetta (Novagen), including a PreScission protease cleavage site between the GST or His and stomatin portions. Bacteria were grown to an OD_{600} of 0.5 in TB medium when protein expression was induced with 80 µM IPTG, followed by overnight (ON) expression at 18 °C. Cells from 1 L of bacterial culture were resuspended in 35 mL ice-cold lysis buffer (50 mM HEPES/NaOH, pH 7.5, 500 mM NaCl, 0.1 mM Pefabloc SC (Roth), 1 µM DNase (Roth) and lysed by passing twice through a microfluidizer (Microfluidics, Newton, USA). After centrifugation at 35.000 rpm for 45 min at 4 °C, the supernatant was applied to a GSH-column which was pre-equilibrated with lysis buffer and extensively washed with 50 mM HEPES/NaOH, pH 7.5, 500 mM NaCl. In the same buffer, overnight cleavage of the GST tag was performed at 4 °C in the presence of 250 µg PreScission protease, which was directly added to the GSH beads. Five amino acids, Gly-Pro-Leu-Gly-Ser, remained as a cloning artifact at the N-terminus after proteolytic cleavage.

2.3.3 Affinity chromatography

The protein was eluted, concentrated and further purified by size exclusion chromatography on a Superdex75 26/60 column pre-equilibrated with 10 mM HEPES/NaOH, pH 7.5, 150 mM NaCl. Peak fractions of the protein were pooled and concentrated to approximately 30 mg/mL.

2.3.4 Protein concentration

Protein solutions were concentrated using Amicon centrifugal filter devices with a 50 kDa cutoff according to the manufacturer's protocol.

2.3.5 Protein concentration determination

To determine the protein concentration the absorption at 280 nm was measured using a NanoDrop.

2.3.6 Protein storage

Protein samples were pooled and concentrated to 5-50 mg/mL. Protein was either directly used or 30 µL aliquots were flash-frozen in liquid nitrogen and stored at -80°C.

2.3.7 Sodium dodecyl sulfate polyacrylamide gel electrophoresis (SDS-PAGE)

NuPAGE Novex 4-12% Bis-Tris PAGE gels were used in the Xcell Sure Lock system according to the manufacturer's protocol.

2.4 Biochemical methods

2.4.1 Isothermal Titration Calorimetry (ITC)

Experiments were carried out at 20 °C or 4°C using a VP-ITC (Microcal) in buffer containing 10 mM HEPES/NaOH pH 7.5, 150 mM NaCl, 5% EtOH. 50 µM stomatin$^{86-213}$ or the LI91,92AA mutant was used. In each step, 10 µL of a 1 mM 25-hydroxy-cholesterol (25HC) solution in the same buffer was titrated in the reaction chamber. For peptide binding experiments, 1-3 mM of an ASIC3 peptide consisting of residues 483-494 (RSGNTLLQEELN) was used in the same buffer excluding EtOH with a stomatin concentration ranging from 50-150 µM; data were analyzed using Microcal ORIGIN software.

2.4.2 Sedimentation equilibrium Analytical Ultracentrifugation (AUC)

Molecular mass studies of stomatin constructs in 10 mM HEPES/NaOH, pH 7.5, 150 mM NaCl were performed in an XL-A type analytical ultracentrifuge (Beckman) equipped with UV absorbance optics. Sedimentation equilibrium experiments were carried out

using six-channel cells with 12 mm optical path length and the capacity to handle three solvent-solution pairs of about 70 µL liquid. Sedimentation equilibrium was reached after an equilibrium speed of 24,000 rpm for about 30 h at 10 °C. The radial absorbance in each compartment was recorded at 290 nm depending on the concentration used in the experiments. Molecular mass determinations employed the global fit of the three radial distributions using the programs POLYMOLE (Behlke and Ristau, 2003) or POLYMOLA (Behlke et al., 1997). When proteins adopt monomer-dimer equilibrium, the molecular mass, M, can be treated approximately as a weight average parameter (M_w). This value is a composite of the monomer molecular mass (M_m) and that of the dimer (M_d) and the partial concentrations of monomers, c_m, and dimers, c_d.

$M_w=(c_m \times M_m + c_d \times M_d)/(c_m + c_d)$ (eq. 1)

Therefore, the equilibrium constant, K_d, can be derived with

$K_d=c_m^2/c_d$ (eq. 2).

2.4.3 Circular Dichroism (CD)

Protein samples were diluted to 0.2 g/L in a buffer containing 150 mM NaF and 10 mM Na_2HPO_4, pH7.4 in a 100 µl quart cuvette with a band width of 1 nm. The CD measurements with three replicates were performed using a Chirascan spectrometer (Applied Photophysics) in the wavelength spectrum of 190 nm to 240 nm, 1 nm step width, and 2 sec integration time. For data analysis the web DICHROWEB server with the CDSSTR algorithm was used (Whitmore and Wallace, 2004).

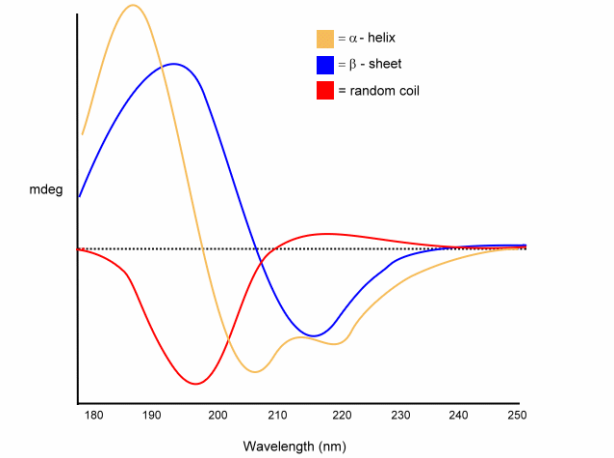

Figure 2. 1: Secondary structure measurements using CD spectroscopy
The different curves represent different secondary structure elements. In yellow a pure alpha helical protein, blue a protein consisting of beta strands and in red a random coiled protein. Picture taken from web page http://mach7.bluehill.com/proteinc/cd/cdspec.html

2.4.4 Right Angle Light Scattering (RALS)

A coupled RALS-refractive index detector (Malvern) was connected in line to an analytical gel filtration column Superdex75 10/300 (GE-Healthcare) to determine absolute molecular masses of the applied proteins. Data were analyzed with the provided OmniSec software. The running buffer contained 100 mM HEPES/NaOH, pH 7.5, 150 mM NaCl. For each protein sample, 100 µl of a 1.5 mg/mL solution were applied.

2.4.5 Lipid Binding Assays

For liposome co- sedimentation assays, wild-type or mutated Stomatin protein was sedimented in the absence or presence of liposomes. Lipids were mixed in 1.8 mL glass vials on ice with a methanol/chloroform solution (1:4.3) to a final lipid concentration of 1 mg/mL. Chloroform/methanol was evaporated using slow-flow Argon stream to produce a uniform lipid-layer on the glass surface. Residual solvent was evaporated O/N using a vacuum evacuated dessicator. The dried lipids were resuspended in filtered gel filtration buffer containing to a final lipid concentration of 1 mg/mL and incubated 5 min. at RT for hydration. Liposome formation was initiated using a bath sonicator (3 x 10 sec.). The samples were incubated at RT for 30 min. and subsequently pelleted at 100,000 x g using a Beckman TLA 100 rotor. After the centrifugation step the supernatant (SN) and

the pellet (P) fraction was mix with SDS sample buffer and used directly for SDS PAGE together with a marker.

2.4.6 Cross linking Experiments

BS^3 (bis sulfosuccinimidyl suberate) (Thermo 21580) has spacer arm of 11.4 Å and can crosslink primary amino groups (-NH_2 present in lysines or the N-terminus of the protein) to form stable amide bonds. 3 mg of BS^3 were dissolved in 250 µl protein buffer which results in a ~20 mM or 10 times cross linker solution. Purified protein was mixed with 2 mM of the cross linker BS^3 for 30 min. at RT and after the incubation time the sample was used directly for SDS PAGE together with a marker.

2.5 Crystallographic and computational methods

2.5.1 Protein crystallization

Before crystallization, protein constructs were diluted with 10 mM HEPES/NaOH, pH 7.5, 150 mM NaCl. Crystallization trials were performed using the sitting-drop vapor diffusion method in 96-well plate format. 300 nL Stomatin$^{86-213}$ at 6 mg/mL was mixed with an equal amount of reservoir solution containing 50 mM cadmium sulfate, 1 M sodium acetate and 100 mM HEPES/NaOH, pH 7.5. After 6 days, hexagonal crystals appeared. Cryo-cooling of single crystals was done by a brief transfer to a solution containing 100 mM HEPES/NaOH pH 7.5, 150 mM NaCl, 50 mM cadmium sulfate, 1 M sodium acetate and 25% glycerol. For crystal form 2, the hanging-drop vapor diffusion method was used in 24-well plates containing 0.7 mL reservoir solution at 20 °C. Crystallization drops were composed of 1 µl protein and 1 µl reservoir solution. Rhombohedral crystals were grown in 100 mM HEPES/NaOH, pH 7.5, 7 % ethanol, 5 % glycerol, 800 mM sodium acetate. For cryo-cooling, crystals were transferred to a solution containing 200 mM HEPES/NaOH, pH 7.5, 100 mM NaCl, 800 mM sodium acetate, 25% glycerol. Stomatin$^{86-213}$ (LI91,92AA) crystallized in 100 mM HEPES/NaOH, pH7.5, 5% ethanol, 20 mM cadmium sulfate. The cryo solution contained 100 mM HEPES/NaOH, pH 7.5, 150 mM NaCl, 20 mM cadmium sulfate and 25% glycerol. All crystals were cryo-cooled by plunging into liquid nitrogen.

2.5.2 Data collection

Datasets of single crystals of crystal form 2 and 3 were recorded at beamline 14.1, BESSY I, Berlin, Germany equipped with an Rayonics MX-225 CCD detector. For all datasets the crystals were rotated with increment of 1° at a temperature of -173°C.

The dataset for the single crystals in crystal form 1 were collected at the micro focus setup at the Swiss Light Source (SLS). At the Paul Scherrer Institut (PSI) Villingen in Switzerland the PX06SA beam line is equipped with a PILATUS M6 detector. Data were collected with a rotation increment of 0.25° per frame due to the long axes of the crystal lattice at a temperature of -173 °C.

Initial indexing and determination of an optimal data collection strategy was done using the program MOSFLM (Leslie, 1999).

2.5.3 Protein structure solution

Recorded intensities were integrated with the program XDS (Kabsch, 2010) or HKL-2000 (Otwinowski and Minor, 1997). Molecular replacement was carried out using the programs MOLREP (Vagin and Teplyakov, 1997) via the CCP4 graphical interface version 6.0.2 (COLLABORATIVE COMPUTATIONAL PROJECT, 1994), using the phstomatin (PDB: 3BK6) domain or the mmflotillin2 (PDB: 1WIN) structure as search models.

2.5.4 Atomic model building and refinement

Atomic models were built and fitted into electron density maps using the program Coot (Emsley and Cowtan, 2004). The structures were refined using the program Refmac5 (Murshudov et al., 1997). Standard positional refinement has been applied, preceded by TLS (Translational, libration, screw rotation displacement) refinement (Winn et al., 2003) and 5% of the measured X-ray intensities were set for the refinement for cross-validation (Brunger, 1997).

2.5.5 Protein structure validation and deposition

All atom contacts and geometry of the atomic models were evaluated using the MolProbity server (Davis *et al.*, 2004) and the SFCHECK program (Vaguine *et al.*,

1999). Validated models were deposited in the Protein Data Bank (http://www.pdb.org) under the following codes: 4FVF, 4FVG and 4FVJ.

2.5.6 Figure preparation

Figures were prepared using PyMOL (DeLano, 2002). The plug-In VASCo (Steinkellner et al., 2009) was used to illustrate the hydrophobic surfaces. The cavity was analyzed using the CASTp server (Dundas et al., 2006). The size of the interfaces was calculated with the help of the PISA server (Krissinel and Henrick, 2007).

2.6 Cell biological methods

2.6.1 Cell culture

CHO cells were cultivated in MEM supplemented with 10% fetal calf serum, 2 mM L-glutamine, 100 U/mL penicillin and 0.1 mg/mL streptomycin and were maintained in an incubator at 37°C and 5% CO_2.

2.6.2 Transfection of CHO cells

CHO cells were grown on coverslips in 6-well plates and transfected at <70% confluence using the Roti-Fect reagent according to the manufacturer's protocol. 0.5 µg DNA was applied for each transfection.

2.6.3 Microscopy

CHO cells were grown to a density of 60% in Dulbecco's Modified Eagle's Medium supplemented with 10% bovine serum albumin, 100 units/mL penicillin, 100 µg/mL streptomycin (Roth) and 4.5 mM glucose as supplement. Transfection with mouse stomatin-mCherry and rat eGFP-ASIC3 plasmids was performed using Fugene (Roche) or Rotifect (Roth). 10- 24 h post transfection, cells were fixed with 5% paraformaldehyde (PFA) at room temperature (RT), washed with PBS, water and mounted on cover slides using Mowiol (Roth). Alternately live cell imaging was performed using a Leica SP5 confocal microscope and analyzed using the ImageJ software.

2.6.4 Expression test of full length (fl) stomatin in CHO cells

Proteins from cell lysates were separated by SDS–PAGE and transferred to a nitrocellulose membrane. Blots were probed overnight at 4 °C with a monoclonal mouse antibody directed against the c-Myc tag (sc-40 9E10 Santa Cruz, California), or anti-Tubulin (T6793, Sigma-Aldrich, Munich) in 5% milk powder in TBST (50 mM TRIS, pH 7.4, 150 mM NaCl, 0.1% Tween 20), followed by incubation for 1 h at RT with a secondary horseradish peroxidase-conjugated antibody. After three times washing with TBST, the ECL kit (Amersham) was used to develop the blot.

2.6.5 Immunoprecipitation and Immunoblotting

CHO cells were co- transfected with plasmids for expression of Myc-His-tagged stomatin or the indicated stomatin mutants and plasmids for expression of Flag-tagged ASIC3. 24 h later, cells were solubilized with lysis buffer containing 1% TritonX-100, 0.1% SDS, 10 mM Tris-HCl, pH 7.6, 150 mM NaCl, 100 µM 0.1 mM Pefabloc SC (Roth). Following ultracentrifugation at 100,000 g for 20 min at 4 °C, 500 µg of detergent-soluble protein was subjected to immunoprecipitation using Myc antibody and protein A-Sepharose and then washed three times in lysis buffer. Proteins were eluted from the beads with SDS sample buffer (4% SDS, 0.4% Bromphenol blue, 40% glycerol, 200 mM Tris-HCl, pH 6.8) by incubation for 5 min at 60 °C and separated on SDS-PAGE. The proteins were transferred to nitrocellulose membranes and blocked by incubation in 5% milk powder in TBST (50 mM TRIS, pH 7.4, 150 mM NaCl, 0.1% Tween 20) for 1 h. Immunoblots were incubated with anti-polyhistidine peroxidase conjugate (1:2000) or anti-FLAG (1:1000) antibodies o/n at 4 °C. The blots were washed three times with TBST in 5% milk powder in TBST and incubated with horseradish-peroxidase-conjugate anti mouse antibody and washed three times with TBST. Bound antibodies were detected using the enhanced chemiluminescence kit (Amersham).

2.6.6 Bimolecular Fluorescence Complementation (BiFC) Assays

BiFC was used to determine the localization of interaction between ASIC3 and stomatin variants in CHO cells. A construct of ASIC3 fused at its C-terminus to a C-terminal fragment of YFP was co- expressed with a construct of stomatin fused at its C-terminus

with an N-terminal fragment of YFP according to (Hu et al., 2002). A fluorescent signal develops if the N- and C-terminal fragments of YFP come within 5 nm of each other. The BiFC signal was visualized 24 hours after transfection in living cells using epifluorescent microscopy (Olympus IX71, 100x oil-immersion objective).

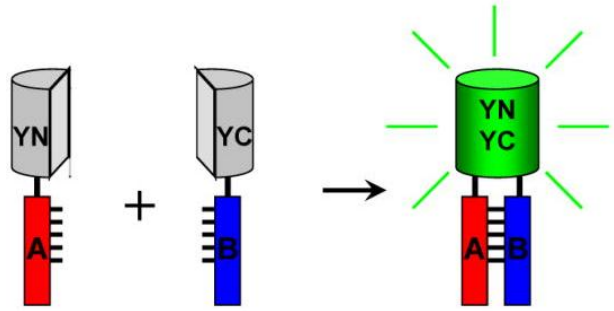

Figure 2. 2: Bimolecular Fluorescence Complementation (BiFC)
BiFC experiments are used to track protein/protein interactions *in vivo*. For this purpose each of the interaction partners, in this case ASIC3 and Stomatin were fused to one half of YFP. Approximation of both interaction partners closer that 5 nm can be monitored by fluorescence signal by microcopy. Picture taken from (Kerppola, 2006).

2.7 Electrophysiological measurements

2.7.1 Electrophysiological measurement and analysis.

(All electrophysiological measurements were performed by Dr. Ewan Smith from the AG Lewin at the MDC in Berlin).

CHO cell transfections were conducted with Lipofectamine LTX (Invitrogen) according to the manufacturer's protocol. Plasmids were diluted into Opti-MEM (Gibco) at a ratio of 4:1 (Stomatin:ASICx), with a DNA concentration of 2 µg/ 40 mm dish and Lipofectamine LTX was subsequently added. During the 30-minute incubation period, the culture medium was replaced with Opti-MEM followed by adding the transfection mixture by careful dropping. After 4 hours, the transfection medium was replaced and cells were used 24 hours later for whole-cell electrophysiology. The following solutions were used: extracellular (in mM) - NaCl (140), KCl (4), $CaCl_2$ (2), $MgCl_2$ (1), glucose (4), HEPES (10), adjusted to pH 7.4 with NaOH (for solutions below pH 6.0, MES was used in place of HEPES) and intracellular - KCl (110), NaCl (10), $MgCl_2$ (1), EGTA (1) and HEPES (10), adjusted to pH 7.3 with KOH. Patch pipettes were pulled (Flaming-

Brown puller, Sutter Instruments) from borosilicate glass capillaries (Hilgenberg) and had a resistance of 3-6 MΩ. Recordings were made using an EPC-9 amplifier (HEKA) and Patchmaster© software (HEKA). Whole-cell currents were recorded at 20 kHz, pipette and membrane capacitance were compensated using Patchmaster macros and series resistance was compensated by 70%. Cells were stimulated with a 5 second pulse of an acidic solution, pH 4 and 6 for ASIC3 transfected cells (randomly applied, 2 minute wash between stimulations) and pH 5 for ASIC2a transfected cells. Analysis was carried out using Fitmaster (HEKA) and GraphPad Prizm (GraphPad Software, Inc.), current amplitudes were normalized to cell capacitance and values expressed as pA/pF. Stomatin displays dose-related effects upon ASICs (Price *et al.*, 2004) and upon transfection of stomatin with ASIC3; we also observed proton-gated currents of varying amplitudes. Differences between peak current densities (ASIC3 experiments) and inactivation times (ASIC2a experiments) were assessed using the Kruskal-Wallis test followed by Dunn's post test.

3. Results

3.1 Screening for soluble protein

To obtain sufficient protein amount for biochemical and structural analyses, various constructs (**Appendix 9. 1**) of the mouse podocin, SLP1, SLP2, SLP3 and stomatin were cloned as His- or GST- fusions and expressed in bacteria (**Methods 2. 3. 2)**. All of the expression constructs contained the SPFH domain which comprises approximately 110 residues **(Figure 3. 1**).

Figure 3. 1: Domain architecture of the SPFH domain of the mouse stomatin.
HP - hydrophobic hairpin in red, SPFH domain in orange and CTD - C-terminal domain in green.

Most of the constructs lacked the hydrophobic hairpin at the N- terminus to avoid potential solubility problems. From a total of 38 expression constructs, 17 were insoluble or precipitated after cleavage of the affinity tag. From the remaining 21 constructs soluble protein was obtained in sufficient amounts for the SLP2 and stomatin proteins for both wild type (wt) and mutated versions.

One example for the purification of the construct comprising the SPFH domain of the mouse stomatin is shown **(Figure 3. 2** and **Methods 2. 3. 2**). A construct comprising amino acids 86-213 (stomatin$^{86\text{-}213}$) was expressed in *Escherichia coli* (*E. coli*) and purified to homogeneity. Protein bands of the predicted size were cut out from the SDS-PAGE and confirmed by mass spectrometry analysis by Dr. Gunnar Dittmar at the MDC.

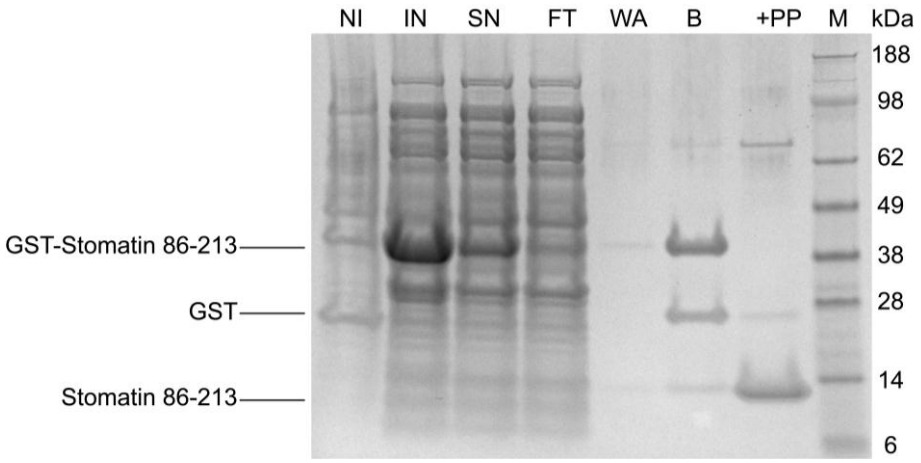

Figure 3. 2: Purification of mouse stomatin$^{86-213}$.
SDS PAGE loaded with samples from protein purification. Mouse stomatin$^{86-213}$ was expressed as N-terminal GST-fusion protein including a PreScission protease cleavage site between the GST and stomatin portions. Lane description: NI – Not induced, IN- Induced, SN- Supernatant, FT- Flow through, WA- wash step, B- beads, +PP- precision protease, M- Marker. The size of the protein bands are indicated in kDa at right.

After cleavage of the tag, a gel filtration run was performed to further purify the protein sample. The gel filtration profile showed a distinct peak, indicating a monodisperse protein sample **(Figure 3. 3A)**. The corresponding fractions of the main peak were pooled, concentrated and snap frozen in liquid nitrogen.

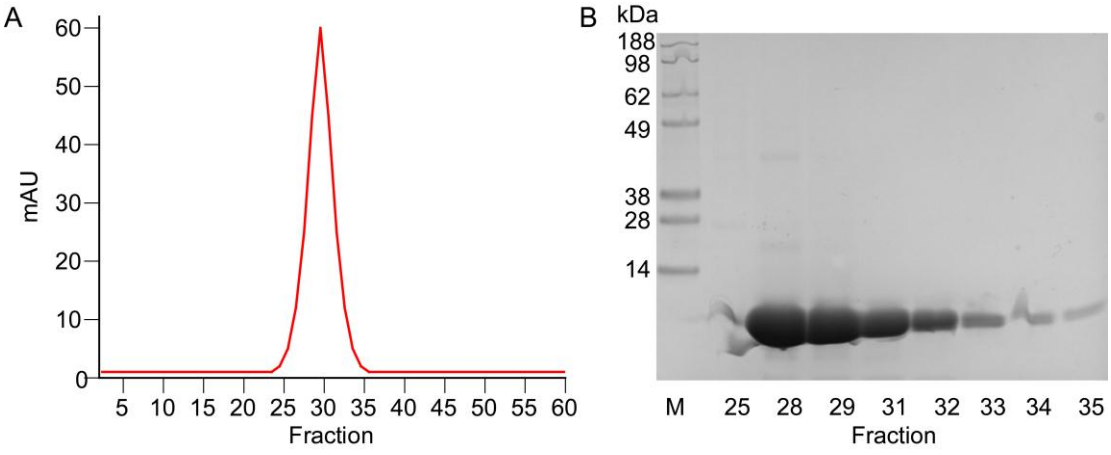

Figure 3. 3: Gel filtration of mouse stomatin.
(A) Gel filtration profile of the stomatin$^{86-213}$ construct with the sample fraction on the x-axis and the 280 nm UV absorption in red. (B) SDS-PAGE with the individual fraction from the preparative gel filtration. M- Marker and the size of the protein bands are indicated in kDa.

All protein samples used for crystallisation trials contained less than 5 % impurities **(Figure 3. 3B)**. The constructs stomatin$^{86-213}$, stomatin$^{86-255}$, SLP-2$^{67-238}$ and SLP-2$^{67-248}$ were used for crystallisation trials at 4 °C or 20 °C using the vapor diffusion method with Hampton standard screens as starting crystallisation condition.

3.2 Crystallisation and structure determination

To obtain insight into the structure of the mouse stomatin, crystallization trials of the stomatin$^{86-213}$ protein lacking the predicted N- terminal membrane anchor were set up. Crystals of the stomatin$^{86-213}$ protein appeared after 4 days and grew to their final size of 10 µm within 14 days in cadmium containing crystallization buffer at 4 °C (**Figure 3. 4**).

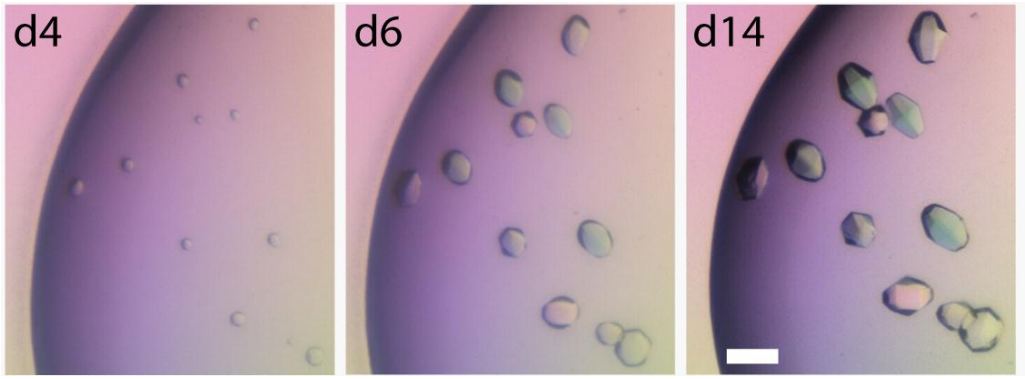

Figure 3. 4: Crystal form 1 of mouse stomatin.
The stomatin$^{86-213}$ protein was used at a concentration of 6 mg/mL and 300 nL were mixed with 300 nL of the crystallisation condition. Crystals grew after 4 days at 4 °C and were mounted after 14 days, when no further growth was seen. 25% glycerol was added as cryoprotectant. Scale bar in white corresponds to 10 µm.

The crystals belonged to the hexagonal space group $P6_522$ with cell dimensions of a=55.5 Å, b=55.5 Å, c=343.4 Å and diffracted the X-ray beam at BESSY synchrotron to 2.5 Å (**Table 1**). The phase problem was solved by molecular replacement using the structure of the *Pyrococcus horikoshii* (ph) stomatin (pdb: 3BK6). Two stomatin molecules were found in the asymmetric unit cell and the final model was refined to a R_{work}/R_{free} of 21.7% / 26.8% (**Table 1**).

Table 1: Data collection and refinement statistics

Protein	**stomatin$^{86-213}$**	**stomatin$^{86-213}$**	**stomatin$^{86-213}$ LI91,92AA**
Crystal form	**1**	**2**	**3**
Data collection			
Space group	$P6_522$	C2	$P6_422$
Molecules / asymmetric unit	2	8	1
Cell dimension			
a, *b*, *c* / Å	55.5, 55.5, 343.4	179.5, 91.4, 86.1	84.5, 84.5, 69.9
α, β , γ / °	90, 90, 120	90, 111.9, 90	90, 90, 120
Wavelength / Å	0.9184	0.9184	0.9184
Resolution / Å*	50(2.61)-2.46	50(2.74)-2.69	73(1.91)-1.8
R_{sym} / %*	7.5 (60.6)	10.8 (32.8)	3.8 (48.4)
(I/σ□I) *	22.67 (4.12)	6.8 (2.7)	38.43 (5.47)
Completeness / %*	99.3 (95.8)	91.3 (76.2)	99.7 (98.9)
Redundancy*	10.8(10.7)	3.4(2.3)	11.6(11.8)
Refinement			
Resolution / Å	50- 2.46	50-2.69	73-1.8
No. reflections	11753	30899	13259
R_{work}/R_{free} / %	21.7/26.8	24.4/29.0	19.4/24.5
No. atoms			
Protein	1811	6765	851
Ligand/ion	14	-	2
Water	77	19	96
B-factors / $Å^2$			
Protein	51	53	37
Ligand/ion	57	-	35
Water	49	34	22
R.m.s. deviations			
Bond lengths / Å	0.006	0.005	0.025
Bond angles / °	0.954	0.918	1.319

* Numbers in brackets correspond to the highest resolution shell.

In total, 13 cadmium ions were found in the electron density with an average B factor of 57$Å^2$ and occupancies ranging from 20 to 95%. The cadmium ions were present in the crystallisation condition and were coordinated by histidine, arginine and glutamate side chains.

Stomatin$^{86-213}$ crystallized also in a second crystal form in slightly different crystallisation conditions containing glycerol and ethanol as precipitants **(Methods 2. 5. 1)**. These crystals appeared after 2 days and grew to their final size of 40 µm after 8 days at 20 °C (**Figure 3. 5A** and **Table 1**).

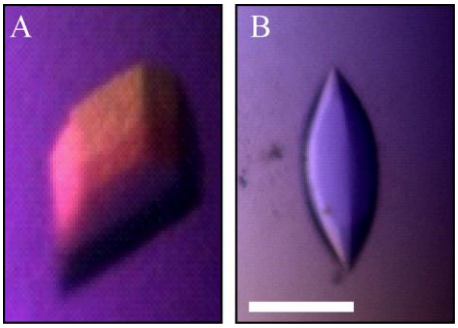

Figure 3. 5: Crystal form 2 and 3 of mouse stomatin$^{86-213}$.
(A) Crystals of stomatin$^{86-213}$ grew within 8 days at 20 °C in 100 mM HEPES/NaOH, pH 7.5, 7 % ethanol, 5 % glycerol, 800 mM sodium acetate to give rise to crystal form 2. Scale bar in white corresponds to 30 µm. (B) Crystal of the construct stomatin$^{86-213}$ with the mutation LI91, 92AA crystallized in 100 mM HEPES/NaOH, pH 7.5, 5% ethanol and 20 mM cadmium sulfate and gave rise to crystal form 3.

Crystals diffracted X-rays up to 2.7 Å and belonged to the monoclinic space group C2 with cell dimensions of a=179.5 Å, b=91.4 Å, c=86.1 Å and β=111.9°. Eight stomatin molecules were found in the asymmetric unit and the structure was solved by molecular replacement using the previously solved mouse stomatin structure as search model. The final model was refined to a R_{work} / R_{free} of 24.4% / 29.0% (**Table 1**).

Stomatin$^{86-213}$ where the residues isoleucine and leucine at position 91 and 92 were replaced by site directed mutagenesis **(Methods 2. 2. 9)** with alanines, (IL91, 92AA stomatin$^{86-213}$) crystallized in a cadmium, glycerol and ethanol containing condition (**Figure 3. 5B**). The protein crystallized in the hexagonal space group $P6_422$ with cell dimensions a=84.5 Å, b=84.5Å, c=69.9Å. The crystals diffracted X-rays to a maximal resolution of 1.7 Å and one stomatin molecule and two cadmium atoms were found in the asymmetric unit. The final model was refined to a R_{work} / R_{free} of 19.4% / 24.5%. All data collection details and refinement statistics are summarized in **(Table 1)**.

3.3 Analysis of the SPFH domain of the mouse stomatin

Analysis of the mouse stomatin$^{86-213}$ structure revealed that stomatin has a mixed α/β fold **(Figure 3. 6)**. The amino (N-) terminal β-strand 1 is subdivided into β1a and β1b by a short loop and together with β2 and β3 forms an antiparallel, curved β-sheet. Helices α2 and α4 extend in parallel and occupy the groove of the sheet, whereas the short α1 and α3 helices are oriented perpendicularly at both ends of the sheet. The N- and C- termini are located on opposite sides of the molecule.

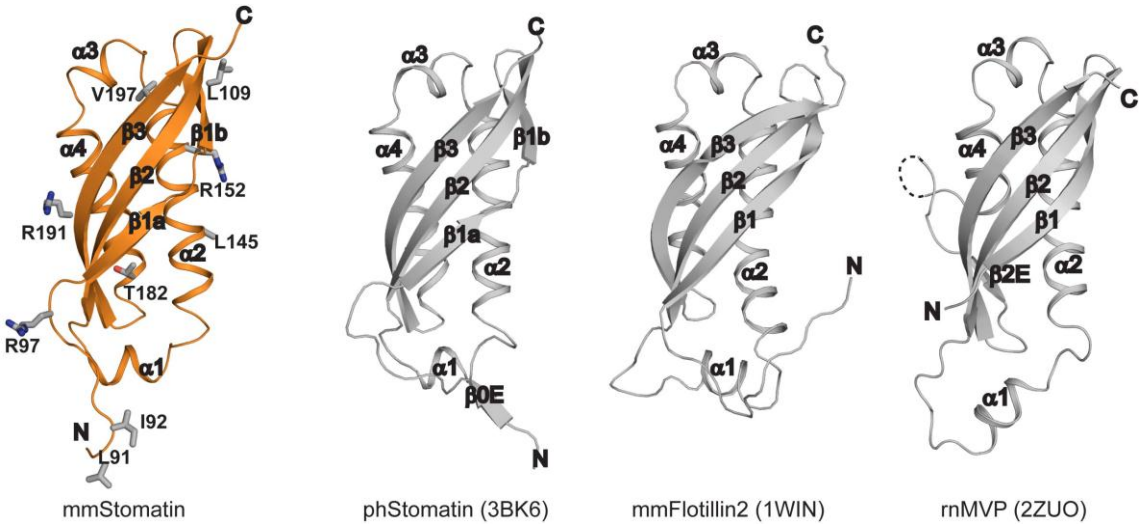

Figure 3. 6: Structural comparison of SPFH domains.
Structure of the mouse stomatin (left) with residues mutated in this work shown as gray sticks. The crystal structure of the phstomatin (pdb 3BK6), the NMR structure of mouse flotillin 2 (pdb 1WIN), and the crystal structure of the SPFH domain (amino acids 519-646) of the rat major vault protein (pdb 2ZUO) are shown for comparison. All structures contain a central antiparallel β–sheet composed of three β-strands and a similar arrangement of their α-helices. phstomatin features an additional β-strand, while flotillin 2 has an elongated loop connecting β2 and α1. The SPFH domain of the major vault protein contains an extra β-sheet β2E inserted immediately before β3 and an unresolved loop of unknown function. See also secondary structure elements in the alignment in **Figure 3. 7**.

The overall fold of mouse stomatin is very similar to those of other SPFH domain structures **(Figure 3. 6).** Mouse and phstomatin can be superimposed with a root mean square deviation (r.m.s.d.) of 1.5 Å along 107 aligned residues, with only minor deviations in α1, α2 and β1a. The phstomatin harbors an additional β-strand (β0) at the N-terminus which mediates trimerization by forming an inter-strand contact to the neighboring molecule **(Figure 1. 2)**. Also, the mouse flotillin 2 (pdb 1WIN) and the SPFH domain of the major vault protein (Tanaka *et al.*, 2009) have very similar structures (r. m. s. d. of 2 Å along 106 amino acids and of 2.6 Å along 109 aligned residues). The alignment in **(Figure 3. 7)** shows the degree of conservation among some SPFH domain containing proteins with respect to the solved structure of the mouse stomatin.

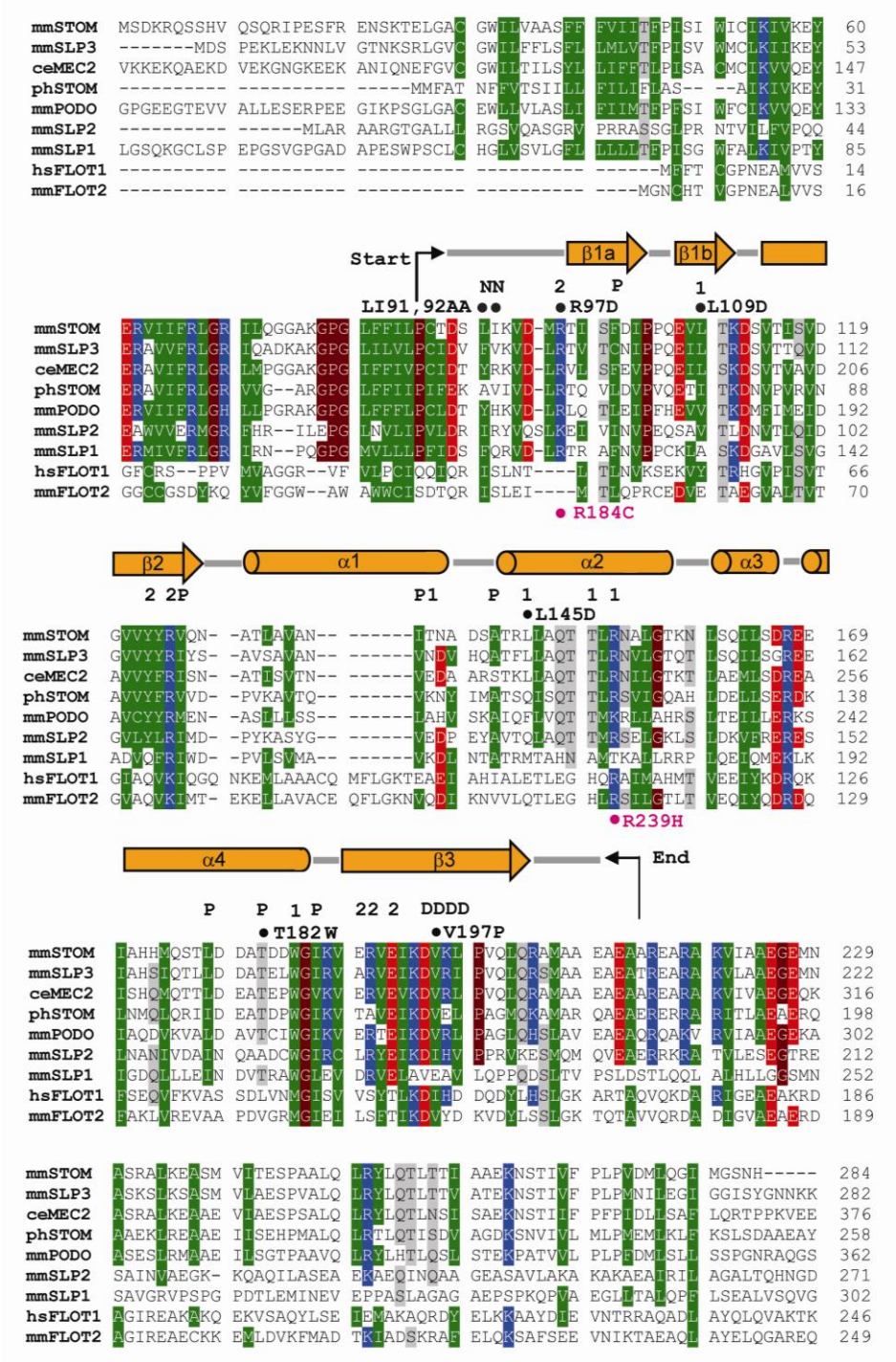

Figure 3. 7: Sequence alignment of SPFH containing proteins.

Sequences of mmstomatin (Expasy accession number P54116), mmSLP-1 (Q8CI66), mmSLP-2 (Q99JB2), mmSLP-3 (Q6PE84), mmpodocin (Q91X05), hsflotillin 1(O75955), mmflotillin 2 (Q60634), ceMEC-2 (Q27433) and phstomatin (O59180) were aligned using ClustalW (Thompson et al., 1994), and the alignment was manually adjusted. Secondary structure elements are shown on top. D - dimerization interface, 1- oligomerization interface-1, 2 -oligomerization interface-2. P - hydrophobic pocket. N – N-terminal interaction site. Selected mutations in MEC-2 causing touch insensitivity in *C. elegans* (Chalfie and Sulston, 1981; Zhang *et al.*, 2004) are indicated in pink. Residues with a conservation of greater than 70% are color -coded (D, E in red; R, K, H in blue; N, Q, S, T in grey; A, L, I, V, F, Y, W, M, C in green).

3.4 Biochemical analysis of the stomatin dimer

The analyses of all three crystal forms revealed that the mouse stomatin domain dimerized in the crystal via the C-terminal four residues of β3 (amino acids 196-199), which form a symmetric intermolecular β-sheet with the opposing molecule burying 600 $Å^2$ surface area per monomer **(Figure 3. 8)**. The interaction between the monomers features only main chain, and no side chain interactions. The resulting stomatin dimer has a banana-shape, where α2-α4 forms the outer and the β-sheet the inner surface of the banana **(Figure 3. 8)**. The N-termini are located at opposite ends of the dimerization interface.

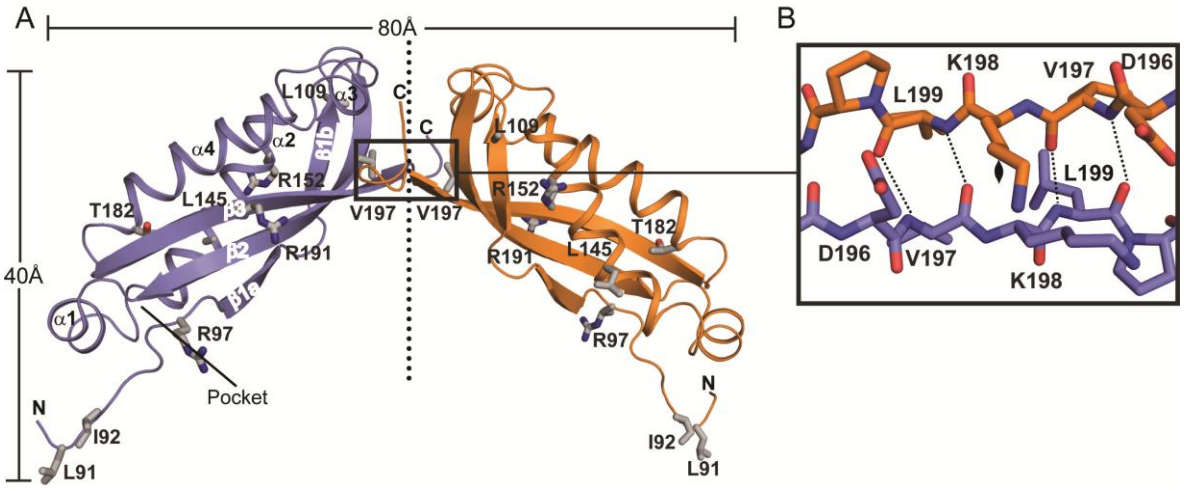

Figure 3. 8: Structural detail of the stomatin dimer.
A) Cartoon representation of the stomatin dimer, with the N- and C-termini and the size dimensions indicated. Residues mutated in this study are shown in stick representation. B) Details of the dimerization site at the C-terminus, featuring an intermolecular β-sheet.

To analyze the relevance of the stomatin dimer for assembly in solution, AUC experiments were carried out **(Figure 3. 9A** and **Methods 2. 4. 2)**. In these experiments, stomatin$^{86-213}$ was observed in a monomer-dimer equilibrium with a dissociation constant (K_D) of 37 µM. In analytical gel filtration (AG) experiments coupled to a right-angle light scattering device **(Methods 2. 4. 4)**, stomatin$^{86-213}$ also showed a monomer-dimer equilibrium **(Figure 3.9B)**. To exclude the possibility that the C-terminal truncation of the crystallized construct caused artificial dimer formation, we analyzed a C-terminally extended construct, stomatin$^{86-255}$, which corresponds in length to the crystallized trimeric phstomatin construct (Yokoyama *et al.*, 2008). The stomatin$^{86-255}$ construct also showed a

monomer-dimer equilibrium in AG **(Figure 3. 9B)**, indicating that residues 214-255 of mouse stomatin do not influence the oligomerisation status of stomatin.

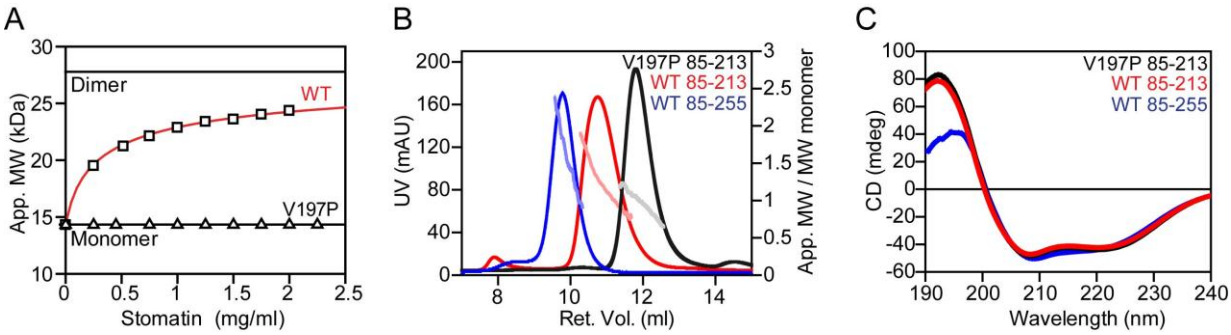

Figure 3. 9: Biochemical analysis of the stomatin dimer

A) Sedimentation equilibrium experiments to determine apparent molecular masses at different protein concentrations. Data for stomatin$^{86-213}$ were fit to a monomer-dimer equilibrium with a K_D of 37±1 µM. The V197P mutation prevented dimerization. B) Analytical gel filtration of stomatin$^{86-213}$, stomatin$^{86-255}$ and stomatin$^{86-213}$ V197P. The absolute molecular masses as determined by right angle laser scattering analysis are indicated in light colors and refer to the right y-axis. C) CD spectra of stomatin$^{86-213}$ (red) stomatin$^{86-255}$ (blue) and stomatin$^{86-213}$ V197P (black).

To test whether the dimer interface in the crystal corresponds to the observed dimer in solution, a mutagenesis approach was applied **(Methods 2. 2. 9)**.

Since the intermolecular β-sheet dimer interface employed only main chain contacts, we initially sought to disrupt the interface by electrostatic repulsion, using the V197D mutation, where the two negatively charged aspartate side chains from different monomers would directly oppose each other.

However, this mutant remained insoluble after three individual purification attempts. In contrast the V197P mutant was soluble and the resulting V197P stomatin$^{86-213}$ protein showed a very similar CD spectrum as stomatin$^{86-213}$, indicating that the mutation did not disturb the fold of the stomatin domain **(Figure 3. 9C)**. In analytical ultracentrifugation, however, the V197P mutation completely prevented dimerization **(Figure 3. 9A)**. Also in AG experiments, the V197P mutant was mostly monomeric **(Figure 3. 9B)**. Taken together, the V197P mutation did not affect the folding of stomatin$^{86-213}$ but disrupted dimerization. For all subsequent structural, AUC, CD, AG and lipid binding assays, the truncated constructs stomatin$^{86-213}$ or stomatin$^{86-255}$ were used in the wild type or mutated version. All cellular localization, electrophysiological recordings, expression and co-immunoprecipitation analyses were made with the full length stomatin in the wild type or mutated version.

3. 5 Expression of stomatin and interaction of stomatin with ASIC3.

Previous data showed that stomatin can be co-immunoprecipitated with ASICs from COS cells (Price et al., 2004). To elaborate on these findings and to see whether mutations in the stomatin protein, discussed later in the text **(Appendix 9. 1** and **9. 2)** cause any degradation in the cell and if the mutations influence the interaction with ASIC3, co-immunoprecipitation assays were performed **(Methods 2. 5. 5)**.

As control experiment for the co-immunoprecipitation assays, the expression of the mutants used in this study, was compared. For the expression tests, CHO cells were transfected with plasmids coding for either wt or mutated His-tagged stomatin; 24h post transfection the cells were lysed and subjected to western blot analysis using α- His antibodies and α- tubulin antibodies as a loading control **(Methods 2. 6. 4)**.

The result of these assays was that all mutated versions of the stomatin protein were expressed to a very similar level **(Figure 3. 10)**.

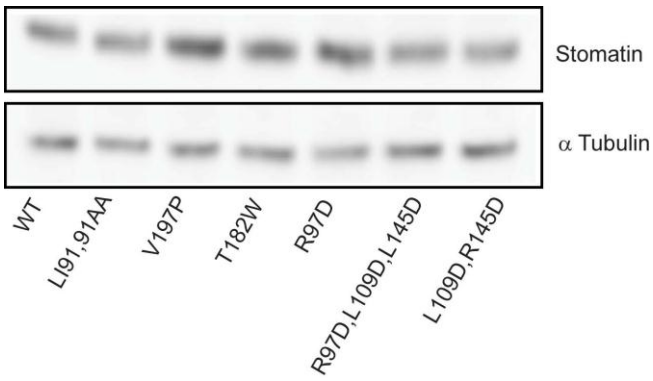

Figure 3. 10: Expression of stomatin and mutants in CHO cells.
Western blot analysis of CHO cells transfected with different stomatin plasmids showing a comparable expression level for all mutants. Antibodies used in the assay: anti-His for stomatin detection and anti-tubulin as loading control see **(Methods 2. 6. 4)**.

For the co-immunoprecipitation assays, CHO cells were transfected either with ASIC3 alone or together with the corresponding stomatin plasmids **(Methods 2. 6. 5**); 24h post transfection the cells were lysed, incubated with anti-Myc antibody and proteinA sepharose beads. After extensive washing, the samples were analyzed by western blot using anti-Flag or anti-His antibodies. In the cells transfected with ASIC3 alone, the protein was expressed and could be detected in the input fraction **(Lane 1, Figure 3. 11)**

after incubation with anti-Flag antibodies. To exclude non-specific binding of proteins to the proteinA sepharose beads, CHO cells alone were used for the same experiments; in this negative control, no protein was detected in the western blot **(Lane 2, Figure 3. 11)**. Upon cotransfection of CHO cells with ASIC3 and the corresponding stomatin plasmid in with wt or mutated version, similar levels of expression for stomatin and ASIC were seen in the input fraction **(Lanes 3-6, Figure 3. 11)**. In the co-immunoprecipitaion experiments, all mutated stomatin proteins were able to pull down ASIC3 as effectively as the wt stomatin protein **(Lanes 3-6, Figure 3. 11).**

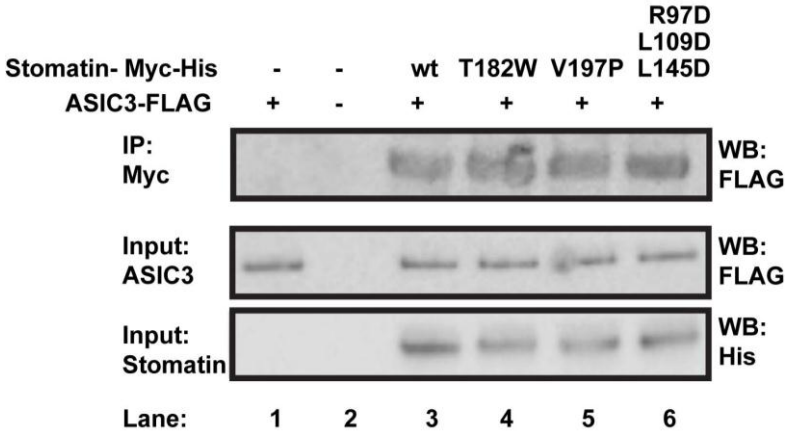

Figure 3. 11: CoIP of stomatin and ASIC3 expressed in CHO cells.
CHO cells were co- transfected with Myc-His-tagged stomatin and Flag-tagged ASIC3 plasmids. 24 h later, cells were lysed and the soluble protein was subjected to immunoprecipitation using an anti-Myc antibody and protein A-Sepharose. After three washing steps, the proteins were eluted from the beads with SDS sample buffer and analyzed via western blot (WB) **(Methods 2. 6. 5)** with an anti-His-peroxidase conjugate or an anti-FLAG antibody. All stomatin mutants were able to immunoprecipitate ASIC3 with the same efficiency as the wt stomatin.

In agreement with the previous findings (Price et al., 2004), Myc-tagged stomatin was able to co- immunoprecipitate ASIC3 upon co- expression in CHO cells **(Figure 3. 11)**. The expression levels in CHO cells of all mutants were comparable to that of the wt stomatin protein.

These findings indicate that none of the functional mutations exert their effect due to reduced expression or degradation of the protein in CHO cells **(Figure 3. 11)**. The mutated versions of the stomatin protein could also immunoprecipitate ASIC3 with no significant difference compared with the wt stomatin protein, meaning that all of the mutations in the stomatin protein which showed the most significant effect in the electrophysiological recordings do not influence the binding to ASIC3.

3. 6 Localization studies of the stomatin dimerization mutants in CHO cells.

Previous studies reported a membrane localization of stomatin in COS cells (Mairhofer *et al.*, 2009; Price *et al.*, 2004) and a co-localization of the mouse stomatin and ASIC3 in different cell types (Price *et al.*, 2004).

In order to identify the localization of the stomatin and to see whether the V197P mutant in the full length protein results in different localization, CHO cells were co- transfected with stomatin-mCherry and ASIC3-EGFP plasmids **(Methods 2. 6. 2)**, 24h post transfection the cells were fixed and analyzed via confocal microscopy **(Methods 2. 6. 3)**. The stomatin protein localizes to membranes of the ER, perinuclear compartments and plasma membrane staining was evident. Furthermore, the over- expressed stomatin protein co- localized with ASIC3 **(Figure 3. 12A)**. Also the V197P stomatin protein mutant co- localizated with ASIC3 and the confocal micrographs **(Figure 3. 12A)** revealed that the impaired dimerization of the V197P mutant does not affect the cellular localization of the protein.

To confirm the results of the co- localization experiments of stomatin and ASIC3 with an alternative technique, the Bimolecular Fluorescence Complementation (BiFC) method was used (**Methods 2. 6. 6**). With BiFC it is possible to visualize the interaction of two interaction partners *in vivo* (Hu *et al.*, 2002; Kerppola, 2006). The protein/protein interactions can be monitored by the development of a fluorescent complex comprising the N- and C-terminal fragments of YFP (each fused to the C-terminal end of stomatin or a stomatin variant and ASIC3). The stomatin V197P mutant showed a similar cellular distribution in the BiFC localization- assays and co- localized with ASIC3 at intracellular structures and at the plasma membrane like the wt stomatin **(Figure 3. 12B)**.

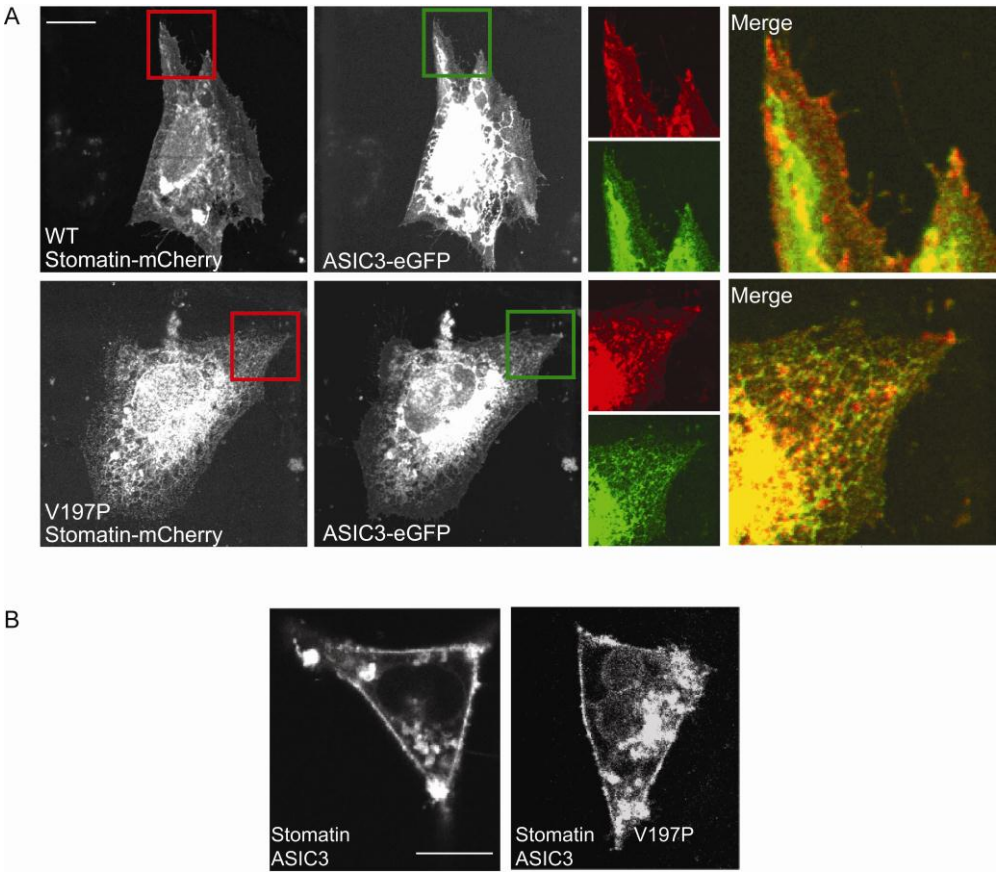

Figure 3. 12: Localization of stomatin dimerization mutants in CHO cells.
(A) CHO cells were grown to a density of 60% before co- transfection with mouse stomatin-mCherry or the indicated stomatin mutants and wt eGFP-ASIC3. 24 h post transfection, cells were fixed and analyzed by confocal microscopy and pictures were processed using the ImageJ software. Representative cells are shown. Sections marked by red or green boxes are magnified and merged on the right. Scale bar 20 µm.
(B) CHO cells were co- transfected with plasmids encoding ASIC3 fused to a C-terminal fragment of YFP and stomatin fused to an N-terminal fragment of YFP. 24 h post transfection, cells were subjected to live cell imaging using epifluorescence microscopy (**Methods 2. 6. 6**). The white scale bar corresponds to 20 µm.

These findings indicate that the wt, and the V197P mutant stomatin protein can reach the plasma membrane and co-localize with ASIC3.

3. 7 Functional analysis of the stomatin dimer

To determine the function of the stomatin dimer in the modulation process of ASICs, electrophysiological recordings were performed in Chinese Hamster Ovary (CHO) cells **(Methods 2. 7)**. ASIC3 over- expressed in CHO cells elucidated current immediately after the application of a low pH solution. These currents rapidly diminished and were

followed by a smaller, sustained current throughout the period of low pH stimulation **(Figure 3. 13 A)**.

In agreement with previous data (Price *et al.*, 2004), stomatin co- expressed with ASIC3 led to the inhibition of the ASIC3 peak current amplitude **(Figure 3. 13B)**. CHO cells co-transfected with ASIC3 and stomatin showed significantly smaller currents at both pH 6.0 and pH 4.0 compared to ASIC3 alone **(Figure 3. 13C, D).** In contrast, the stomatin V197P mutant showed no inhibitory action on ASIC3 proton-gated currents.

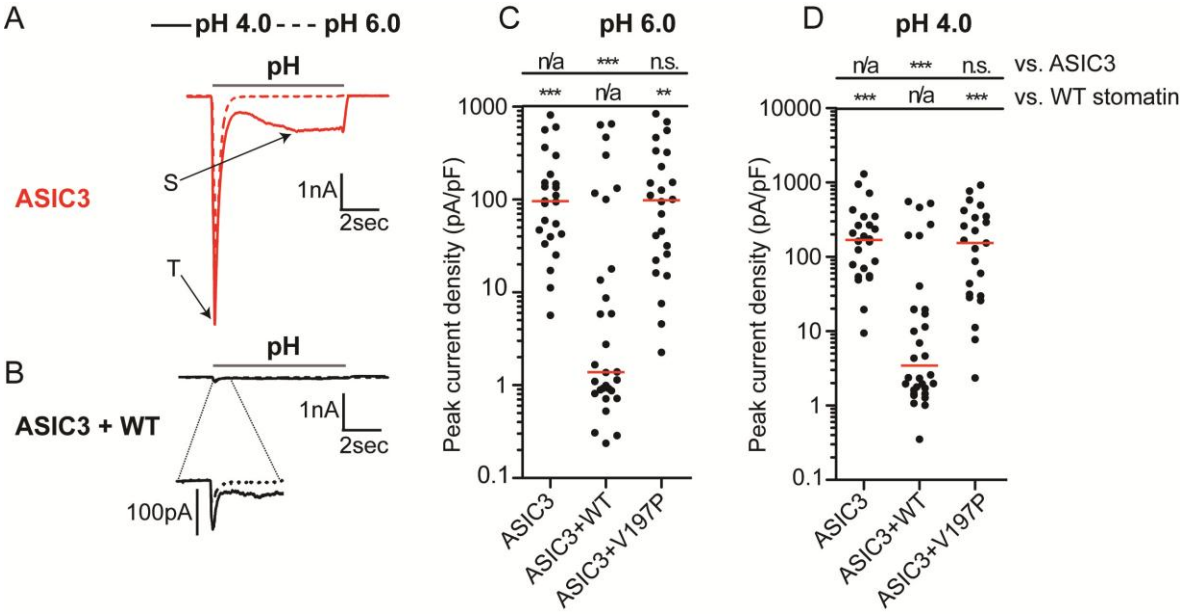

Figure 3. 13: Stomatin dimerization is crucial for the inhibition of ASIC3 current amplitudes.

ASIC3-mediated currents in CHO cells **(A)** have both transient (T) and sustained (S) phases; the S phase is larger at pH 4 (solid line) than at pH 6 (dotted line). Co- transfection with stomatin results in inhibition of proton-gated currents **(B)**. In dot plots of peak current density, each dot represents one cell and the red lines show the median for each data set. The Kruskal-Wallis test followed by Dunn's post test and statistical comparisons of peak current density of ASIC3 expressed alone and ASIC3 co expressed with stomatin are shown **(C and D)**. All electrophysiological recordings were conducted by Dr. Ewan Smith form the AG Lewin at the MDC.

These results indicate that dimerization of stomatin does not affect the correct intracellular targeting but is necessary for ASIC current modulation.

Stomatin is also known to accelerate the inactivation of ASIC2a proton-gated currents (Price et al., 2004). Unlike current amplitude, which is correlated with ion channel plasma membrane expression levels, the inactivation time of ASIC2a-mediated currents is a mechanistic feature of ion channel gating. Therefore, faster ASIC2a inactivation

times in the presence of stomatin are likely representative of a direct interaction between ASIC2a and stomatin or a stomatin-dependent modulation of the local membrane environment. In agreement with previous data, co expression of stomatin accelerated the inactivation time of ASIC2a currents. In contrast the stomatin V197P mutant had no significant effect on the inactivation time of ASIC2a proton-gated currents **(Figure 3. 14)**.

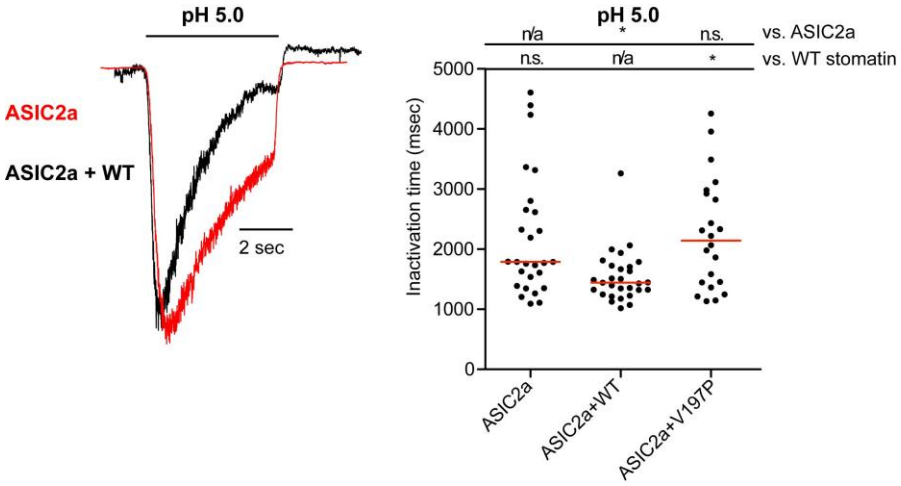

Figure 3. 14: Stomatin dimerization is crucial for the modulation of ASIC2a currents.
ASIC2a-mediated currents in CHO cells, normalized for current amplitude, showing that co- transfection of stomatin (black) decreases the inactivation time of pH 5 activated ASIC2a transient currents (red). In dot plots of inactivation time, each dot represents one cell and the red lines show the median for each data set. The Kruskal-Wallis test followed by Dunn's post test and statistical comparisons of inactivation time of ASIC2a expressed alone and ASIC2a co- expressed with stomatin are shown. n/a, not applicable, n.s., not significant, *, $p < 0.05$.

Taken together, the electrophysiological experiments indicate that the functional minimal building block of eukaryotic stomatin involved in the modulation of ASIC2a and ASIC3 currents is a banana-shaped stomatin dimer.

3. 8 Lipid binding assays

It has been reported that SPFH domain containing proteins can associate with cholesterol-rich membranes (Huber et al., 2006) and localize to lipid microdomains such as lipid rafts (Umlauf *et al.*, 2006).

In order to test the propensity of stomatin$^{86\text{-}213}$ to bind to lipids and cholesterol, spin assays were carried out according to (Gao *et al.*, 2010). For the spin assays, 15 µM

stomatin$^{86-213}$ protein was incubated with liposomes composed of four different lipid mixtures **(Figure 3. 15)**. After a centrifugation step at 60,000 rpm for 10 min, which is known to sediment the liposomes, supernatant and pellet fractions were separately analyzed via SDS PAGE **(Mehtods 2. 4. 5)**.

In these experiments, the majority of the protein was found in the supernatant, indicating that the protein did not bind to the sedimented liposomes **(Figure 3. 15)**.

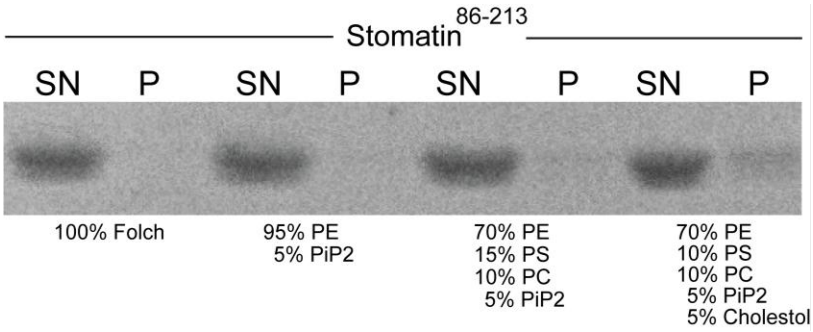

Figure 3. 15: Spin assay experiments
For the lipid binding experiments, 15 µM of the stomatin$^{86-213}$ protein was mixed 1:1 with the indicated lipid mixtures. After centrifugation of the sample at 60,000 rpm for 10 minutes, the supernatant and the pellet were separately mixed with SDS sample buffer and analyzed using SDS PAGE **(Methods 2. 4. 5)** SN- Supernatant, P- Pellet. PC (Phosphatidylcholine), PE (Phosphatidylethanolamine), PS (Phosphatidylserine), PiP2 (L-a-phosphatidylinositol-4,5-bisphosphate).

A small portion of the protein incubated with a lipid mixture containing 5% cholesterol did appear to co- sediment with liposomes, as indicated be the slight band in the pellet fraction **(Figure 3. 15),** suggesting a weak affinity of stomatin$^{86-213}$ for cholesterol containing liposomes.

To follow up on the results of the lipid binding assays and in agreement with the reported binding of MEC-2 and podocin to cholesterol (Huber et al., 2006), ITC experiments were performed **(Methods 2. 4. 1)**. In order to increase the solubility of cholesterol in aqueous buffers, the cholesterol analogue 25-hydroxy-cholesterol (25HC) was used; however ITC experiments gave no clear results for an interaction of 25HC with stomatin$^{86-213}$ **(Figure 3. 16)**.

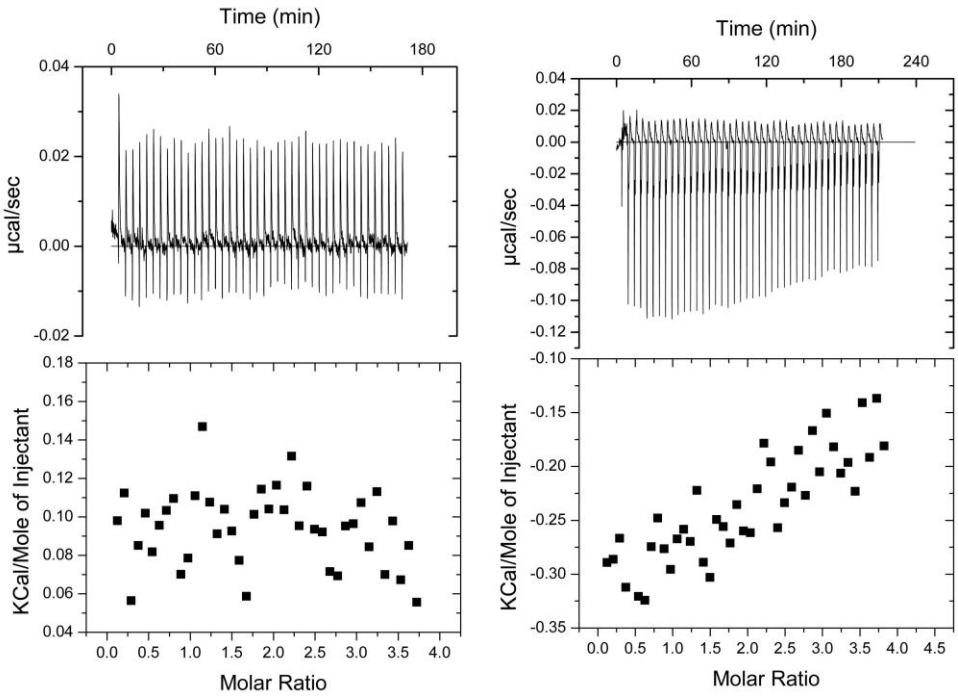

Figure 3. 16: ITC binding experiments of stomatin with 25-hydroxycholesterol
Isothermal Titration Calorimetry (ITC) experiments were carried out at 20 °C using a VP-ITC in buffer containing 10 mM HEPES/NaOH pH 7.5, 150 mM NaCl, 5% EtOH and 50 (left) or 150 µM (right) stomatin$^{86\text{-}213}$. In each step, 10 µl of a 1 mM (left) or 3 mM (right) 25HC solution in the same buffer was titrated into the reaction chamber; data were analyzed using Microcal ORIGIN software.

It was concluded that stomatin$^{86\text{-}213}$ did not bind with high affinity to 25HC. This might be due to the lack of the posttranslational modifications like palmitoylation and the missing hydrophobic hairpin at the N- terminus **(Figure 1. 5).**

In summary, neither the spin assay nor ITC experiments demonstrated convincing binding of the tested lipids to stomatin, suggesting that other domains than the SPFH domain contributed to the lipid association of SPFH domain containing proteins.

3. 9 Biochemical and structural analysis of a hydrophobic pocket

Analysis of the molecule packing in the first crystal form showed that interaction of the monomers resulted in a linear oligomeric structure, which was further intertwined with an opposing oligomer resulting in a double helical architecture **(Figure 3. 17A)**. In the second crystal form, a similar double helical structure containing was observed **(Figure 3. 17B)**.

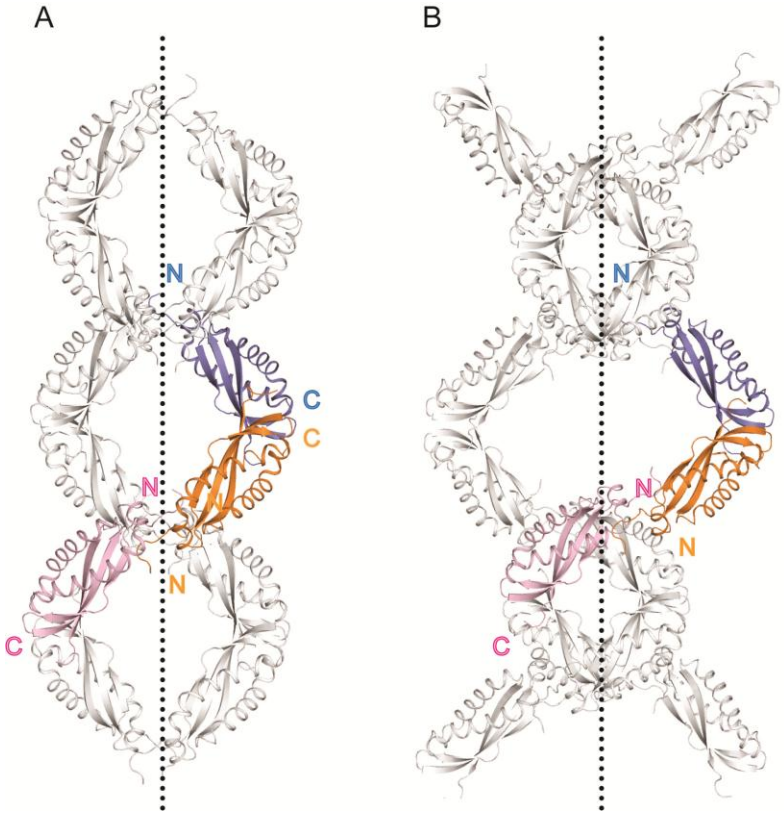

Figure 3. 17: Oligomerisation of mouse stomatin.
In crystal forms 1 and crystal forms 2 a stomatin dimer (molecules in blue and orange) with a C-terminal dimerization interface was observed. In crystal form 1 (A) and crystal form 2 (B), the dimers display an intertwined helical crystal packing, formed by additional contacts of the N-terminal loop preceding the SPFH domain of the mouse stomatin (including L91 and I92) with the hydrophobic pocket of the adjacent dimer. In (A), the dimers form a uniform helix, whereas in (B), a irregular helix is formed. The dotted line indicates the helix axis.

Analysis of the crystal form 1 and 2 revealed that residues L91 and I92 located in the N-terminal loop preceding the SPFH domain of the mouse stomatin protrude into a hydrophobic pocket on the concave face of an opposing stomatin dimer **(Figure 3. 18A)**. The volume of the open hydrophobic pocket was calculated to be 350 $Å^3$ **(Methods 2. 5. 6) (Figure 3. 18A).** Surface exposed hydrophobic residues are indicated in green, polar

residues in yellow **(Figure 3. 18A, B)** and the inner surface of the hydrophobic pocket is formed by the partially conserved residues F101, Y124, V126, I136 and T182 **(Figure 3. 18C)**.

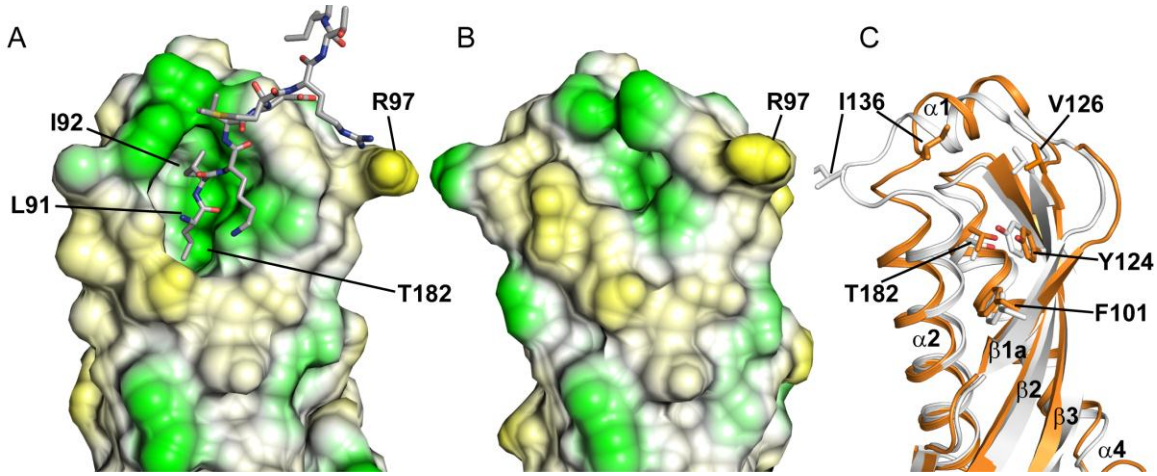

Figure 3. 18: A hydrophobic pocket is essential for stomatin function
(A) Lipophilic surface potential of stomatin$^{86\text{-}213}$ where hydrophobic residues are indicated in green and polar residues in yellow. A hydrophobic pocket is filled by residues Leu91 and Ile92 of an opposing dimer. (B) In a construct where Leu91 and Ile92 are mutated to alanine, the pocket is partially closed. (C) Pocket closure is caused by structural rearrangements in α1, α2 and β2, as seen by a superposition of the open (orange) and closed (white) pocket structures.

To analyze the architecture of the pocket in the absence of L91 and I92, these two residues were mutated to alanine, which result in the construct stomatin$^{86\text{-}213}$ LI91,92AA which crystallized in crystal form 3 **(Table 1)**. In this structure, the binding site for L91 was completely occupied by Y124, whereas the cleft occupied by I92 in the stomatin$^{86\text{-}213}$ constructs was still present and even widened by a movement of I136 **(Figure 3. 18B, C).** The pocket closure of the L91 binding site was caused by rearrangements in α1, α2 and β2, which moved towards the pocket **(Figure 3. 18C)**.

To test the importance of this pocket in the inhibition of ASICs, a mutation expected to completely fill the pocket was introduced (stomatin$^{86\text{-}213}$ T182W). The stomatin$^{86\text{-}213}$ T182W and LI91,92AA mutants eluted in a monomer/dimer in AG experiments, as the wt construct **(Figure 3. 19A)**, indicating that the dimer formation was not affected by this mutation. In addition, the T182W and L191, 92AA mutants showed no apparent difference in secondary structure content in CD measurements **(Figure 3. 19B)**. Furthermore, these mutants were expressed to a similar level as the wt stomatin protein

(Figure 3. 10) and were still able to interact with ASIC3 in pull-down experiments **(Figure 3. 11).**

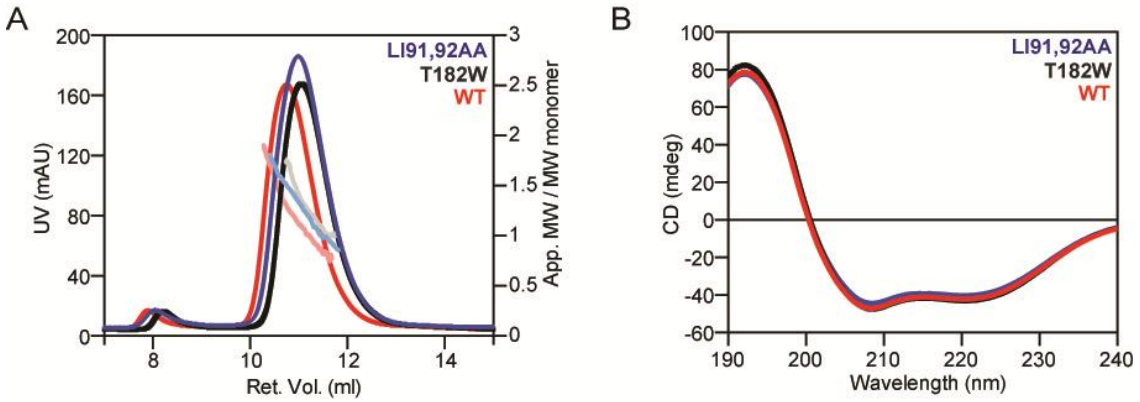

Figure 3. 19: Biochemical analysis of pocket mutants.
A) Analytical gel filtration with static light scattering experiments (AG) for stomatin$^{86\text{-}213}$ wt (red) and the LI91, 92AA (blue) and T182W mutants (black). B) CD measurements for the same mutants with the same color code used.

The detailed analysis of the T182W and L191, 92AA mutants revealed no differences in the behavior of these mutants from that of stomatin, suggesting that these mutations cause no folding or dimerization defects in the protein.

3. 10 Localization analysis the pocket mutants in CHO cells.

To determine whether the L191, 92AA and T182W mutants show altered behavior in their cellular localization, mCherry tagged constructs were co- expressed with eGFP-tagged ASIC3 in CHO cells. When overexpressed in CHO cells, both the T182W and LI91, 92AA stomatin mutants displayed a similar distribution in the fluorescence analysis as the wt stomatin protein **(Figure 3. 20A)** and co-localization with ASIC3 was observed. In BiFC localization studies, the LI91,92AA and the T182W mutants showed a similar co- localization with ASIC3 at the plasma membrane as was shown for the wt stomatin protein **(Figure 3. 20B)**.

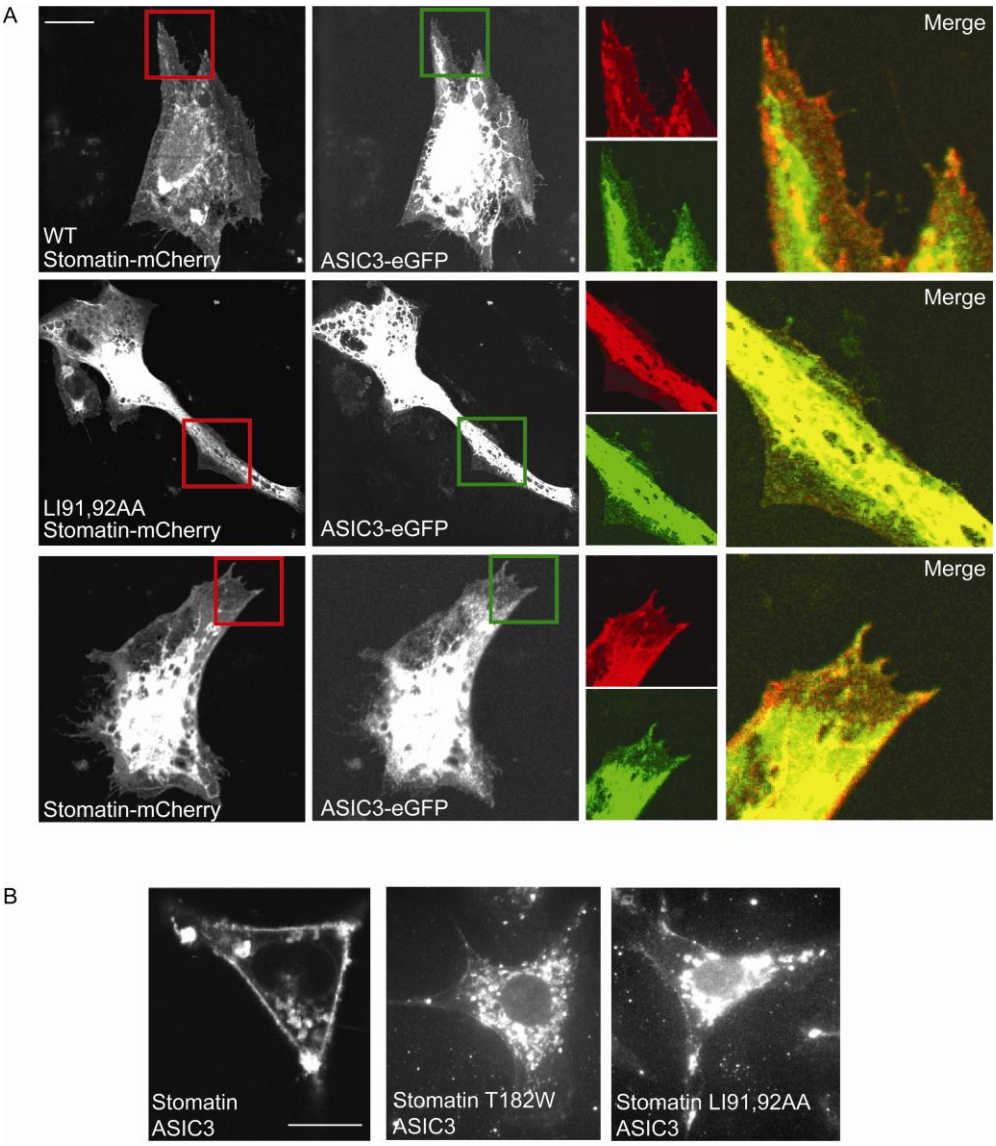

Figure 3. 20: Localization of stomatin mutants in CHO cells.
(A) CHO cells were grown to a density of 60% before co- transfection with mouse stomatin-mCherry or the indicated stomatin mutants and wt eGFP-ASIC3. 24 h post transfection, cells were fixed and analyzed by confocal microscopy and pictures were processed using the ImageJ software. Representative cells are shown. Sections marked by red or green boxes are magnified and merged on the right. Scale bar 20 µm.
(B) CHO cells were co- transfected with plasmids encoding ASIC3 fused to a C-terminal fragment of YFP and stomatin fused to an N-terminal fragment of YFP. 24 h post transfection, cells were subjected to live cell imaging using epifluorescence microscopy (**Methods 2. 6. 6**). The white scale bar corresponds to 20 µm.

Taken together, both pocket mutants localize in a comparable way as the wt stomatin protein in punctuated structures and to the plasma membrane. Both mutants co- localized with the over- expressed ASIC3 protein in two different experiments, indicating that the introduced mutations did not alter the cellular localization of the protein

3. 11 Functional analysis of a hydrophobic pocket

To test the mutations LI91, 92AA and T182W for their functional relevance, both mutations were introduced in the full length protein and used for electrophysiological recordings. The LI91, 92AA mutant was still able to inhibit ASIC2a and ASIC3 **(Figure 3. 21)**, indicating that L91 and I92 in the loop preceding the SPFH domain of mouse stomatin are not the physiological targets of this pocket required for ASICs modulation.

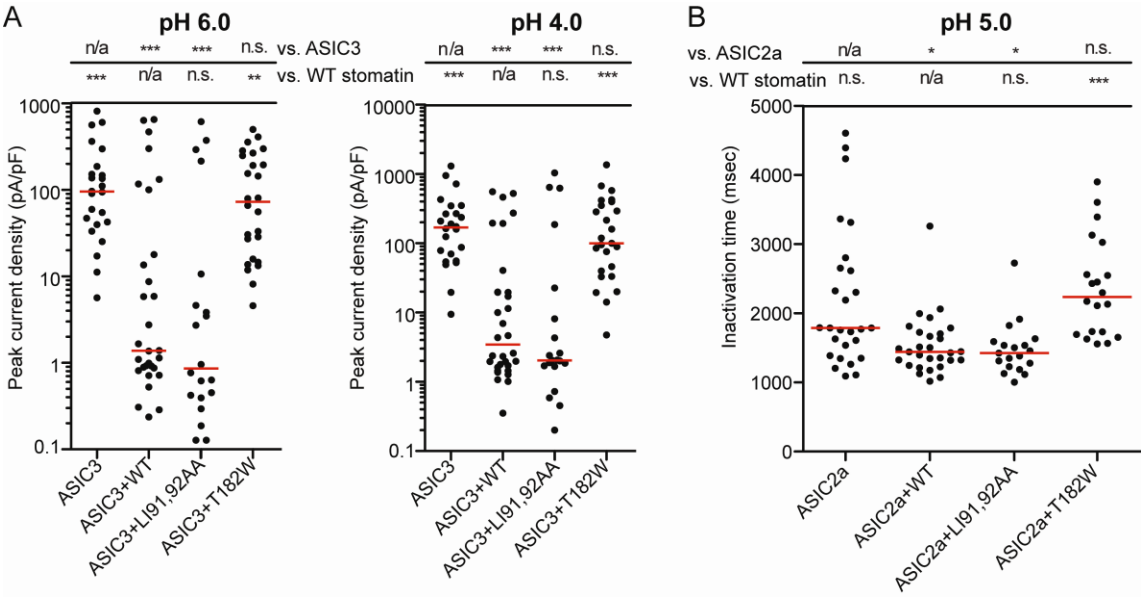

Figure 3. 21: The stomatin pocket is crucial for the modulation of ASIC3 and ASIC2a currents.

A) Electrophysiological recordings of CHO cells co-transfected with ASIC3 and the indicated stomatin mutants at pH 4.0 and pH 6.0 as described in **(Methods 2. 7)**. B) Inactivation times for CHO cells transfected with ASIC2a and the indicated stomatin mutants. The Kruskal-Wallis test followed by Dunn's post test and statistical comparisons of inactivation time of ASIC2a expressed alone and ASIC2a co-expressed with stomatin are shown. n/a, not applicable, n.s., not significant, *, $p < 0.05$; **, $p < 0.01$ and ***, $p < 0.001$.

In contrast, the T182W mutant was unable to modulate proton gated currents of ASIC3 and ASIC2a as shown in whole-cell recordings **(Figure 3. 21)**. The T182W mutant, which was expected to fill the pocket, exhibited a significant effect on ASIC3 and ASIC2a in the electrophysiological experiments **(Figure 3. 21)**, suggesting that the pocket has a physiological role in the modulation of ASIC3 by stomatin.

3. 12 Mapping the site for stomatin- ASIC3 interaction

The C-terminus of ASIC3 contains consecutive leucines at position L488, L489 and this motif resembles the N-terminal Leu91, Ile92 in stomatin **(Figure 3. 22A)**. Assuming that these residues in the ASIC3 C-terminus might interact with the stomatin hydrophobic pocket, both amino acids were mutated to aspartic acid (ASIC3 LL488,489DD) to disrupt this putative interaction site **(Figure 3. 22A)**.

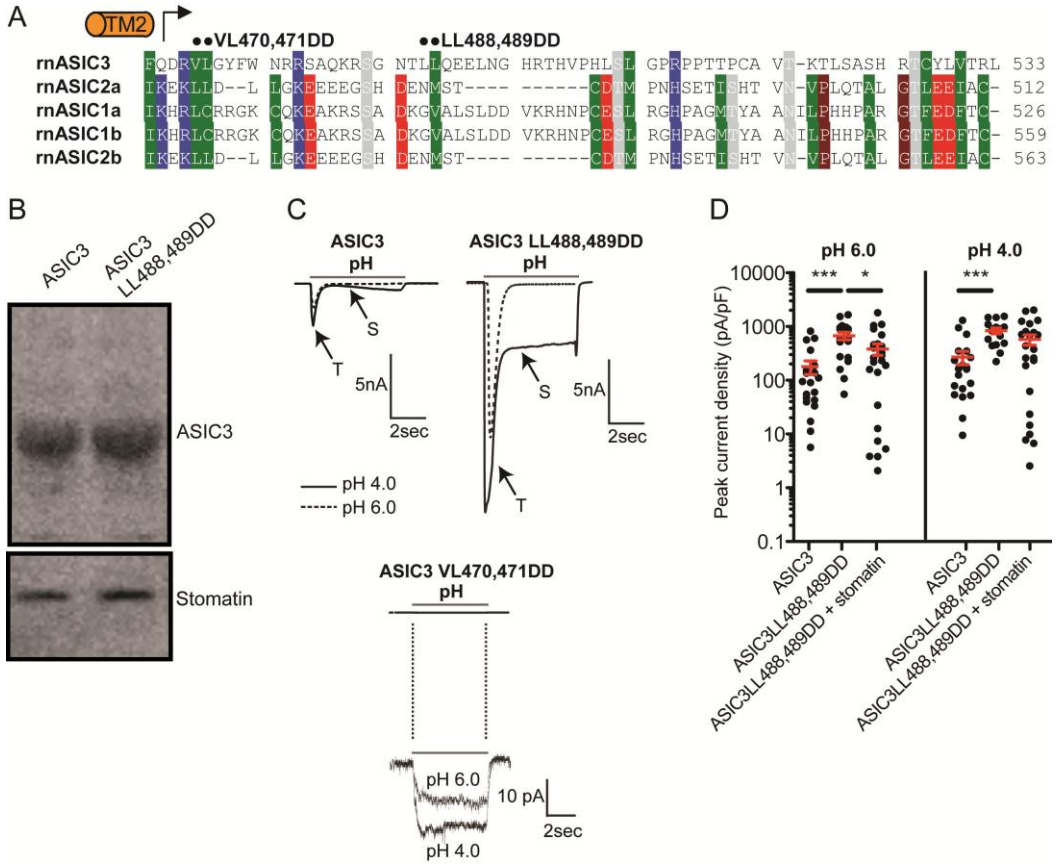

Figure 3. 22: A mutation in the C-terminus of ASIC3 affects modulation by stomatin.

(A) Sequence alignment of the rnASICs proteins at the C-termini. The positions of the mutations analyzed in this study are indicated by black dots. Conserved residues are labeled as in **(Figure 3. 7)**. (B) Co-immunoprecipitation of LL488,489DD mutants and ASIC3 together with stomatin described in **(Methods 2. 6. 5)**. (C) Example traces of proton-evoked currents in cells over- expressing either ASIC3, ASIC3 LL488,489DD or ASIC3 VL470,471DD. The ASIC3 LL488, 489DD mutant showed increased transient (T) and sustained (S) current amplitudes compared to ASIC3. (D) Quantification of transient currents mediated by ASIC3 and ASIC3 LL488,489DD together with stomatin. Each dot corresponds to the measurements in one cell. ***, $p < 0.001$; *, $p < 0.05$.

The ASIC3 LL488, 489DD mutant also interacted with stomatin in pull down assays **(Figure 3.22B),** indicating that these two amino acids are not crucial for the interaction with stomatin.

However, the transient currents from the ASIC3 LL488, 489DD after a pH shift in the environment was substantially increased compared to the wt ASIC3 channel **(Figure 3.22C)**. Furthermore, the regulation of the ASIC3 LL488, 489DD mutant by stomatin was partially lost **(Figure 3. 22D)**. Transient amplitudes of the ASIC3 LL488, 489DD mutant at pH 6.0 were still affected by the presence of stomatin **(Figure 3. 22D)**, but stomatin did not cause an effect on sustained current amplitudes at pH 6.0 or transient and sustained current amplitudes at pH 4.0 **(Figure 3. 22D)**. These data suggest that the C-terminus of ASIC3 may be important for the modulation by stomatin.

Mutations in a second hydrophobic motif in the C-terminus of ASIC3 (VL470, 471DD) resulted in a non-functional ASIC3 channel **(Figure 3. 22C)**.

To confirm the electrophysiological results, the C-terminus of ASIC3 was subjected to an interaction study using ITC. A peptide comprising the identified motif in the C-terminal of ASIC3 (RSGNT**LL**QEELN) was subjected to ITC experiments with stomatin$^{86\text{-}213}$ (**Methods 2. 4. 1**).

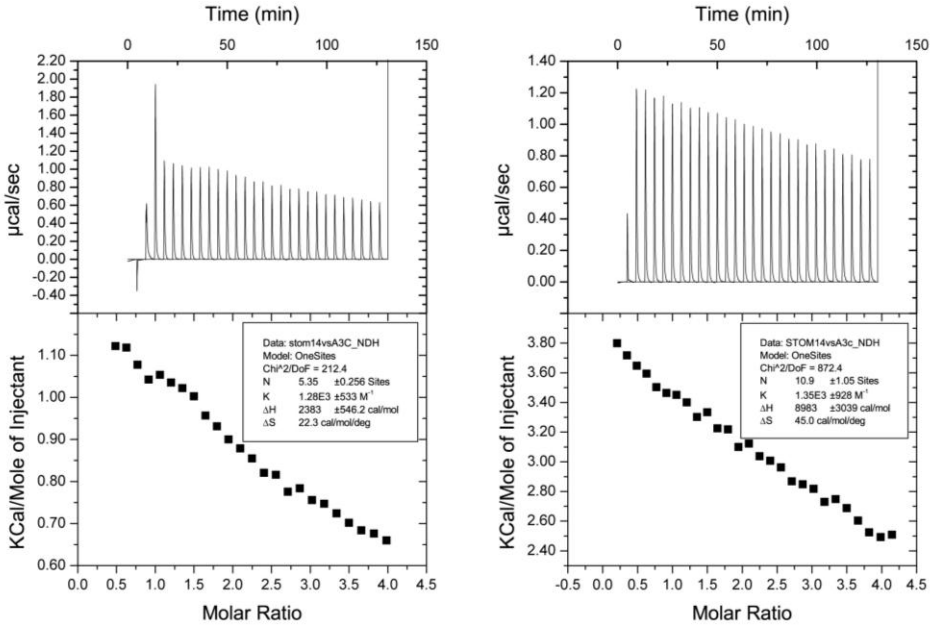

Figure 3. 23: ITC experiments of stomatin with C -terminal peptide of ASIC3.
The ITC experiments were carried out at 20 °C using a VP-ITC. In each step, 10 µl of a 1 or 3 mM solution of an ASIC3 peptide consisting of residues 483-494 (RSGNT**LL**QEELN) was titrated into the reaction chamber filled with stomatin at a concentration of 50 or 150 µM; data were analyzed using Microcal ORIGIN software. In both experiments, no binding of the C- terminal ASIC3 peptide with stomatin protein were seen.

However, no binding of the ASIC3 C- terminal peptide and the stomatin$^{86-213}$ was detected (**Figure 3. 23)**. These results indicated that the identified peptide, if at all, binds with very low affinity to the SPFH domain of the mouse stomatin. Furthermore, the stability of the interaction may require the association of both proteins with membranes.

3. 12 Localization analysis of the ASIC3 mutant in CHO cells.

To investigate the localization of the ASIC3 LL488,489DD mutant CHO cells were transfected with the corresponding plasmids. The ASIC3 LL488,489DD mutant co-localized with stomatin at internal membranes and the plasma membrane **(Figure 3.24A)**.

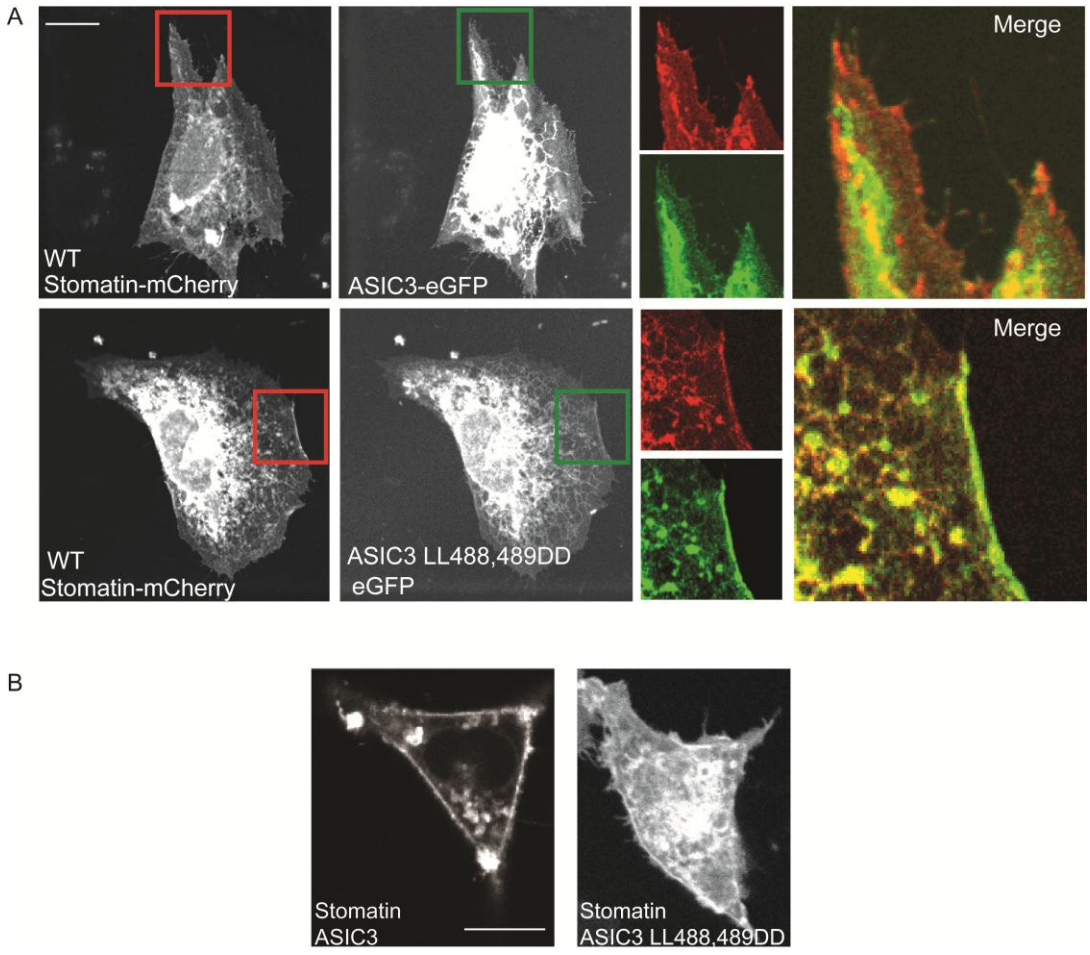

Figure 3. 24: A mutation in the C-terminus of ASIC3 does not affect the cellular localization.

(A) CHO cells were grown to a density of 60% before co- transfection with mouse stomatin-mCherry or the indicated stomatin mutants and wt eGFP-ASIC3. 24 h post transfection, cells were fixed and analyzed by confocal microscopy and pictures were processed using the ImageJ software. Representative cells are shown. Sections marked by red or green boxes are magnified and merged on the right. Scale bar 20 µm.

(B) CHO cells were co- transfected with plasmids encoding ASIC3 fused to a C-terminal fragment of YFP and stomatin fused to an N-terminal fragment of YFP. 24 h post transfection, cells were subjected to live cell imaging using epifluorescence microscopy (**Methods 2. 6. 6**). The white scale bar corresponds to 20 µm.

The same results were obtained from BiFC localization experiments, were the LL488,489DD mutant co- localized with ASIC3, mainly at the plasma membrane and to membrane compartments in the cell **(Figure 3. 24B)**. Indicating that the LL488,489DD mutation in the C- terminus of ASIC3 doest not affect the localization of this ion channel.

3. 13 Analysis of the stomatin oligomerisation

Previous investigations showed that stomatin and other members of the SPFH domain containing proteins can form homo and hetero oligomers (Tanaka *et al.*, 2009; Tatsuta *et al.*, 2005a; Umlauf *et al.*, 2006). To examine the self-assembly and to further investigate the oligomeric state of stomatin, cross linking experiments **(Methods 2. 4. 6)** with recombinant produced protein were performed. For the cross linking experiments, constructs comprising stomatin$^{96-204}$, stomatin$^{86-255}$ and stomatin$^{86-213}$ were tested for their ability to form oligomers in the presence or absence of the cross linking reagent BS^3 (bis sulfosuccinimidyl suberate). BS^3 contains a spacer arm of 11.4 Å and can crosslink primary amino groups to form stable amide bonds. After determination of the optimal protein concentration for the experiments (data not shown), all assays were carried out with 15 µM of the purified protein. After incubation of the protein with BS^3 for 30 minutes, samples were analyzed by SDS- PAGE **(Figure 3. 25)**.

The results from the cross lining experiments showed that all of the tested proteins have the propensity to form oligomers in the presence of the cross linker BS^3 with the exception of the LI91, 92AA mutant, which showed a reduced oligomerisation ability **(Figure 3. 25)**.

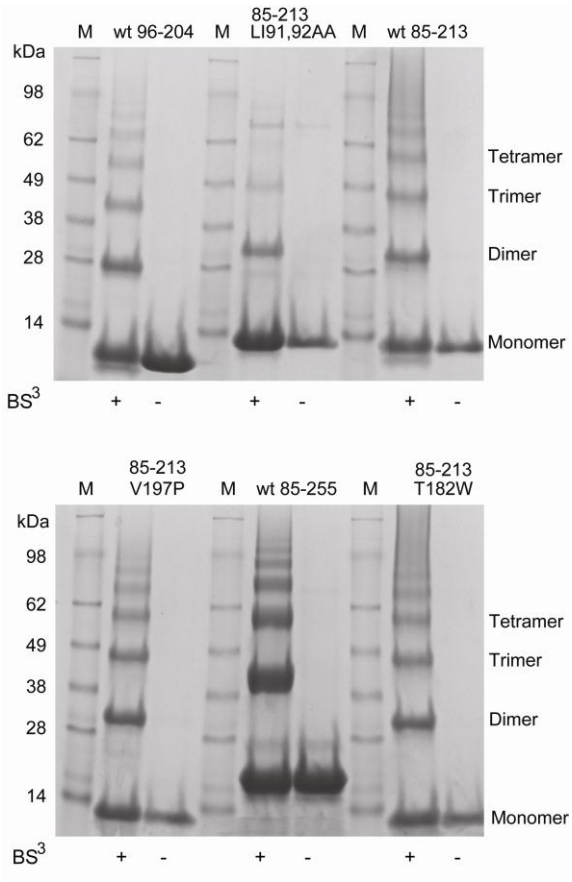

Figure 3. 25: Stomatin oligomers in the presents of BS^3 cross linker.
Various mouse stomatin proteins were applied to SDS gels in the presence (+) or absence (-) of 2 mM BS^3 cross linker for 30 min at RT. M- Marker with the size of the protein bands indicated on the left in kDa and the resulting oligomeric state on the right.

However, the results from the cross linker experiments can be questioned because the V197P mutant, which was biochemically identified to be monomeric showed the propensity to form higher order oligomers. This leads to the suggestion that the oligomerisation of the V197P is an artefact and caused by the not specific cross linker BS^3.

To further investigate the olgomeric character of the mouse stomatin stomatin$^{86\text{-}213}$ LI91, 92AA, in crystal form 3 was analyzed in detail. The dimerization site remained the same as in the other two crystal forms but the dimers formed a tubular oligomeric arrangement via lateral interaction **(Figure 3. 26)**.

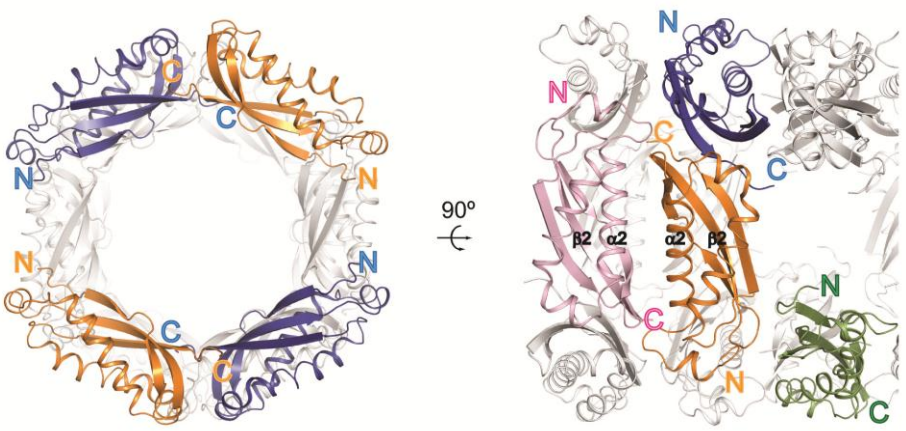

Figure 3. 26: Oligomerisation of mouse stomatin^{LI91,92AA}
In crystal form 3 the LI91, 92AA mutant of the stomatin$^{86-213}$ protein forms lateral interaction which results in a tubular oligomeric arrangement. This was established by symmetric contacts of the SPFH domain.

A sequence conservation plot of the solvent accessible residues according to the alignment **(Figure 3. 7)** of the mammalian SPFH domain containing family was mapped to the surface of the structure **(Figure 3. 27A)**. This conservation blot indicated that the residues involved in higher order oligomerisation in crystal form 3 were conserved.

The tubular arrangement is established by symmetric contacts of the stomatin subunits via two patches of surface exposed residues **(Figure 3. 27A)**. The conserved symmetric interfaces were named interface-1 and interface-2 and indicated with black lines in **(Figure 3. 27A)**.

The symmetric interface-1 has a buried surface area of 700 $Å^2$ per molecule **(Figure 3. 27C)**. The hydrophobic patch is built up by W185 and L145 from one molecule and the L109 of the opposing molecule. In the center of interface-1, R152 forms a hydrogen bond with T149 of the opposing molecule.

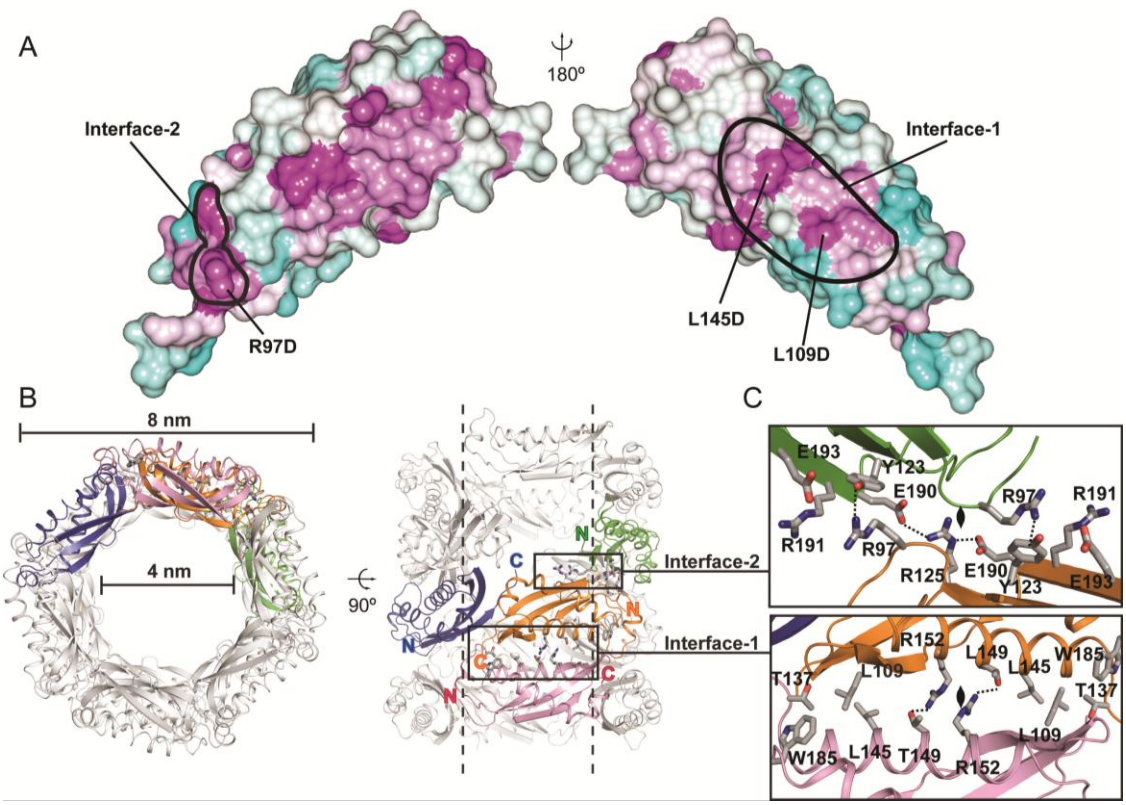

Figure 3. 27: Higher-order oligomerisation of stomatin$^{86-213}$ LI91, 92AA
(A) Solvent-accessible residues in the stomatin domain are colored according to sequence conservation within the mammalian stomatin family, using a gradient from violet (highly conserved) to cyan (not conserved). The oligomerisation interfaces in crystal form 3 are indicated by the black line. (B) Two views of the tubular structures formed by stomatin dimers in crystal form 3. (C) Detailed views of the conserved interfaces.

Interface-2 is smaller in size with a buried surface area of 300 Å^2 and features an interaction of the invariant R97 with a conserved surface-exposed amino acid triplet formed by Y123, E193 and R191 **(Figure 3. 27C).**

To test the relevance of these interfaces for the function of stomatin as a modulator of ASIC3, mutagenesis studies were performed. In interface-1 the L109D, L145D double mutant eluted with the same retention volume as stomatin$^{86-213}$ in AG experiments **(Figure 3. 28A)** and gave an identical CD spectrum **(Figure 3. 28B)**.

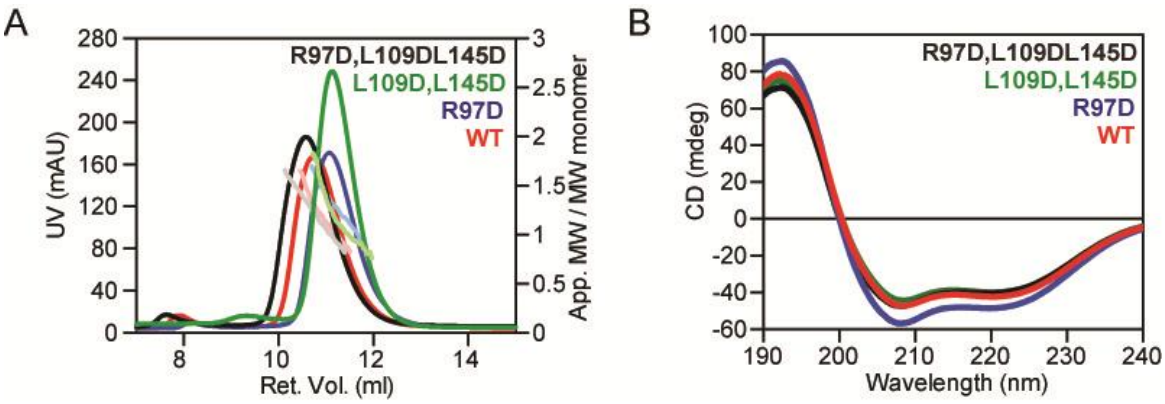

Figure 3. 28: Biochemical analysis of the oligomerisation interface mutants.
(A) Result from the analytical gel filtration for stomatin$^{86\text{-}213}$(red) and the R97D (blue), L109D, L145D (green) and R97D, L109D, L145D (black) mutants. (B) CD measurements for the stomatin$^{86\text{-}213}$ mutants using the same colour code as in A.

To test the function of interface-2, R97 was mutated to aspartate; the resulting mutant showed a monomer dimer equilibrium via analytical gel filtration, similar to the wt protein **(Figure 3. 28A),** and no folding defect seemed to be present, as probed by CD spectroscopy **(Figure 3. 28B)**.

Also for a construct combining mutations in both interface-1 and interface-2 (R97D, L109D, L145D) no notable deviations in either the analytical gel filtration profile **(Figure 3. 28A)** or in the CD spectrum were seen **(Figure 3. 28B)**.

Taken together, none of the interface mutants showed any significant folding or oligomerisation defects.

3. 14 Localization of the oligomerisation interface mutants in CHO cells

To test the effect of these interface mutants on cellular localization, CHO cells were transfected with the corresponding plasmids.

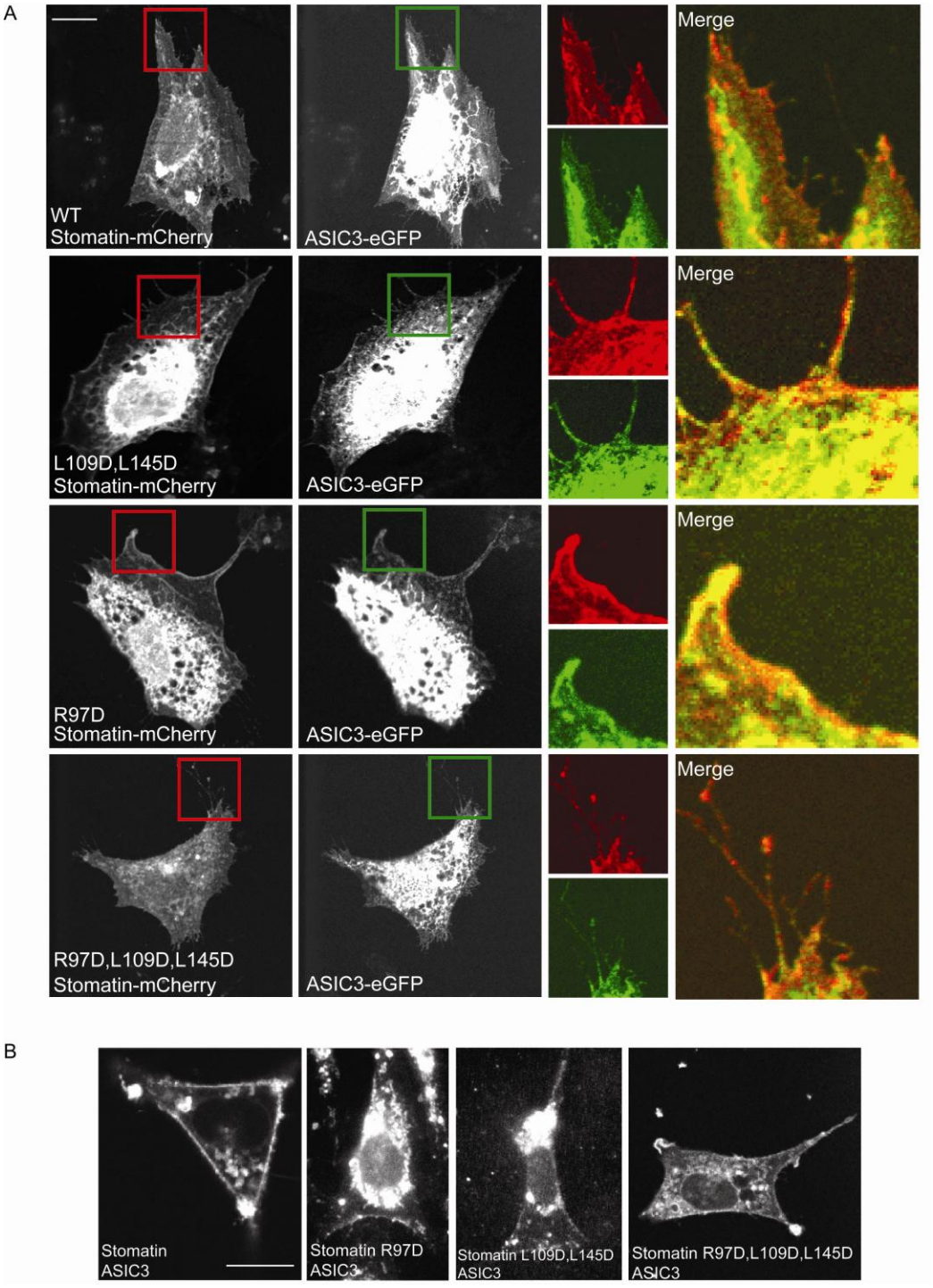

Figure 3. 29: Localization of oligomerisation mutants in CHO cells.
(A) CHO cells were grown to a density of 60% before co- transfection with mouse stomatin-mCherry or the indicated stomatin mutants and wt eGFP-ASIC3. 24 h post transfection, cells were fixed and analyzed by

confocal microscopy and pictures were processed using the ImageJ software. Representative cells are shown. Sections marked by red or green boxes are magnified and merged on the right. Scale bar 20 µm.
(B) CHO cells were co- transfected with plasmids encoding ASIC3 fused to a C-terminal fragment of YFP and stomatin fused to an N-terminal fragment of YFP. 24 h post transfection, cells were subjected to live cell imaging using epifluorescence microscopy (**Methods 2. 6. 6**). The white scale bar corresponds to 20 µm.

The L109D, L145D double mutant showed a similar localization in CHO cells when compared with the wt stomatin protein, as did the R97D mutant. For both mutants, co-localization with ASIC3 was seen **(Figure 3. 29A)**. The R97D, L109D, L145D triple mutant also co- localized with ASIC3 and no obvious differences from the localization profiles between the interface- 1 or interface-2 mutants and wt stomatin were detected **(Figure 3. 29A)**. The same results where obtained from BiFC localization experiments, were all interface mutants co- localized with ASIC3, at internal membranes and at the plasma membrane **(Figure 3. 29B).**

Furthermore, all stomatin oligomerisation mutants were produced to comparable levels with ASIC3 **(Figure 3. 10)** and could co- immunoprecipitate ASIC3 with a similar efficiency as the wt stomatin **(Figure 3. 11)**.

3. 15 Functional analysis of the stomatin oligomer

To test the relevance of these interface mutants on the modulation of ASIC3, electrophysiological assays were performed and compared with those of the stomatin protein.

In whole-cell recordings, the stomatin L109D, L145D mutant failed to inhibit ASIC3 at pH 6.0. However, at pH 4.0 the peak current density of ASIC3 was significantly reduced **(Figure 3. 30)**. In contrast the R97D single point mutant in interface-2 showed no significant inhibitory action of stomatin on ASIC3 proton-gated peak current density at either pH value **(Figure 3. 30)**. At pH 6.0, the L109D, L145D mutant displayed an intermediate inhibitory effect; although peak current density was significantly lower at pH 4.0 for this mutant **(Figure 3. 30)**. The R97D, L109D, L145D triple mutant showed at pH 6.0, an intermediate inhibitory effect; although peak current density of ASIC3 was highly significantly reduced at pH 4.0 for this triple mutant **(Figure 3. 30)**.

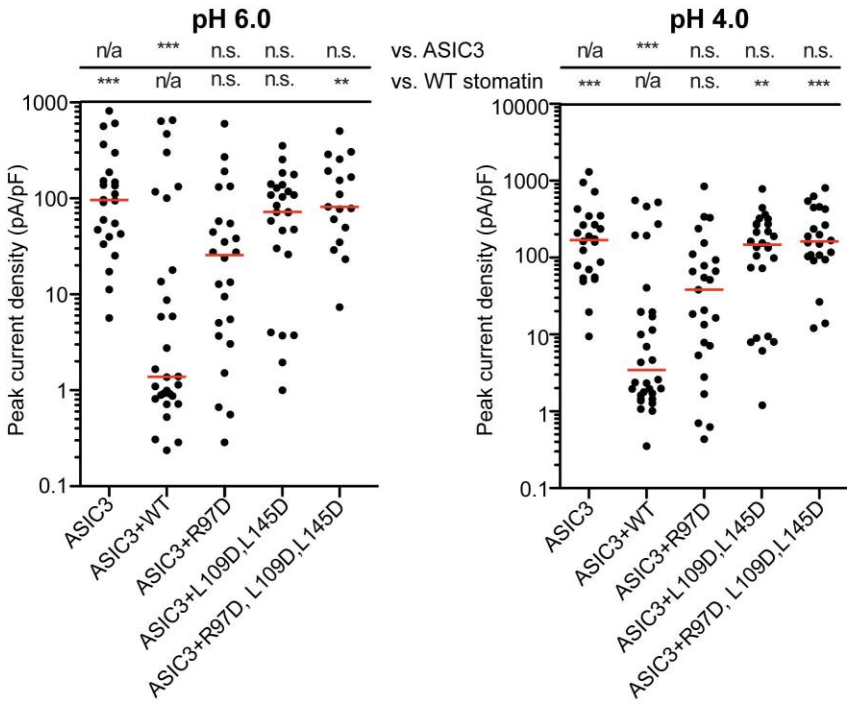

Figure 3. 30: Functional analysis of the oligomerisation interface mutants. Electrophysiological recordings of CHO cells transfected with ASIC3 and the indicated stomatin mutants at pH 4.0 and pH 6.0. The Kruskal-Wallis test followed by Dunn's post test and statistical comparisons of inactivation time compared to ASIC3 expressed alone and ASIC3 co-expressed with stomatin are shown. n/a, not applicable, n.s., not significant, **, $p < 0.01$ and ***, $p < 0.001$.

It was finally possible to identify individual residues in both oligomerisation interfaces that have a clear effect on the function of stomatin in the modulation of ASIC3.

This finding suggests a synergistic action of these two interfaces in the inhibition of ASIC currents and might indicate that higher-order stomatin assembly proceeds in a similar way as in crystal form 3 **(Figure 3. 26).** It might also involve hetero-oligomerisation between different stomatin members as suggested in (Mairhofer et al., 2009). Furthermore, these data are consistent with our model **(Figure 4. 4)** where the SPFH domain of stomatin assembles in a tubular fashion to regulate ASIC ion channel activity.

4. Discussion

SPFH domain containing proteins exert powerful physiological effects on ion channels (Lapatsina *et al.*, 2012b; Martinez-Salgado *et al.*, 2007; Price *et al.*, 2004; Wetzel *et al.*, 2007). Proton-gated ASIC3-mediated currents are suppressed and ASIC2a current inactivation is accelerated in the presence of stomatin (Price *et al.*, 2004; Wetzel *et al.*, 2007). By solving the core structure of the mouse stomatin and performing structural and functional analyses, three key regions of the stomatin molecule necessary for its ability to modulate ASICs were identified

First, it was show that the basic building block of stomatin is a banana-shaped dimer, which is formed by an intermolecular β-sheet at the C-terminus and is necessary for the modulation of ASICs.

Second, a hydrophobic pocket in each stomatin monomer was identified, the closure of which prevents modulation of ASICs without affecting the dimerization.

Finally, additional conserved oligomerisation surfaces in stomatin in one crystal form were found which are involved in the formation of ring-like structures with an outside diameter of 8 nm. Each of the findings will be discussed in the following paragraphs.

4. 1. The dimerization site

By solving the structure of the mouse stomatin$^{86\text{-}213}$ protein in three different crystal forms a dimer in the crystal packing was found. In order to determine the physiological relevance of this dimer, AUC and AG in combination with mutagenesis studies were conducted **(Figure 3. 9)**.

To disrupt β3 locally, we then introduced the V197P mutation in stomatin and the resulting protein was stable and could be purified in amounts sufficient for biochemical and crystallographic investigation.

Analytical ultracentrifugation showed that the V197P mutation completely prevented dimerization **(Figure 3. 9A)**. Also in AG experiments, the V197P mutant was mostly monomeric **(Figure 3. 9B)**. CD measurements of this mutant showed a spectrum similar to that of stomatin$^{86\text{-}213}$, indicating that the mutation did not perturb the fold of the protein **(Figure 3. 9C)**. These biochemical results indicate that the dimer is indeed present in solution and not a crystallographic artefact.

The fact that the basic building block of the mouse stomatin is a banana-shaped dimer, formed by an intermolecular β-sheet at the C-terminus, was surprising in light of the previously published trimeric structure of the archaebacterial phstomatin (Yokoyama *et al.*, 2008). In this structure, phenylalanine 55, which is not conserved and exclusively present in the phstomatin protein, is buried in a pocket of the opposing protomer and thereby plays a central role in trimer assembly **(Figure 1. 2** and **Figure 3. 7)**. In fact, trimerization has so far only been proposed for the archaebacterial stomatin and is not observed in any of the mammalian SPFH domain structures reported so far (Tanaka *et al.*, 2009). Further support for a physiological dimer comes from the fact that dimer formation is mediated by the same C-terminal interface in all three crystal forms obtained in this work. Results from the cross linking experiments were inconclusive **(Figure 3. 25)**. Nevertheless, all biochemical experiments revealed that the mouse stomatin$^{86\text{-}213}$ in solution is present in a monomer/dimer equilibrium (**Figure 3. 9A** and **B)** with a Kd of 37 µM. In addition, the construct stomatin$^{86\text{-}255}$ containing a C-terminal extension similar to the phstomatin protein used for the crystallisation trials, also showed a monomer/dimer equilibrium in AG experiments **(Figure 3. 9B)**, indicating that the C- terminal coiled coil does not lead to a trimerization of the mouse stomatin.

Furthermore, there is experimental evidence that some SPFH domain containing proteins are able to form dimers and it has been shown that dimerization is essential for the function of these proteins (Frick *et al.*, 2007; Tatsuta *et al.*, 2005a). This includes studies showing that homo- or hetero dimerization is important for the stability and function of prohibitin (Artal-Sanz *et al.*, 2009; Coates *et al.*, 1997) and flotillins (Frick *et al.*, 2007). This lead to investigation of whether different members of the SPFH domain containing family can hetero- oligomerise with other members of the family. Interestingly, a study from Mairhofer et al showed a functionally relevant hetero-assembly of stomatin and SLP-1 (Mairhofer *et al.*, 2009). Another study proved that SLP-3 and stomatin co-localize in DRG (Lapatsina *et al.*, 2012b). Unpublished data from our group on stomatin co-expressed with SLP1 or SLP-2 in *E. coli* cells showed it was possible to purify a complex of stomatin with both proteins (data not shown), suggesting heterodimerization of these proteins.

By comparing the overall fold of the mouse stomatin dimer with the well known BAR domain family proteins, we found striking parallels **(Figure 4. 1)**.

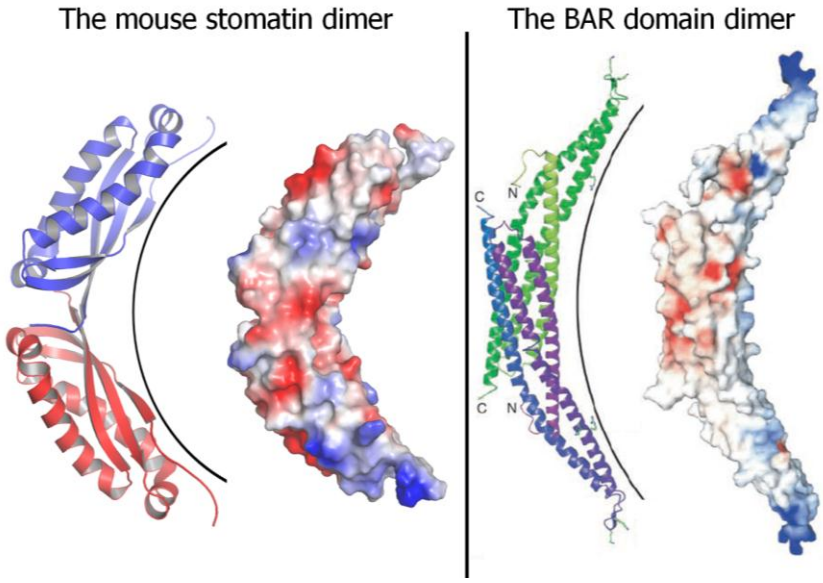

Figure 4. 1: Comparison of the mouse stomatin dimer with the BAR domain dimer of Drosophila.
The banana shaped dimer of the mouse stomatin and the Drosophila BAR domain in cartoon and surface representations (Peter *et al.*, 2004). The color code indicates the charged surface exposed residues in red and the hydrophobic residues in blue.

BAR domain proteins also assemble into banana-shaped dimers and the dimers are formed with similar µM affinities as that shown in this work for the stomatin dimer (Frost *et al.*, 2009; Peter *et al.*, 2004). In addition, the F- BAR domain dimers can further assemble into helical structures **(Figure 4. 2)**.

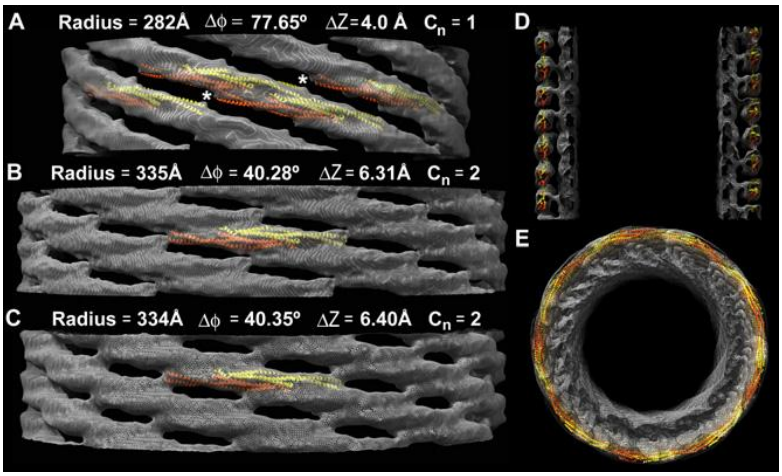

Figure 4. 2: Cryo EM reconstruction of the BAR domain oligomer.

Cryo EM reconstruction of the BAR domain dimers individual subunits in yellow and orange, and assembly in a ring structure showing the ability to form tubular structures of different diameters (compare (A) with (B) and (C)). Longitudinal view (E) and lateral view (D). Taken form (Frost *et al.*, 2008).

These interactions at the tip and the lateral side of the dimer and may thus exert changes in membrane curvature, which often are supported by the insertion of N-terminal amphipathic helices (Frost *et al.*, 2008; Shimada *et al.*, 2007).

The membrane insertion domain of stomatin and the palmitoylation sites (Snyers *et al.*, 1999) might exert a similar function in inducing membrane curvature and a tubular assembly of the stomatin dimers was also observed in the crystal lattice of the stomatin LI91,92AA protein **(Figure 3. 26** and **Figure 3. 27)**.

The SPFH domain of the mouse stomatin has, except for the hydrophobic pocket **(Figure 3. 18)**, no particular charged patches on the inside of the banana shaped dimer; despite the suggested propensity to bind to lipids (Huber *et al.*, 2006), and no lipid binding of the mouse stomatin could be detected in the biochemical experiments reported in this work.

4. 2. The hydrophobic pocket in stomatin

A hydrophobic pocket in each stomatin monomer were identified **(Figure 3. 18)**. To further investigate the pocket and to elucidate its putative function, mutagenesis of residues composing the pocket or protruding into the pocket were performed. The mouse T182, which is located in the bottom of the pocket, was mutated to a bulky tryptophan residue with which we expected to close the pocket. Furthermore, it was speculated that this pocket might be able to accommodate cholesterol or other lipids.

To test this hypothesis, lipid binding assays and ITC experiments with stomatin$^{86\text{-}213}$ and 25 HC were performed **(Figure 3. 15** and **Figure 3. 16)**. Despite earlier studies which suggested cholesterol binding by MEC-2 and podocin (Huber *et al.*, 2006), all attempts to show an interaction between stomatin and cholesterol or other lipids failed in this study **(Figure 3. 15** and **Figure 3. 16).**

The result that no lipid protein interaction was detected in the lipid binding assays can be explained by the fact that the construct used for these experiments is devoid of the palmitoylation sites. Also the construct excludes the hydrophobic hairpin regions, which are most likely important for the association of stomatin with membranes.

However, it still cannot be excluded that a low affinity interaction of the SPFH domain of the mouse stomatin with certain lipids is important for its function *in vivo*. Such an effect has been shown for flotillin, where cyclodextrin depletion of cholesterol led to altered localization and impaired function of the protein (Liu *et al.*, 2005). To conduct these experiments with stomatin could give new insights into its lipid binding propensity.

Since no differences in the localization of the T182W mutant compared to stomatin in CHO cells were detected **(Figure 3. 20)**, it was concluded that the pocket is not necessary for targeting stomatin to the plasma membrane. Co- immunoprecipitaion assays also showed that the ASIC3/stomatin interaction is not affected by the T182W mutation **(Figure 3. 11)**. In previous density gradient centrifugation experiments, mutation of T182A was shown not to alter the oligomerisation state of human stomatin (Umlauf *et al.*, 2006).

For the electrophysiological recordings CHO cells were used which provided a background-free system for investigating the modulation effect, due to their lack of ASIC channels (Smith *et al.*, 2007). To compare all functional and localization studies all cellular experiments were performed in the same cell type.

The functional assays clearly showed that the T182W mutation had a strong effect on the ability of stomatin to modulate ASIC3 and ASIC2a **(Figure 3. 21)**. To explain this effect, it was proposed that the pocket might be able to accommodate a short hydrophobic peptide motif. So the functionality of the pocket was further investigated and tested for the ability to bind to peptides. As seen from stomatin crystal forms 1 and 2, the pocket can accommodate a dipeptide of two amino acids with branched aliphathic side chains (L, I). Two similar motifs in the ASIC3 C-terminus were identified **(Figure 3. 22)** (V470, L471 and a L488, L489).

Replacement of the dileucine motif at positions 488 and 489 with two aspartates resulted in a loss of ASIC regulation by stomatin. Nevertheless, this effect was not supported by biochemical experiments where no interaction between the stomatin protein and the C-terminal peptide of ASIC3 were detected **(Figure 3. 23)**. Still, the electrophysiological data show that the C-terminus of ASIC3 is important for the currents regulation and that stomatin can modulate ASIC3 function via this motif.

4. 3. Oligomerisation

In this work it was demonstrated that the minimal functional unit of the SPFH domain of the mouse stomatin is a dimer. Furthermore, in crystal form 3, two conserved interfaces are involved in the formation of a ring-like structure with an outside diameter of 8 nm **(Figure 3. 27B)**. Slight alterations in the assembly interfaces might lead to oligomers of different diameters in the cell. Previously, the C-terminal region of stomatin was shown to contribute additional oligomerization sites (Umlauf *et al.*, 2006). For the cyanobacterial stomatin (Boehm *et al.*, 2009) and yeast prohibitin (Tatsuta *et al.*, 2005b), ring-like oligomers were identified by single-particle electron microscopy analysis, supporting the idea that SPFH domain containing proteins may assemble at the membrane in ring-like structures with a banana-shaped dimer as the building block.

Two conserved interfaces were identified to contribute to the formation of a ring-like or tubular oligomerisation. In the symmetric interface-1, residues L109 and L145 were mutated to aspartic acids with no resulting change in either folding or dimerization. The double mutation L109D, L145D showed a strong effect on ASIC3 regulation, indicating that interface-1 is functionally important and that the ring-like oligomer could be indeed physiologically relevant.

The second conserved interface was also tested by introducing point mutations. None of the interface-2 mutations showed any effect on the folding or dimerization of stomatin. The R97D mutant showed a moderate effect on ASIC3 regulation. Interestingly, it was shown in previous experiments that the R184C mutation in MEC-2, corresponding to R97 in the mouse stomatin, renders worms touch insensitive, suggesting that this interface is important for the mechanotransduction (Chalfie and Sulston, 1981).

A triple mutation comprising L109D and L145D in interface-1 and R97D in interface-2 showed a strong effect on the ASIC3 modulation, as the triple mutant rendered the stomatin molecule ineffective in modulating ASICs. This suggests that stomatin might assemble in a similar ring-like fashion at the plasma membrane.

There is abundant evidence that stomatin and other stomatin-domain proteins can form higher-order oligomers (Snyers *et al.*, 1998; Umlauf *et al.*, 2006). Ring-like stomatin oligomers were identified by single-particle analysis of the cyanobacterial stomatin (Boehm *et al.*, 2009) and yeast prohibitin (Tatsuta *et al.*, 2005a), supporting the idea that

stomatin domain proteins may assemble *in vivo* as ring structures with a banana-shaped dimer as the building block. Furthermore, heterodimerization of flotillins and, possibly, higher-order oligomerisation, induces membrane curvature and vesicle budding at the plasma membrane (Frick *et al.*, 2007). Thus, the here proposed model of the mouse stomatin oligomerisation might be relevant for many other SPFH domain containing proteins, although the SPFH domain can also be engaged in different oligomerisation modes **(Figure 1. 2, Figure 1. 10, Figure 1. 11** and **Figure 3. 17)**.

The fact that higher order stomatin oligomers in solution were not detect, either in AUC or in AG experiments, can be explained by the possibly low affinity of these interactions. When the proteins are in closer proximity upon insertion into the membrane there might be cooperative binding. The fact that the constructs used in these assays lacked the N-terminal membrane insertion sequence **(Figure 3. 1)** and that all biochemical assays took place in the absence of lipid bilayer might be the reason that higher oligomers were never detected *in vitro*.

Attempts to show the oligomer of the recombinantly expressed protein in the presence and absence of lipids by electron microscopy were not successful (data not shown). Beside these attempts, the Myc- His- tagged stomatin expressed in CHO cells was subjected to native gel analysis (data not shown). In these preliminary experiments, a protein complex of approximately 600 kDa was detected. This is in agreement with previous sucrose gradient centrifugation results from (Umlauf *et al.*, 2006) and (Salzer *et al.*, 2001) where stomatin oligomers of the same size were described.

4. 4. Possible modulation mechanism of ASICs

The structure of the chicken ASIC1a confirmed a previously proposed trimeric assembly of the protein in its native state with a majority of the channel located in the extracellular space (Gonzales *et al.*, 2009; Jasti *et al.*, 2007).

The activation of ASICs was shown to be influenced by extracellular stimulus like the drop of pH in the environment. Furthermore, it was reported that the ASICs function can be regulated by extracellular protease treatment (Hughey *et al.*, 2004). A recent crystallographic and electrophysiological study showed a co crystal structure of the trimeric chicken ASIC1a channel with the tarantula Psalmotoxin (PcTx1) bound to the

ECR (Baconguis and Gouaux, 2012). The functional data demonstrates that (PcTx1) binding results in an activated form ASIC1a form at pH 7.25 and pH 5.5.

Beside this extracellular modulation mechanism, also intracellular modulating mechanisms were described. It was shown that the activity of ASICs can be modulated by phosphorylation. This requires the interaction of the ASICs C-termini with the PDZ domain of PICK1 (protein interacting with C-kinase1) (Baron *et al.*, 2002; Deval *et al.*, 2004; Duggan *et al.*, 2002; Leonard *et al.*, 2003). Other PDZ domain containing proteins, like PSD-95 and Lin-7b, have also been shown to interact with the C- terminus of ASICs and can exert either positive or negative modulation of pH gated currents (Hruska-Hageman *et al.*, 2004). In these cases, it is thought that channel activity is primarily modulated by regulating the number of channels on the plasma membrane. In my PhD-thesis I could identify a C-terminal di-leucine motif in ASIC3 which appears to be involved in stomatin modulation without affecting ASIC3 membrane targeting. Mutation of the di-leucine motif to aspartic acid greatly increased current amplitudes without affecting the physical interaction with stomatin **(Figure 3. 22)**.

This suggests that stomatin primarily regulates functional properties of the ASIC3 channel via this di-leucine motif. Conversely, closure of the hydrophobic pocket in stomatin with the T182W mutation abolished stomatin's ability to negatively regulate ASIC3 **(Figure 3. 18)**.

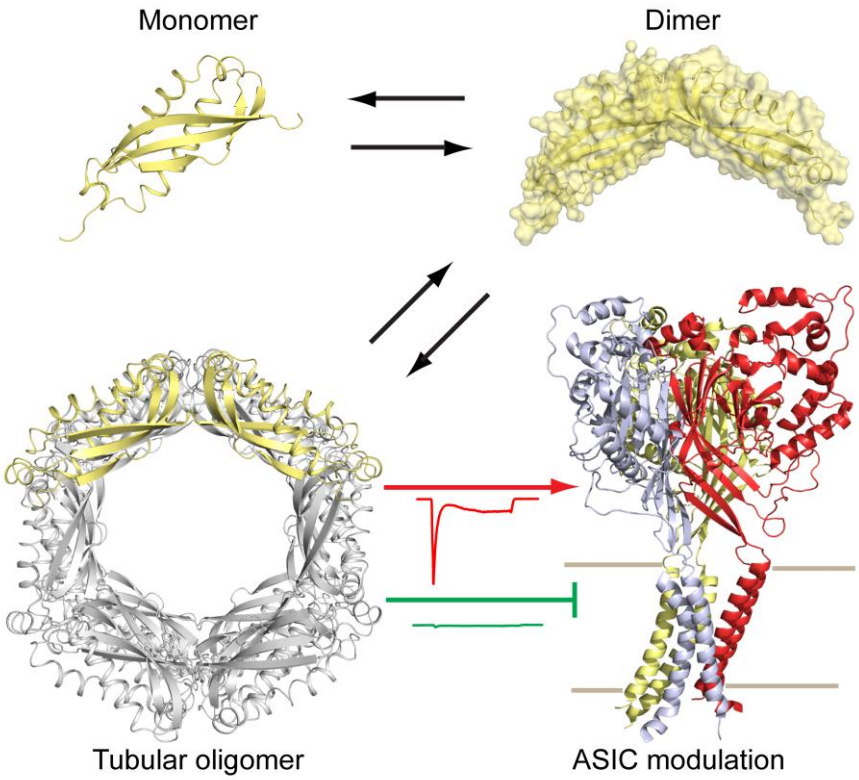

Figure 4. 4: Proposed model for ASIC modulation by the mouse stomatin oligomer.
The key findings of this work are summarized in a putative model where the stomatin dimers oligomerize into a tubular assembly. This tubular structure could be the cytoplasmic modulator of the ASIC3 transduction channel, which was shown by electrophysiological recordings interface- 1 and interface- 2 of stomatin **(Figure 3. 27)**.

So far, no structural information about the cytoplasmatic N- or C- termini of ASICs is available. This could be the missing link in understanding the function of this class of proteins in greater detail **(Figure 4. 4)**. It has been reported that TRPV1 channels can be modulated by the cytoplasmic protein calmodulin which interacts directly with the cytoplasmic N-terminus of the channel which features ankyrin repeats (Lishko *et al.*, 2007). Furthermore, it was shown that this modulating event is cholesterol-dependent.

For the SPFH domain containing proteins, a similar cholesterol-dependent gating mechanism is conceivable and some evidence points in this direction. A structural or biochemical characterization of a stomatin/ASIC complex as a whole or a stomatin structure with ASIC peptides bound would provide more detailed insights into the mechanism of how these important proteins exert their physiological effects**.**

5. Outlook

For the future, the structure of a full length version of mouse stomatin, or the full length protein of other members of the SPFH domain protein family, would be helpful for obtaining more detailed information on the biochemical and structural mechanisms of this class of proteins. Initial attempts to purify the native protein from mouse erythrocytes were not successful due to the lack of a specific antibody against stomatin.

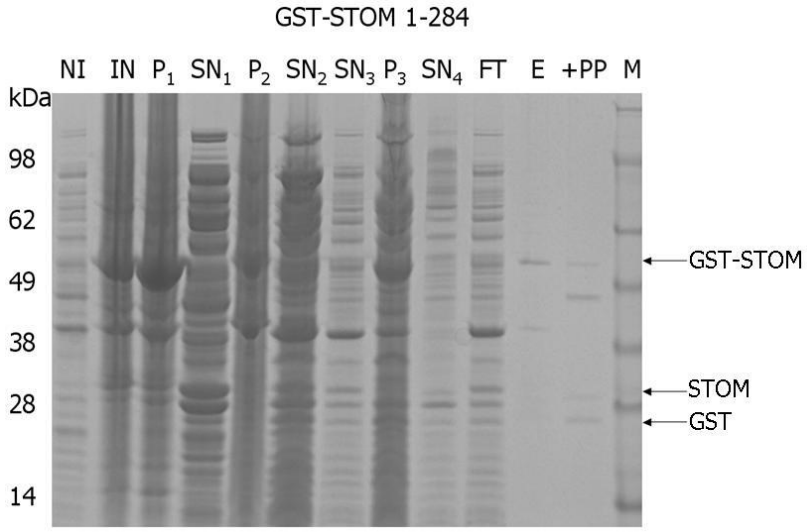

Figure 5. 1: Expression and purification of the fl mouse stomatin.
The purification was performed according to **(Methods 2. 3. 7)** with the exception that 1% LDAO from the harvesting step remained in all buffers as reported in (Halbhuber *et al.*, 2003). The pellets (P) after each sedimentation step and the supernatant (SN) were tested for the presence of the partially insoluble full length GST–stomatin fusion protein. After elution from GSH-sepharose (E) the GST tag was cleaved with precision protease (+PP). The Protein marker (M) reveals that a small amount of the GST-stomatin fusion protein could be purified and the GST tag was partially cleaved by the precision protease. The protein subsequently precipitated and no further purification via preparative gel filtration could be employed.

Other attempts to obtain full length stomatin protein in the presence of detergents have been partially successful **(Figure 5. 1).** The next step is to perform a detailed detergent screen and to search for the appropriate detergent concentration.

To more precisely investigate the stomatin oligomer, it would be useful to isolate the eukaryotic over-expressed stomatin protein complex via gel filtration and improve the native PAGE western blot analysis.

Cell free expression would be a productive way to rapidly test different stabilizing conditions and different host organisms like eukaryotic cell lines cells with an inducible promoter should also be tested. The advantage of eukaryotic cells would be the

introductions of posttranslational modifications like palmitoylation and phosphorylation. Furthermore, eukaryotic expression would allow the association of stomatin with the native lipid environment, and the lipids could also stabilize the N- terminal hydrophobic patch.

6. Acknowledgements/Danksagung

Ich will Prof. Dr. Oliver Daumke zunächst dafür danken, dass er mir dieses Projekt zur Bearbeitung überlassen hat und mich im Laufe meiner Doktorarbeit immer sehr gut mit seiner überragenden Fachkompetenz betreut hat. Im weiteren will ich Oli dafür danken, dass er mich mit seiner stets motivierenden, klaren und offenen Art auch in dickflüssigeren Zeiten mit seiner Geduld gut zur Seite stand. Im ganzen danke ich Oli, dass du ein sehr guter Betreurer und Mentor bist, ich habe sehr viel von dir gelernt.

Prof. Dr. Udo Heinemann danke ich für die vielen interessanten Gedankenanstöße, die durch Kommentare in Vorlesungen und Seminaren mich zum Nachdenken angeregt haben. Im weiteren danke ich ihm dafür, die Aufgaben des Erstprüfer zu übernehmen.

Prof. Dr. Gary Lewin danke ich für die vielen Diskussionen und Anmerkungen zum Manuskript und dem Projekt.

Mein Dank gilt der gesamten Daumke Gruppe für die tolle Arbeitsumgebung, in der Erfolge gemeinsam gefeiert und Rückschläge gemeinsam gelöst werden.

Im speziellen will ich David Schwefel für seine Hilfe bei der Strukturaufklärung danken. Es waren zum Teil langen Stunden im Computerraum mit Dir, aber sie waren immer lehrreich und lustig.

Chris Fröhlich und Claudio Shah danke ich für die vielen Ratschläge im Labor und am Computer. Im weiteren habe ich mich stets gefreut, euch im Labor anzutreffen. Danke Chris und Alexej Dick für die vielen tollen SK49 Abende.

Sabine Werner und Marion Papst danke ich für die große Unterstützung im Labor. Ihr haltet uns so gut den Rücken frei, und einen solchen Service habe ich in keinem anderen Labor bis jetzt erlebt.

Song Gao, I want to thank you for you good suggestions and the interesting conversation about biological or other topics.

Katja Fälber, ich danke dir für die vielen Dinge, die ich von dir lernen konnte, und die guten Gespräche mit Dir.

Stephen Marino, I want to thank you especially for the proof reading of this manuscript and the inspiring conversations we had.

Mein Dank geht an Kathrin Schulte, Verena Ezerski, Ullrike Maschke, Stefan Grabiger, Isabell Orf, Daniel Olal, Arasu Balasubramaniyam Sivanandam und Eva Rosenbaum für die gute Unterstützung.

Prof. Dr. Behlke und Dr. Otto Ristau danke ich für die Durchführung und Analyse der AUZ Daten.

Dem BESSY2 und SLS Team danke ich für die Hilfe am Synchrotron.

Im weiteren will ich dem gesamten MDC ein Lob für den reibungslosen Ablauf meiner Doktorarbeit aussprechen, ich habe bis jetzt noch kein besser funktionierendes Institut erlebt!

Ich will meinen Freunden Frido, Carlos, Max, all meinen Freunden sowie Janka und meinen beiden Mitbewohnerinnen Eva und Steffie für die wichtige Unterstützung fernab von Buch danken.

I want to thanks the following Bands: Europe, Pearl Jam, Bonaparte, Tina Turner, Peter Fox and Johnossi for the soundtrack of this work.

7. Erklärung

Ich versichere, daß ich die von mir vorgelegte Dissertation selbständig angefertigt, die benutzten Quellen und Hilfsmittel vollständig angegeben und die Stellen der Arbeit einschließlich Tabellen, Karten und Abbildungen -, die anderen Werken im Wortlaut oder dem Sinn nach entnommen sind, in jedem Einzelfall als Entlehnung kenntlich gemacht habe.

Die von mir vorgelegte Dissertation ist von Prof. Dr. Oliver Daumke und Prof. Dr. Gary Lewin betreut worden.

Berlin, 17. 08. 2012

Janko Brand

8. References

Artal-Sanz M and Tavernarakis N (2009) Prohibitin couples diapause signalling to mitochondrial metabolism during ageing in C. elegans. ***Nature*** **461: 793-797**

Artal-Sanz M, Tsang WY, Willems EM, Grivell LA, Lemire BD, van der Spek H, Nijtmans LG (2003) The mitochondrial prohibitin complex is essential for embryonic viability and germline function in Caenorhabditis elegans. ***J Biol Chem*** **278: 32091-32099**

Askwith CC, Wemmie JA, Price MP, Rokhlina T, Welsh MJ (2004) Acid-sensing ion channel 2 (ASIC2) modulates ASIC1 H+-activated currents in hippocampal neurons. ***J Biol Chem*** **279: 18296-18305**

Baconguis I and Gouaux E (2012) Structural plasticity and dynamic selectivity of acid-sensing ion channel-spider toxin complexes. ***Nature***

Bao L, Locovei S, Dahl G (2004) Pannexin membrane channels are mechanosensitive conduits for ATP. ***FEBS Lett*** **572: 65-68**

Barnes TM, Jin Y, Horvitz HR, Ruvkun G, Hekimi S (1996) The Caenorhabditis elegans behavioral gene unc-24 encodes a novel bipartite protein similar to both erythrocyte band 7.2 (stomatin) and nonspecific lipid transfer protein. ***J Neurochem*** **67: 46-57**

Baron A, Deval E, Salinas M, Lingueglia E, Voilley N, Lazdunski M (2002) Protein kinase C stimulates the acid-sensing ion channel ASIC2a via the PDZ domain-containing protein PICK1. ***J Biol Chem*** **277: 50463-50468**

Bassilana F, Champigny G, Waldmann R, de Weille JR, Heurteaux C, Lazdunski M (1997) The acid-sensitive ionic channel subunit ASIC and the mammalian degenerin MDEG form a heteromultimeric H+-gated Na+ channel with novel properties. ***J Biol Chem*** **272: 28819-28822**

Behlke J and Ristau O (2003) Sedimentation equilibrium: a valuable tool to study homologous and heterogeneous interactions of proteins or proteins and nucleic acids. ***Eur Biophys J*** **32: 427-431**

Behlke J, Ristau O, Schonfeld HJ (1997) Nucleotide-dependent complex formation between the Escherichia coli chaperonins GroEL and GroES studied under equilibrium conditions. ***Biochemistry*** **36: 5149-5156**

Bickel PE, Scherer PE, Schnitzer JE, Oh P, Lisanti MP, Lodish HF (1997) Flotillin and epidermal surface antigen define a new family of caveolae-associated integral membrane proteins. ***J Biol Chem*** **272: 13793-13802**

Boehm M, Nield J, Zhang P, Aro EM, Komenda J, Nixon PJ (2009) Structural and mutational analysis of band 7 proteins in the cyanobacterium Synechocystis sp. strain PCC 6803. ***J Bacteriol*** **191: 6425-6435**

Borner GH, Sherrier DJ, Weimar T, Michaelson LV, Hawkins ND, Macaskill A, Napier JA, Beale MH, Lilley KS, Dupree P (2005) Analysis of detergent-resistant membranes in Arabidopsis. Evidence for plasma membrane lipid rafts. ***Plant Physiol*** **137: 104-116**

Boute N, Gribouval O, Roselli S, Benessy F, Lee H, Fuchshuber A, Dahan K, Gubler MC, Niaudet P, Antignac C (2000) NPHS2, encoding the glomerular protein podocin, is mutated in autosomal recessive steroid-resistant nephrotic syndrome. ***Nat Genet*** **24: 349-354**

Browman DT, Hoegg MB, Robbins SM (2007) The SPFH domain-containing proteins: more than lipid raft markers. ***Trends Cell Biol*** **17: 394-402**

Brunger AT (1997) Free R value: cross-validation in crystallography. ***Methods Enzymol*** **277: 366-396**

Cadiou H, Studer M, Jones NG, Smith ES, Ballard A, McMahon SB, McNaughton PA (2007) Modulation of acid-sensing ion channel activity by nitric oxide. ***J Neurosci*** **27: 13251-13260**

Carnally SM, Dev HS, Stewart AP, Barrera NP, Van Bemmelen MX, Schild L, Henderson RM, Edwardson JM (2008) Direct visualization of the trimeric structure of the ASIC1a channel, using AFM imaging. ***Biochem Biophys Res Commun*** **372: 752-755**

Carruthers A and Naftalin RJ (2009) Altered GLUT1 substrate selectivity in human erythropoiesis? ***Cell*** **137: 200-201**

Chalfie M (2009) Neurosensory mechanotransduction. ***Nat Rev Mol Cell Biol*** **10: 44-52**

Chalfie M and Sulston J (1981) Developmental genetics of the mechanosensory neurons of Caenorhabditis elegans. ***Dev Biol*** **82: 358-370**

Christie DA, Kirchhof MG, Vardhana S, Dustin ML, Madrenas J (2012) Mitochondrial and Plasma Membrane Pools of Stomatin-Like Protein 2 Coalesce at the Immunological Synapse during T Cell Activation. ***PLoS One*** **7: e37144**

Chugani DC, Rome LH, Kedersha NL (1993) Evidence that vault ribonucleoprotein particles localize to the nuclear pore complex. ***J Cell Sci*** **106 (Pt 1): 23-29**

Chung CT, Niemela SL, Miller RH (1989) One-step preparation of competent Escherichia coli: transformation and storage of bacterial cells in the same solution. ***Proc Natl Acad Sci U S A*** **86: 2172-2175**

Coates PJ, Jamieson DJ, Smart K, Prescott AR, Hall PA (1997) The prohibitin family of mitochondrial proteins regulate replicative lifespan. ***Curr Biol*** **7: 607-610**

COLLABORATIVE COMPUTATIONAL PROJECT (1994) The CCP4 Suite: Programs for Protein Crystallography. ***Acta Crystallogr D*** **50: 760-763**

Coric T, Passamaneck YJ, Zhang P, Di GA, Canessa CM (2008) Simple chordates exhibit a proton-independent function of acid-sensing ion channels. ***FASEB J*** **22: 1914-1923**

Coric T, Zheng D, Gerstein M, Canessa CM (2005) Proton sensitivity of ASIC1 appeared with the rise of fishes by changes of residues in the region that follows TM1 in the ectodomain of the channel. ***J Physiol*** **568: 725-735**

Davis IW, Murray LW, Richardson JS, Richardson DC (2004) MOLPROBITY: structure validation and all-atom contact analysis for nucleic acids and their complexes. ***Nucleic Acids Res*** **32: W615-W619**

DeLano WL (2002) The PyMol Molecular Graphics System. ***DeLano Scientific*** **DeLano Scientific, Palo Alto, CA, USA, www.pymol.org**

Dundas J, Ouyang Z, Tseng J, Binkowski A, Turpaz Y, Liang J (2006) CASTp: computed atlas of surface topography of proteins with structural and topographical mapping of functionally annotated residues. ***Nucleic Acids Res*** **34: W116-W118**

Emsley P and Cowtan K (2004) Coot: model-building tools for molecular graphics. ***Acta Cryst D*** **60: 2126-2132**

Firsov D, Robert-Nicoud M, Gruender S, Schild L, Rossier BC (1999) Mutational analysis of cysteine-rich domains of the epithelium sodium channel (ENaC). Identification of cysteines essential for channel expression at the cell surface. ***J Biol Chem*** **274: 2743-2749**

Foster LJ, de Hoog CL, Mann M (2003) Unbiased quantitative proteomics of lipid rafts reveals high specificity for signaling factors. ***Proc Natl Acad Sci U S A*** **100: 5813-5818**

Frick M, Bright NA, Riento K, Bray A, Merrified C, Nichols BJ (2007) Coassembly of flotillins induces formation of membrane microdomains, membrane curvature, and vesicle budding. ***Curr Biol*** **17: 1151-1156**

Fricke B, Jarvis HG, Reid CD, Aguilar-Martinez P, Robert A, Quittet P, Chetty M, Pizzey A, Cynober T, Lande WF, Mentzer WC, During M, Winter S, Delaunay J, Stewart GW (2004) Four new cases of stomatin-deficient hereditary stomatocytosis syndrome: association of the stomatin-deficient cryohydrocytosis variant with neurological dysfunction. ***Br J Haematol*** **125: 796-803**

Frost A, Perera R, Roux A, Spasov K, Destaing O, Egelman EH, De CP, Unger VM (2008) Structural basis of membrane invagination by F-BAR domains. ***Cell*** **132: 807-817**

Frost A, Unger VM, De CP (2009) The BAR domain superfamily: membrane-molding macromolecules. ***Cell*** **137: 191-196**

Gao S, von der Malsburg A, Paeschke S, Behlke J, Haller O, Kochs G, Daumke O (2010) Structural basis of oligomerization in the stalk region of dynamin-like MxA. ***Nature*** **465: 502-506**

Gilles F, Glenn M, Goy A, Remache Y, Zelenetz AD (2000) A novel gene STORP (STOmatin-Related Protein) is localized 2 kb upstream of the promyelocytic gene on chromosome 15q22. ***Eur J Haematol*** **64: 104-113**

Glebov OO, Bright NA, Nichols BJ (2006) Flotillin-1 defines a clathrin-independent endocytic pathway in mammalian cells. ***Nat Cell Biol*** **8: 46-54**

Gonzales EB, Kawate T, Gouaux E (2009) Pore architecture and ion sites in acid-sensing ion channels and P2X receptors. ***Nature*** **460: 599-604**

Green JB and Young JP (2008) Slipins: ancient origin, duplication and diversification of the stomatin protein family. ***BMC Evol Biol*** **8: 44**

Halbhuber Z, Petrmichlova Z, Alexciev K, Thulin E, Stys D (2003) Overexpression and purification of recombinant membrane PsbH protein in Escherichia coli. ***Protein Expr Purif*** **32: 18-27**

Haney CH and Long SR (2010) Plant flotillins are required for infection by nitrogen-fixing bacteria. ***Proc Natl Acad Sci U S A*** **107: 478-483**

Hu ZL, Huang C, Fu H, Jin Y, Wu WN, Xiong QJ, Xie N, Long LH, Chen JG, Wang F (2010) Disruption of PICK1 attenuates the function of ASICs and PKC regulation of ASICs. ***Am J Physiol Cell Physiol*** **299: C1355-C1362**

Huang M, Gu G, Ferguson EL, Chalfie M (1995) A stomatin-like protein necessary for mechanosensation in C. elegans. ***Nature*** **378: 292-295**

Huber TB and others (2006) Podocin and MEC-2 bind cholesterol to regulate the activity of associated ion channels. ***Proc Natl Acad Sci U S A*** **103: 17079-17086**

Huber TB, Simons M, Hartleben B, Sernetz L, Schmidts M, Gundlach E, Saleem MA, Walz G, Benzing T (2003) Molecular basis of the functional podocin-nephrin complex: mutations in the NPHS2 gene disrupt nephrin targeting to lipid raft microdomains. ***Hum Mol Genet*** **12: 3397-3405**

Hughey RP, Bruns JB, Kinlough CL, Harkleroad KL, Tong Q, Carattino MD, Johnson JP, Stockand JD, Kleyman TR (2004) Epithelial sodium channels are activated by furin-dependent proteolysis. ***J Biol Chem*** **279: 18111-18114**

Jasti J, Furukawa H, Gonzales EB, Gouaux E (2007) Structure of acid-sensing ion channel 1 at 1.9 A resolution and low pH. ***Nature*** **449: 316-323**

Kabsch W (2010) XDS. ***Acta Crystallogr D Biol Crystallogr*** **66: 125-132**

Kadurin I, Golubovic A, Leisle L, Schindelin H, Grunder S (2008) Differential effects of N-glycans on surface expression suggest structural differences between the acid-sensing ion channel (ASIC) 1a and ASIC1b. ***Biochem J*** **412: 469-475**

Kadurin I, Huber S, Grunder S (2009) A single conserved proline residue determines the membrane topology of stomatin. ***Biochem J*** **418: 587-594**

Kashlan OB and Kleyman TR (2011) ENaC structure and function in the wake of a resolved structure of a family member. ***Am J Physiol Renal Physiol*** **301: F684-F696**

Kedersha NL, Miquel MC, Bittner D, Rome LH (1990) Vaults. II. Ribonucleoprotein structures are highly conserved among higher and lower eukaryotes. ***J Cell Biol*** **110: 895-901**

Kedersha NL and Rome LH (1986) Preparative agarose gel electrophoresis for the purification of small organelles and particles. ***Anal Biochem*** **156: 161-170**

Kerppola TK (2006) Design and implementation of bimolecular fluorescence complementation (BiFC) assays for the visualization of protein interactions in living cells. ***Nat Protoc*** **1: 1278-1286**

Kleyman TR, Carattino MD, Hughey RP (2009) ENaC at the cutting edge: regulation of epithelial sodium channels by proteases. ***J Biol Chem*** **284: 20447-20451**

Kong LB, Siva AC, Kickhoefer VA, Rome LH, Stewart PL (2000) RNA location and modeling of a WD40 repeat domain within the vault. ***RNA*** **6: 890-900**

Kong LB, Siva AC, Rome LH, Stewart PL (1999) Structure of the vault, a ubiquitous celular component. ***Structure*** **7: 371-379**

Krissinel E and Henrick K (2007) Inference of macromolecular assemblies from crystalline state. ***J Mol Biol*** **372: 774-797**

Lapatsina L, Brand J, Poole K, Daumke O, Lewin GR (2012a) Stomatin-domain proteins. ***Eur J Cell Biol*** **91: 240-245**

Lapatsina L, Jira J, Smith ES, Poole K, Kozlenkov A, Bilbao D, Lewin GR, Heppenstall PA (2012b) Regulation of ASIC channels by a stomatin/STOML3 complex located in a mobile vesicle pool in sensory neurons. ***Open Biology*** **in press:**

Lechner SG and Siemens J (2011) Sensory transduction, the gateway to perception: mechanisms and pathology. ***EMBO Rep*** **12: 292-295**

Leslie AG (1999) Integration of macromolecular diffraction data. ***Acta Crystallogr D Biol Crystallogr*** **55: 1696-1702**

Lingueglia E (2007) Acid-sensing ion channels in sensory perception. ***J Biol Chem*** **282: 17325-17329**

Liu J, Deyoung SM, Zhang M, Dold LH, Saltiel AR (2005) The stomatin/prohibitin/flotillin/HflK/C domain of flotillin-1 contains distinct sequences that direct plasma membrane localization and protein interactions in 3T3-L1 adipocytes. ***J Biol Chem*** **280: 16125-16134**

Llobet A, Gallop JL, Burden JJ, Camdere G, Chandra P, Vallis Y, Hopkins CR, Lagnado L, McMahon HT (2011) Endophilin drives the fast mode of vesicle retrieval in a ribbon synapse. ***J Neurosci*** **31: 8512-8519**

Locovei S, Bao L, Dahl G (2006) Pannexin 1 in erythrocytes: function without a gap. ***Proc Natl Acad Sci U S A*** **103: 7655-7659**

Lopez D and Kolter R (2010) Functional microdomains in bacterial membranes. ***Genes Dev*** **24: 1893-1902**

Mairhofer M, Steiner M, Mosgoeller W, Prohaska R, Salzer U (2002) Stomatin is a major lipid-raft component of platelet alpha granules. ***Blood*** **100: 897-904**

Mairhofer M, Steiner M, Salzer U, Prohaska R (2009) Stomatin-like protein-1 interacts with stomatin and is targeted to late endosomes. ***J Biol Chem*** **284: 29218-29229**

Martinez-Salgado C, Benckendorff AG, Chiang LY, Wang R, Milenkovic N, Wetzel C, Hu J, Stucky CL, Parra MG, Mohandas N, Lewin GR (2007) Stomatin and sensory neuron mechanotransduction. ***J Neurophysiol*** **98: 3802-3808**

Merkwirth C and Langer T (2009) Prohibitin function within mitochondria: essential roles for cell proliferation and cristae morphogenesis. ***Biochim Biophys Acta*** **1793: 27-32**

Mim C, Cui H, Gawronski-Salerno JA, Frost A, Lyman E, Voth GA, Unger VM (2012) Structural basis of membrane bending by the N-BAR protein endophilin. ***Cell*** **149: 137-145**

Montel-Hagen A, Kinet S, Manel N, Mongellaz C, Prohaska R, Battini JL, Delaunay J, Sitbon M, Taylor N (2008) Erythrocyte Glut1 triggers dehydroascorbic acid uptake in mammals unable to synthesize vitamin C. ***Cell*** **132: 1039-1048**

Mossink MH, van ZA, Franzel-Luiten E, Schoester M, Kickhoefer VA, Scheffer GL, Scheper RJ, Sonneveld P, Wiemer EA (2002) Disruption of the murine major vault protein (MVP/LRP) gene does not induce hypersensitivity to cytostatics. ***Cancer Res*** **62: 7298-7304**

Murshudov GN, Vagin AA, Dodson EJ (1997) Refinement of macromolecular structures by the maximum-likelihood method. ***Acta Cryst D*** **53: 240-255**

Neumann-Giesen C, Falkenbach B, Beicht P, Claasen S, Luers G, Stuermer CA, Herzog V, Tikkanen R (2004) Membrane and raft association of reggie-1/flotillin-2: role of myristoylation, palmitoylation and oligomerization and induction of filopodia by overexpression. ***Biochem J*** **378: 509-518**

Otto GP and Nichols BJ (2011) The roles of flotillin microdomains--endocytosis and beyond. ***J Cell Sci*** **124: 3933-3940**

Otwinowski Z and Minor W (1997) Processing of X-ray Diffraction Data Collected in Oscillation Mode. ***Methods Enzymol*** **276: 307-326**

Owczarek CM, Treutlein HR, Portbury KJ, Gulluyan LM, Kola I, Hertzog PJ (2001) A novel member of the STOMATIN/EPB72/mec-2 family, stomatin-like 2 (STOML2), is ubiquitously expressed and localizes to HSA chromosome 9p13.1. ***Cytogenet Cell Genet*** **92: 196-203**

Passero CJ, Mueller GM, Rondon-Berrios H, Tofovic SP, Hughey RP, Kleyman TR (2008) Plasmin activates epithelial Na+ channels by cleaving the gamma subunit. ***J Biol Chem*** **283: 36586-36591**

Pearce MM, Wang Y, Kelley GG, Wojcikiewicz RJ (2007) SPFH2 mediates the endoplasmic reticulum-associated degradation of inositol 1,4,5-trisphosphate receptors and other substrates in mammalian cells. ***J Biol Chem*** **282: 20104-20115**

Peter BJ, Kent HM, Mills IG, Vallis Y, Butler PJ, Evans PR, McMahon HT (2004) BAR domains as sensors of membrane curvature: the amphiphysin BAR structure. ***Science*** **303: 495-499**

Price MP, Snyder PM, Welsh MJ (1996) Cloning and expression of a novel human brain Na+ channel. ***J Biol Chem*** **271: 7879-7882**

Price MP, Thompson RJ, Eshcol JO, Wemmie JA, Benson CJ (2004) Stomatin modulates gating of acid-sensing ion channels. ***J Biol Chem*** **279: 53886-53891**

Rivera-Milla E, Stuermer CA, Malaga-Trillo E (2006) Ancient origin of reggie (flotillin), reggie-like, and other lipid-raft proteins: convergent evolution of the SPFH domain. ***Cell Mol Life Sci*** **63: 343-357**

Roselli S, Gribouval O, Boute N, Sich M, Benessy F, Attie T, Gubler MC, Antignac C (2002) Podocin localizes in the kidney to the slit diaphragm area. ***Am J Pathol*** **160: 131-139**

Roselli S, Heidet L, Sich M, Henger A, Kretzler M, Gubler MC, Antignac C (2004) Early glomerular filtration defect and severe renal disease in podocin-deficient mice. ***Mol Cell Biol*** **24: 550-560**

Saleem MA, Ni L, Witherden I, Tryggvason K, Ruotsalainen V, Mundel P, Mathieson PW (2002) Co-localization of nephrin, podocin, and the actin cytoskeleton: evidence for a role in podocyte foot process formation. ***Am J Pathol*** **161: 1459-1466**

Salzer U, Ahorn H, Prohaska R (1993) Identification of the phosphorylation site on human erythrocyte band 7 integral membrane protein: implications for a monotopic protein structure. ***Biochim Biophys Acta*** **1151: 149-152**

Salzer U and Prohaska R (2001) Stomatin, flotillin-1, and flotillin-2 are major integral proteins of erythrocyte lipid rafts. ***Blood*** **97: 1141-1143**

Scheffer GL, Schroeijers AB, Izquierdo MA, Wiemer EA, Scheper RJ (2000) Lung resistance-related protein/major vault protein and vaults in multidrug-resistant cancer. ***Curr Opin Oncol*** **12: 550-556**

Scheffer GL, Wijngaard PL, Flens MJ, Izquierdo MA, Slovak ML, Pinedo HM, Meijer CJ, Clevers HC, Scheper RJ (1995a) The drug resistance-related protein LRP is the human major vault protein. ***Nat Med*** **1: 578-582**

Scheffer GL, Wijngaard PL, Flens MJ, Izquierdo MA, Slovak ML, Pinedo HM, Meijer CJ, Clevers HC, Scheper RJ (1995b) The drug resistance-related protein LRP is the human major vault protein. ***Nat Med*** **1: 578-582**

Scheper RJ, Broxterman HJ, Scheffer GL, Meijer CJ, Pinedo HM (1992) Drug-transporter proteins in clinical multidrug resistance. ***Clin Chim Acta*** **206: 25-32**

SCHERER WF, SYVERTON JT, Gey GO (1953) Studies on the propagation in vitro of poliomyelitis viruses. IV. Viral multiplication in a stable strain of human malignant epithelial cells (strain HeLa) derived from an epidermoid carcinoma of the cervix. ***J Exp Med*** **97: 695-710**

Schneider U, Schwenk HU, Bornkamm G (1977) Characterization of EBV-genome negative "null" and "T" cell lines derived from children with acute lymphoblastic leukemia and leukemic transformed non-Hodgkin lymphoma. ***Int J Cancer*** **19: 621-626**

Schroeder WT, Stewart-Galetka S, Mandavilli S, Parry DA, Goldsmith L, Duvic M (1994) Cloning and characterization of a novel epidermal cell surface antigen (ESA). ***J Biol Chem*** **269: 19983-19991**

Schulte T, Paschke KA, Laessing U, Lottspeich F, Stuermer CA (1997) Reggie-1 and reggie-2, two cell surface proteins expressed by retinal ganglion cells during axon regeneration. ***Development*** **124: 577-587**

Seidel G and Prohaska R (1998) Molecular cloning of hSLP-1, a novel human brain-specific member of the band 7/MEC-2 family similar to Caenorhabditis elegans UNC-24. ***Gene*** **225: 23-29**

Shono A, Tsukaguchi H, Yaoita E, Nameta M, Kurihara H, Qin XS, Yamamoto T, Doi T (2007) Podocin participates in the assembly of tight junctions between foot processes in nephrotic podocytes. ***J Am Soc Nephrol*** **18: 2525-2533**

Smith M, Filipek PA, Wu C, Bocian M, Hakim S, Modahl C, Spence MA (2000) Analysis of a 1-megabase deletion in 15q22-q23 in an autistic patient: identification of candidate genes for autism and of homologous DNA segments in 15q22-q23 and 15q11-q13. ***Am J Med Genet*** **96: 765-770**

Snyers L, Umlauf E, Prohaska R (1999) Cysteine 29 is the major palmitoylation site on stomatin. ***FEBS Lett*** **449: 101-104**

Steglich G, Neupert W, Langer T (1999) Prohibitins regulate membrane protein degradation by the m-AAA protease in mitochondria. ***Mol Cell Biol*** **19: 3435-3442**

Steinkellner G, Rader R, Thallinger GG, Kratky C, Gruber K (2009) VASCo: computation and visualization of annotated protein surface contacts. ***BMC Bioinformatics*** **10: 32**

Stewart GW (1997) Stomatin. ***Int J Biochem Cell Biol*** **29: 271-274**

Stewart GW, Hepworth-Jones BE, Keen JN, Dash BC, Argent AC, Casimir CM (1992) Isolation of cDNA coding for an ubiquitous membrane protein deficient in high Na+, low K+ stomatocytic erythrocytes. ***Blood*** **79: 1593-1601**

Takei K, Slepnev VI, Haucke V, De CP (1999) Functional partnership between amphiphysin and dynamin in clathrin-mediated endocytosis. ***Nat Cell Biol*** **1: 33-39**

Tanaka H, Kato K, Yamashita E, Sumizawa T, Zhou Y, Yao M, Iwasaki K, Yoshimura M, Tsukihara T (2009) The structure of rat liver vault at 3.5 angstrom resolution. ***Science*** **323: 384-388**

Tatsuta T, Model K, Langer T (2005a) Formation of membrane-bound ring complexes by prohibitins in mitochondria. ***Mol Biol Cell*** **16: 248-259**

Tatsuta T, Model K, Langer T (2005b) Formation of membrane-bound ring complexes by prohibitins in mitochondria. ***Mol Biol Cell*** **16: 248-259**

Tavernarakis N, Driscoll M, Kyrpides NC (1999) The SPFH domain: implicated in regulating targeted protein turnover in stomatins and other membrane-associated proteins. ***Trends Biochem Sci*** **24: 425-427**

Thompson JD, Higgins DG, Gibson TJ (1994) CLUSTAL W: improving the sensitivity of progressive multiple sequence alignment through sequence weighting, position-specific gap penalties and weight matrix choice. ***Nucleic Acids Res*** **22: 4673-4680**

Umlauf E, Csaszar E, Moertelmaier M, Schuetz GJ, Parton RG, Prohaska R (2004) Association of stomatin with lipid bodies. ***J Biol Chem*** **279: 23699-23709**

Umlauf E, Mairhofer M, Prohaska R (2006) Characterization of the stomatin domain involved in homo-oligomerization and lipid raft association. ***J Biol Chem*** **281: 23349-23356**

Unfried I, Entler B, Prohaska R (1995) The organization of the gene (EPB72) encoding the human erythrocyte band 7 integral membrane protein (protein 7.2b). ***Genomics*** **30: 521-528**

Vagin A and Teplyakov A (1997) MOLREP: an automated program for molecular replacement. ***J Appl Cryst*** **30: 1022-1025**

Vaguine AA, Richelle J, Wodak SJ (1999) SFCHECK: a unified set of procedures for evaluating the quality of macromolecular structure-factor data and their agreement with the atomic model. ***Acta Crystallogr D Biol Crystallogr*** **55: 191-205**

Volonte D, Galbiati F, Li S, Nishiyama K, Okamoto T, Lisanti MP (1999) Flotillins/cavatellins are differentially expressed in cells and tissues and form a hetero-oligomeric complex with caveolins in vivo. Characterization and epitope-mapping of a novel flotillin-1 monoclonal antibody probe. ***J Biol Chem*** **274: 12702-12709**

Waldmann R, Champigny G, Bassilana F, Heurteaux C, Lazdunski M (1997) A proton-gated cation channel involved in acid-sensing. ***Nature*** **386: 173-177**

Waldmann R, Champigny G, Bassilana F, Voilley N, Lazdunski M (1995) Molecular cloning and functional expression of a novel amiloride-sensitive Na+ channel. ***J Biol Chem*** **270: 27411-27414**

Wang Y and Morrow JS (2000) Identification and characterization of human SLP-2, a novel homologue of stomatin (band 7.2b) present in erythrocytes and other tissues. ***J Biol Chem*** **275: 8062-8071**

Wetzel C, Hu J, Riethmacher D, Benckendorff A, Harder L, Eilers A, Moshourab R, Kozlenkov A, Labuz D, Caspani O, Erdmann B, Machelska H, Heppenstall PA, Lewin GR (2007) A stomatin-domain protein essential for touch sensation in the mouse. ***Nature*** **445: 206-209**

Whitmore L and Wallace BA (2004) DICHROWEB, an online server for protein secondary structure analyses from circular dichroism spectroscopic data. ***Nucleic Acids Res*** **32: W668-W673**

Winn MD, Murshudov GN, Papiz MZ (2003) Macromolecular TLS refinement in REFMAC at moderate resolutions. ***Methods Enzymol*** **374: 300-321**

Yokoyama H, Fujii S, Matsui I (2008) Crystal structure of a core domain of stomatin from Pyrococcus horikoshii Illustrates a novel trimeric and coiled-coil fold. ***J Mol Biol*** **376: 868-878**

Zhan H, Moore CS, Chen B, Zhou X, Ma XM, Ijichi K, Bennett MV, Li XJ, Crocker SJ, Wang ZW (2012) Stomatin inhibits pannexin-1-mediated whole-cell currents by interacting with its carboxyl terminal. ***PLoS One*** **7: e39489**

Zorick TS and Echols H (1991) Membrane localization of the HflA regulatory protease of Escherichia coli by immunoelectron microscopy. *J Bacteriol* 173: 6307-6310

9. Appendix

9. 1 Prokaryotic constructs

mmStomatin	Soluble	5´	3´	WT or mutation
pGEX 6P1 mmStomatin 1-284	-	BamH1	Xho1	WT
pGEX 6P1 mmStomatin 86-194	-	BamH1	Xho1	WT
pSLKB2LNB mmStomatin 86-194	-	BamH1	Xho1	WT
pGEX 6P1 mmStomatin 96-204	+	BamH1	Xho1	WT
pGEX 6P1 mmStomatin 86-204	+	BamH1	Xho1	WT
pGEX 6P1 mmStomatin 23-204	-	BamH1	Xho1	WT
pGEX 6P1 mmStomatin 86-255	+	BamH1	Xho1	WT
pSLKB2LNB mmStomatin 86-255	+	BamH1	Xho1	WT
pGEX 6P1 mmStomatin 86-213	+	BamH1	Xho1	WT, LI91,92AA, R97D, R97D/L109D/L145D, L145D/L109D,R152D/L145D, T182W,V197P,R191D
pSLKB2LNB mmStomatin 86-213	+	BamH1	Xho1	WT
pGEX 6P1 mmStomatin 86-213	-	BamH1	Xho1	V197D
mmSLP1				
pGEX 6P1 mmSLP1 108-277	+	BamH1	Xho1	WT
pSLKB2LNB mmSLP1 108-277	-	BamH1	Xho1	WT
pGEX 6P1 mmSLP1 108-237	+	BamH1	Xho1	WT
pSLKB2LNB mmSLP1 108-237	+	BamH1	Xho1	WT
mmSLP2				
pGEX 6P1 mmSLP2 67-238	+	BamH1	Xho1	WT
pSLKB2LNB mmSLP2 67-238	+	BamH1	Xho1	WT
pGEX 6P1 mmSLP2 67-248	+	BamH1	Xho1	WT
pSLKB2LNB mmSLP2 67-248	+	BamH1	Xho1	WT
mmSLP3				
pGEX 6P1 mmSLP3 79-206	-	BamH1	Xho1	WT
pSLKB2LNB mmSLP3 79-206	-	BamH1	Xho1	WT
pGEX 6P1 mmSLP3 79-248	-	BamH1	Xho1	WT
pSLKB2LNB mmSLP3 79-248	-	BamH1	Xho1	WT
pGEX 6P1 mmSLP3 1-287	-	BamH1	Xho1	WT
pGEX 6P1 mmSLP3 79-206	-	BamH1	Xho1	all C to S
pGEX 6P1 mmSLP3 79-248	-	BamH1	Xho1	all C to S
pGEX 6P1 mmSLP3 1-287	-	BamH1	Xho1	all C to S
mmPodocin				
pGEX 6P1 mmPodo 1-99	-	BamH1	Xho1	WT
pGEX 6P1 mmPodo 1-284	-	BamH1	Xho1	WT
pGEX 6P1 mmPodo 119-284	-	BamH1	Xho1	WT

9. 2 Eukaryotic constructs

Electrophysiological recordings	**5´**	**3´**	**WT or mutation**
pIRES2-eGFP mmStomatin1-284	Xho1	EcoR1	
Cellular localization constructs			
mCherryN3-mmStomatin 1-284	Xho1	EcoR1	WT, LI91,92AA, R97D, R97D/L109D/L145D, L145D/L109D,R152D/L145D, T182W, V197P, R191D
mCherryN3-mmStomatin 1-30	Xho1	EcoR1	WT
mCherryN3-mmStomatin 1-58	Xho1	EcoR1	WT
mCherryN3-mmStomatin 1-100	Xho1	EcoR1	WT
mCherryN3-mmStomatin 59-284	Xho1	EcoR1	WT
mCherryN3-mmStomatin 86-213	Xho1	EcoR1	WT
Immunoprecipitation and expression assays			
pcDNA6-mmStomatin 1-284	Xho1	EcoR1	WT, LI91,92AA, R97D, R97D/L109D/L145D, L145D/L109D,R152D/L145D, T182W, V197P, R191D
pcDNA6-rnASIC3 1-530			WT and LL488,489DD
BiFC			
pBiFC-CN155-mmStomatin 1-284	EcoR1	Xho1	R97D,R97D/L109D/L145D, L145D/L109D,T182W, V197P
pBiFC-VN173-mmStomatin 1-284	Hind3	Xba1	R97D,R97D/L109D/L145D, L145D/L109D,T182W, V197P
pBiFC-CN155-rnASIC3 1-530	EcoR1	Xho1	WT and LL488,489DD

9. 3 Instruments and Buffers

Instrument	**Manufacturer**
Agarose Gel Electrophoresis System	OLS, Bremen, D
Amicon centrifugal filter devices	Millipore, Billerica, USA
Benchtop Centrifuge 5415 R	Eppendorf, Hamburg, D
Benchtop Centrifuge 5804 R	Eppendorf, Hamburg, D
GSTrap HP 1 ml	GE Healthcare, Piscataway, USA
Chromatography column material GSH Sepharose	GE Healthcare, Piscataway, USA
Chromatography columns Superdex 75 16/60, 26/60	GE Healthcare, Piscataway, USA
Chromatography columns Superdex 200 16/60, 26/60	GE Healthcare, Piscataway, USA
Chromatography columns XK 16/20, XK 26/20	GE Healthcare, Piscataway, USA
Centrifuge Avanti J-26 XP	Beckman Coulter, Krefeld, D
Fluidizer	Microfluidics, Newton, USA
FPLC Äkta Prime Plus	GE Healthcare, Piscataway, USA

FPLC Äkta Purifier	GE Healthcare, Piscataway, USA
Isothermal Titration Calorimeter VP-ITC	GE Healthcare, Piscataway, USA
PCR Thermocycler	Biometra, Göttingen, D
Peristaltic Pump	Ismatec, Glattbrugg, CH
pH-Meter	Mettler-Toledo, Gießen, D
SDS PAGE System Xcell Sure Lock	Invitrogen, Darmstadt, D
Shaker Incubator	New Brunswick Scientific, Edison, USA
Ultracentrifuge Optima L-100K	Beckman Coulter, Krefeld, D
Western Blot Module Xcell II	Invitrogen, Darmstadt, D

Enzyme	**Manufacturer**
DNAse I	Roche, Mannheim, D
PreScission Protease	GE Healthcare, Piscataway, USA
Pfu DNA Polymerase	ROBOKLON, Berlin, D
Restiction Endonucleases	New England Biolabs, Frankfurt am Main, D
T4 DNA Ligase	New England Biolabs, Frankfurt am Main, D

Kit	**Manufacturer**
2-Log DNA ladder	New England Biolabs, Frankfurt am Main, D
Bradford protein assay	Bio-Rad, München, D
GeneAmp dNTPs	Roche, Mannheim, D
NuPAGE LDS Sample Buffer (4x)	Invitrogen, Darmstadt, D
NuPAGE MES SDS Buffer Kit	Invitrogen, Darmstadt, D
NuPAGE Novex 4-12% Bis-Tris	Invitrogen, Darmstadt, D
QIAprep Spin Miniprep Kit	Qiagen, Hilden, D
QIAquick PCR Purification Kit	Qiagen, Hilden, D
QIAquick Gel Extraction Kit	Qiagen, Hilden, D
QuickChange Stratagene	Stratagene, Amsterdam, NL
Roti-Fect	Carl Roth, Karlsruhe, D
The Classics Suite	Qiagen, Hilden, D
The JSCG+ Suite	Qiagen, Hilden, D
The PEGs Suite	Qiagen, Hilden, D

Medium	**Components**
Opti-MEM	Invitrogen (11058-021)
RPMI 1640	Invitrogen (21875-034)
Luria-Bertani (LB)	5 g/l yeast extract
	10 g/l tryptone
	5 g/l NaCl
DMEM	Invitrogen (10370-047)
Terrific broth (TB)	Roth (HP61.1)

Buffer	**Concentration/Components**
Lysis Buffer	50 mM/HEPES pH 7.5 500 mM/NaCl 0.1 mM/Pefabloc SC 1 µg/mL/DNAse I
Wash Buffer	50 mM/HEPES pH 7.5 500 mM/NaCl
Elution Buffer	50 mM/HEPES pH 7.5 500 mM/NaCl 20 mM/GSH
Gel filtration Buffer	10 mM/HEPES pH 7.5 150 mM/NaCl

Online services	**Domain**
Secundary structure prediction	http://www.compbio.dundee.ac.uk/www-jpred/
Volumen calculation of pockets	http://sts.bioengr.uic.edu/castp/calculation.php
Restriction enzym finder	http://www.neb.com/nebecomm/DoubleDigestCalculator.asp
Alignment tool	http://www.genome.jp/tools/clustalw/
Database for protein domains	http://prosite.expasy.org/
Structure comparison	http://ekhidna.biocenter.helsinki.fi/dali_server/
Structure validation	http://molprobity.biochem.duke.edu/
CD-messuremnts analysis tool	http://dichroweb.cryst.bbk.ac.uk/html/home.shtml
Conservation blot tool	http://consurf.tau.ac.il/

Plug-in	**Service**
VASCo	visualisation of protein surfaces and potentials

9. 4 Chemicals and enzymes

Chemicals and Enzymes	**Cat.-No.**	**Manufacturer (location)**
25-Hydroxycholesterol	H1015	Sigma-Aldrich (Steinheim)
Acetic Acid	3783.5	Roth (Karlsruhe)
Acetone	9372.2	Roth (Karlsruhe)
Acetonitrile	CN20.2	Roth (Karlsruhe)
Additive Screen	HR2-428	Hampton Research (Aliso Viejo, USA)
Agarose	2267.3	Roth (Karlsruhe)
Ammonium acetate	9689	Sigma-Aldrich (Steinheim)
Ammonium chloride	9700	Sigma-Aldrich (Steinheim)
Ammonium citrate dibasic	9833	Sigma-Aldrich (Steinheim)
Ammonium fluoride	9737	Sigma-Aldrich (Steinheim)
Ammonium formate	9735	Sigma-Aldrich (Steinheim)
Ammonium iodide	9874	Sigma-Aldrich (Steinheim)
Ammonium nitrate	9889	Sigma-Aldrich (Steinheim)
Ammonium phosphate monobasic	9709	Sigma-Aldrich (Steinheim)
Ammonium sulfate	9212.2	Roth (Karlsruhe)

Ampicillin sodium salt	K029.3	Roth (Karlsruhe)
Calcium acetate Hydrate	21056	Sigma-Aldrich (Steinheim)
Calcium chloride	A119.1	Roth (Karlsruhe)
Chloramphenicol	3886.3	Roth (Karlsruhe)
Coomassie brillant blue R 250	3862.2	Roth (Karlsruhe)
di-Ammonium hydrogen phosphate (sec)	9839	Sigma-Aldrich (Steinheim)
di-Ammonium tartrate	9986	Sigma-Aldrich (Steinheim)
di-Potassium hydrogen phosphate anhydrous	P749.2	Roth (Karlsruhe)
di-Sodium hydrogen phosphate anhydrous	P030.2	Roth (Karlsruhe)
DNAse I	04 716 728 001	Roche (Mannheim)
DOGS-NTA	790528	Avanti (Alabaster, USA)
*Dpn*I	R0176S	New England Biolabs (Frankfurt am Main)
DTT	6908.2	Roth (Karlsruhe)
EDTA	8040.2	Roth (Karlsruhe)
Ethanol	5054.2	Roth (Karlsruhe)
Ethidium bromide	2218.1	Roth (Karlsruhe)
Folch extract	B1502-1G	Sigma-Aldrich (Steinheim)
GeneAmp© dNTPs	N8080007	Roche Molecular Systems (Branchburg, USA)
Glutathione SepharoseTM 4B	27-4574-01	Amersham (Piscatawy, USA)
Glycerol	3783.1	Roth (Karlsruhe)
GSH reduced	3541	Calbiochem (Darmstadt)
Guanidinehydrochloride	37.1	Roth (Karlsruhe)
HEPES	9105.4	Roth (Karlsruhe)
Imidazole	3899.3	Roth (Karlsruhe)
Isopropanol	9866.5	Roth (Karlsruhe)
Kanamycinsulfate	T823.4	Roth (Karlsruhe)
Lithium acetate Dihydrate	62393	Sigma-Aldrich (Steinheim)
Lithium chloride	62478	Sigma-Aldrich (Steinheim)
Lithium citrate tribasic Tetrahydrate	62484	Sigma-Aldrich (Steinheim)
Lithium nitrate	62574	Sigma-Aldrich (Steinheim)
Lithium sulfate Monohydrate	62612	Sigma-Aldrich (Steinheim)
Magnesium acetate Tetrahydrate	63049	Sigma-Aldrich (Steinheim)
Magnesium chloride Hexahydrate	63065	Sigma-Aldrich (Steinheim)
Magnesium formate Dihydrate	793	Sigma-Aldrich (Steinheim)
Magnesium nitrate	237175-100G	Sigma-Aldrich (Steinheim)
Magnesium sulfate Heptahydrate	63138	Sigma-Aldrich (Steinheim)
Malonic acid	63290	Sigma-Aldrich (Steinheim)
Mark12TM unstained standard	LC5677	Invitrogen (Karlsruhe)
Methanol	4627.5	Roth (Karlsruhe)
MPD	68340	Sigma-Aldrich (Steinheim)
NuPAGE© LDS Sample Buffer (4x)	NP0007	Invitrogen (Karlsruhe)
NuPAGE© MES SDS Buffer Kit	NP0060	Invitrogen (Karlsruhe)
NuPAGE© Novex 4-12% Bis-Tris Gel 1,5 mm, 10 / 15 well	NP0335BOX /NP0336BOX	Invitrogen (Karlsruhe)
Pefabloc© SC-Protease inhibitor	A154.2	Roth (Karlsruhe)
PEG 1000	81188	Sigma-Aldrich (Steinheim)
PEG 2000MME	81321	Sigma-Aldrich (Steinheim)

PEG 3350	88276	Sigma-Aldrich (Steinheim)
PEG 400	91893	Sigma-Aldrich (Steinheim)
PEG 4000	95904	Sigma-Aldrich (Steinheim)
PEG 500MME	71578	Sigma-Aldrich (Steinheim)
PEG 8000	89510	Sigma-Aldrich (Steinheim)
Pfu DNA polymerase	600153	Stratagene (La Jolla, USA)
pGEX-6-P1	27-4597-01	GE Healthcare (München)
Potassium acetate	60035	Sigma-Aldrich (Steinheim)
Potassium chloride	6781.3	Roth (Karlsruhe)
Potassium citrate tribasic monohydrate	25107	Sigma-Aldrich (Steinheim)
Potassium dihydrogen phosphate	3904.1	Roth (Karlsruhe)
Potassium fluoride	60239	Sigma-Aldrich (Steinheim)
Potassium formate	60246	Sigma-Aldrich (Steinheim)
Potassium iodide	60400	Sigma-Aldrich (Steinheim)
Potassium nitrate	60414	Sigma-Aldrich (Steinheim)
Potassium phosphate	3904.3	Roth (Karlsruhe)
Potassium sodium tartrate Tetrahydrate	60413	Sigma-Aldrich (Steinheim)
Potassium sulfate	60528	Sigma-Aldrich (Steinheim)
Potassium thiocyanate	60517	Sigma-Aldrich (Steinheim)
PreScissionTM Protease	27-0843-01	GE Healthcare (München)
Primers	diverse	Eurofins MWG (Ebersberg)
QIAprepTM Spin Miniprep Kit	27106	Qiagen (Hilden)
Sodium acetate Trihydrate	71188	Sigma-Aldrich (Steinheim)
Sodium chloride	9265.2	Roth (Karlsruhe)
Sodium citrate tribasic Dihydrate	71402	Sigma-Aldrich (Steinheim)
Sodium di-hydrogen phosphate 2-hydrate	T879.1	Roth (Karlsruhe)
Sodium fluoride	71519	Sigma-Aldrich (Steinheim)
Sodium formate	71539	Sigma-Aldrich (Steinheim)
Sodium hydroxide	6771.1	Roth (Karlsruhe)
Sodium iodide	71710	Sigma-Aldrich (Steinheim)
Sodium nitrate	71755	Sigma-Aldrich (Steinheim)
Sodium sulfate Decahydrate	71969	Sigma-Aldrich (Steinheim)
Sodium tartrate dibasic dihydrate	71994	Sigma-Aldrich (Steinheim)
Sodium thiocyanate	71938	Sigma-Aldrich (Steinheim)
Terrific-Broth medium	HP61.1	Roth (Karlsruhe)
Tetrabutylammonium bromide	86860-500G	Sigma-Aldrich (Steinheim)
The Classics II Suite	130723	Qiagen (Hilden)
The Classics Suite	130701	Qiagen (Hilden)
The JSCG+ Suite	130720	Qiagen (Hilden)
The MPD Sutie	130706	Qiagen (Hilden)
The pHClear II Suite	130710	Qiagen (Hilden)
Trichloromethane	6340.2	Roth (Karlsruhe)
Zinc acetate Dihydrate	96459	Sigma-Aldrich (Steinheim)
Phosphatidylethanolamine	840021	Avanti (Alabaster, USA)
L-a-phosphatidylinositol-4,5-bisphosphate	840046	Avanti (Alabaster, USA)
Phosphatidylserine	840032	Avanti (Alabaster, USA)
Dodecyldimethylaminoxid	1643-20-5	Sigma-Aldrich (Steinheim)
Phosphatidylcholine	840051	Avanti (Alabaster, USA)

9. 5 Abbreviations:

Å	Angstrom (= 0.1 nm)
aa	Amino acid
AC	Affinity chromatography
AG	Analytical gel filtration
Amp.	Ampicillin sodium salt
AUC	Analytical Ultra Centrifugation
BiFC	Bimolecular Fluorescence Complementation
Cam.	Chloramphenicol
CD	Circular Dichroism
CHO	Chinese Hamster Ovarian
conc.	Concentrated
d	Diameter
D	Dilution factor
dd	Double deionised
DMSO	Dimethyl sulfoxide
DNA	Deoxyribonucleic acid
DNAse	Deoxyribonuclease
dNTP	Deoxynucleotide triphosphate
DOGS-NTA	1,2-dioleoyl-*sn*-glycero-3-{} (ammonium salt)
DTT	Dithiothreitol
DRG	Dorsal Root Ganglion
e.g.	exemplī grātia (for example)
EDTA	Ethylenediaminetetraacetic acid
ER	Endoplasmic reticulum
EtOH	Ethanol
fl	Full length
Folch	Folch extract
fr.	Fraction
FTIR	Fourier transform spectroscopy
fw.	Forward
GSH	Glutathione
GST	Glutathione *S*-transferase
h	Hour
HEPES	4-(2-hydroxyethyl)-1-piperazineethanesulfonic acid
HEK	Human Embryonic Kidney
HeLa	Henrietta Lacks
hs	*Homo Sapiens*
IPTG	Isopropyl β-D-1-thiogalactopyranoside
ITC	Isothermal Titration Calorimetry
kb	Kilobase
K_d	Equilibrium dissociation constant
kDa	Kilodalton
LB	Luria-Bertani
LDAO	Dodecyldimethylaminoxid
mAU	Milli absorbance unit
MDR	Multi Drug Resistant
min	Minute(s)
mm	*Mus musculus*
MPD	2-methyl-2,4-pentandiol
M_W	Molecular weight

NMR	Nuclear magnetic resonance
Nr.	Number(s)
NTP	Nucleoside triphosphate
ON	Over night
OD	Optical density
PAGE	Polyacrylamide gel electrophoresis
PC	Phosphatidylcholine
PCR	Polymerase chain reaction
PDB	Protein Data Bank
PE	Phosphatidylethanolamine
PEG	Polyethylene glycol
Pfu	*Pyrococcus furiosus*
ph	*Pyrococcus horikoshii*
PiP2	L-a-phosphatidylinositol-4,5-bisphosphate
PS	Phosphatidylserine
R.m.s.d.	Root mean square deviation
rn	*Rattus norvegicus*
RNA	Ribonucleic acid
RT	Room temperature
Rt	Retention time
rv.	Reverse
SDS	Sodium dodecyl sulfate
SPFH	Stomatin, Prohibitin, Flotillin, HflC/K
TB	Terrific-Broth
TM	Transmembrane
tRNA	Transfer ribonucleic acid
Ve	Elution volume
λ	Wavelength